

Cover Page



Universiteit Leiden



The handle <http://hdl.handle.net/1887/25141> holds various files of this Leiden University dissertation

Author: Hiruma, Yoshitaka

Title: The structure of the cytochrome P450cam-putidaredoxin complex determined by paramagnetic NMR spectroscopy and crystallography

Issue Date: 2014-04-10

The structure of the cytochrome P450cam-putidaredoxin complex
determined by paramagnetic NMR spectroscopy and crystallography

Yoshitaka Hiruma

The structure of the cytochrome P450cam-
putidaredoxin complex determined by paramagnetic
NMR spectroscopy and crystallography

Doctoral Thesis, Leiden University, 2014

Layout: Off Page, www.offpage.nl

Printed by CPU-Wöhrmann Print Service-Zutphen

ISBN: 978-94-6182-420-2

Cover image: The cover image was kindly provided
by Mitsuko Nakao.

2014, Yoshitaka Hiruma

The structure of the cytochrome P450cam-putidaredoxin complex
determined by paramagnetic NMR spectroscopy and crystallography

Proefschrift

ter verkrijging van
de graad van Doctor aan de Universiteit Leiden,
op gezag van Rector Magnificus Prof. mr. C. J. J. M. Stolker,
volgens besluit van het College voor Promoties
te verdedigen op donderdag 10 april 2014
klokke 13:45 uur

door

Yoshitaka Hiruma

geboren te Tokyo, Japan in 1983

Promotiecommissie

Promotor: Prof. Dr. M. Ubbink
Overige leden: Prof. Dr. R. Bernhardt (Saarland University)
Prof. Dr. J. Brouwer (Leiden University)
Prof. Dr. A. Ramamoorthy (University of Michigan)
Dr. M. Nojiri (Osaka University)
Dr. N. Pannu (Leiden University)

The research described in this thesis was financially supported by the Netherlands Organisation for Scientific Research (NWO)

*To my family, who always support me
To my teachers, who gave me knowledge, passion and dreams
To my mentor, who believes me to become a great individual*

Table of contents

	List of abbreviations	9
Chapter 1	General introduction	11
Chapter 2	Validation and characterization of lanthanoid tags for P450cam by paramagnetic NMR spectroscopy	33
Chapter 3	The structure of the cytochrome P450cam-putidaredoxin complex determined by paramagnetic NMR spectroscopy and crystallography	53
Chapter 4	Hot spot residues in the cytochrome P450cam-putidaredoxin binding interface	73
Chapter 5	Paramagnetic NMR analysis reveals the encounter state of the Pdx-P450cam complex	89
Chapter 6	Structural characterization of the substrate access channel of P450cam with a paramagnetic inhibitor	105
Chapter 7	General discussion	117
Addendum	Summary	127
	Samenvatting	129
	Publication list	133
	Curriculum Vitae	135
	Acknowledgements	137

List of abbreviations

CLaNP-5	caged lanthanoid NMR probe version 5
CLaNP-7	caged lanthanoid NMR probe version 7
CO	carbon monoxide
CSP	chemical shift perturbation
D ₂ O	deuterium oxide
DMC	double-mutant cycle
DTT	dithiothreitol
ET	electron transfer
ET1/ET2	first electron transfer / second electron transfer
FAD	flavin adenine dinucleotide
HSQC	heteronuclear single quantum coherence
K _D	dissociation constant
k _{off}	dissociation rate constant
k _{on}	association rate constant
Ln ³⁺ -CLaNP-7	lanthanoid-containing CLaNP-7
MeOH	methanol
MTS	(1-acetyl-2,2,5,5-tetramethyl-3-pyrroline-3-methyl)-methanesulfonylthioate
MTSL	(1-oxyl-2,2,5,5-tetramethyl-3-pyrroline-3-methyl)-methanesulfonylthioate
NADH	nicotinamide adenine dinucleotide
NMR	nuclear magnetic resonance
NOE	nuclear Overhauser enhancement
ox	oxidized state
P450	cytochrome P450 (CYP)
P450cam	cytochrome P450cam (CYP101A1)
PCS	pseudocontact shift
PdR	putidaredoxin reductase
Pdx	putidaredoxin
PRE	paramagnetic relaxation enhancement
RDC	residual dipolar coupling
red	reduced state
TROSY	transverse relaxation optimized spectroscopy
WT	wild type
$\Delta\delta_{\text{avg}}$	average amide chemical shift
$\Delta\chi$ tensor	magnetic susceptibility tensor
$\Delta\chi_{\text{ax}}$	axial part of magnetic susceptibility tensor
$\Delta\chi_{\text{rh}}$	rhombic part of magnetic susceptibility tensor

CHAPTER 1

General introduction

P450 discovery and history

It was in 1954 in Philadelphia that Klingenberg discovered a novel carbon monoxide-binding pigment in rat liver microsomes.^[1] He added a trace of sodium dithionite and bubbled carbon monoxide while studying the kinetics of cytochrome b_5 in rat liver. Unexpectedly, he observed the appearance of a prominent absorption peak at 450 nm. This unique optical spectral change in the presence of carbon monoxide shared no resemblances with any other known metallo-proteins. In 1962, Omura repeated Klingenberg's experiments and named the mysterious "microsomal carbon monoxide-binding pigment" cytochrome P-450. "P" is the abbreviation of pigment and "450" was named after the unique optical absorption peak at 450 nm. In the first paper of "cytochrome P450", Omura reported that the carbon monoxide-binding pigment in liver microsomes was a novel hemoprotein. The molar extinction coefficient of characteristic 450 nm peak ($\epsilon_{450\text{nm}} = 91 \text{ mM}^{-1}\text{cm}^{-1}$) described in the paper is still widely used today to quantify the P450 content in biological samples.^[1]

P450 research soon expanded into various fields, from physiological functions to industrial chemistry. In the year following the first P450 paper, Estabrook, Cooper and Rosenthal reported that cytochrome P450 was involved in the biosynthesis of steroid hormones in bovine adrenal glands.^[2] They also found that P450 is an enzyme that catalyzes hydroxylation reactions of substrates using molecular oxygen. In 1965, P450 in rat liver microsomes was shown to participate in the oxidative metabolism of pharmaceutical compounds.^[3] At the end of 1960's, the presence of P450 was discovered in various tissues and organisms.^[4] Today, at least 57 different P450 genes are known in human beings;^[5] some of which are involved in the metabolism of sex hormones and others in the biosynthesis of cholesterol. Besides the unique absorption peak at 450 nm, P450 members share conserved amino acid sequences and a similar fold. In 1987, Nebert *et al.* coined the nomenclature of "CYP" to classify various P450 into families and sub-families based on primary sequences.^[6] The family tree generated by CYP classification indicated that all of the P450 in various organisms evolved from a single ancestral P450. Thus, P450 members are all part of the CYP superfamily.^[1]

Practical applications of P450

Nowadays, approximately two thousand papers on CYPs are published annually.^[1] One of the most useful features of P450 is regio- and stereo-specific hydroxylation. For instance, while chemical synthesis of drugs derived from vitamin D_3 requires 20 steps with low yield, P450 (CYP107) dependent conversion proceeds through a single step.^[4] At present several millions of patients are prescribed steroidal medicines, including cortisol and low density lipoprotein (LDL)-cholesterol lowering drugs. In 1952, a microbiologist called Murray published the first report of cortisol production in a single step by the use of the fungus *Curvulavria lunata*.^[7] The mycelium of this fungal species was later discovered to possess P450_{lun}, which converts 11-deoxycortisol to

cortisol.^[8] Even to date, industrial production of cortisol depends on the immobilized *C. lunata* and overexpression of P450_{11β} is attempted to increase the product yield.^[4] The invention of the “blue rose” is one of the most stunning applications of P450. Over the centuries, the creation of blue roses had been believed to be impossible due to the limitation of available colors of roses.^[4] However, in 2007, an industrial team in Japan has made the blue rose possible by introducing P450 gene (CYP75A) from *viola* (Figure 1).^[9]

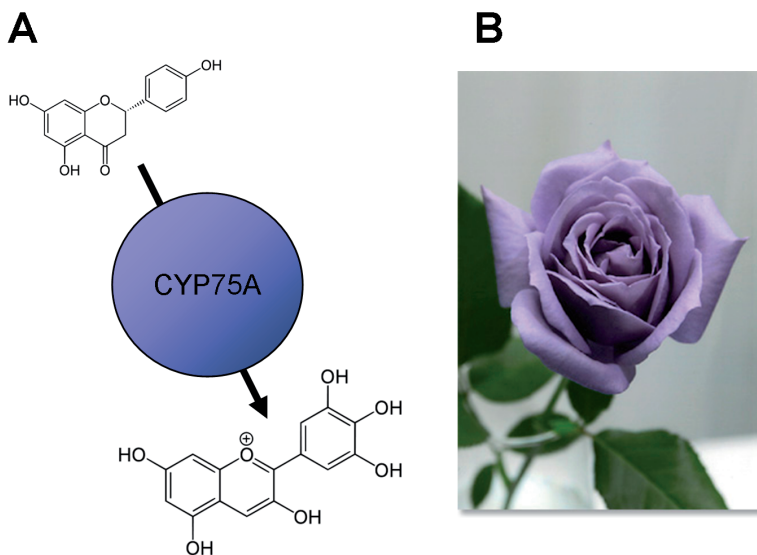


Figure 1. Production of blue roses by CYP75A. (A) CYP75A catalyzes the hydroxylation of flavanone to generate blue pigment, delphinidin. (B) Blue rose created by a Japanese company, Suntory. The picture was taken from www.suntory.com.

P450cam history

For over a decade after the initial discovery of rat liver microsomal P450, CYPs were believed to be present only in higher eukaryotes.^[1] However, in 1968, Katagiri *et al.* reported that an NADH-dependent P450 system was found in *Pseudomonas putida*.^[10] This bacterial P450 system consists of three soluble components, namely, an FAD-containing flavoprotein, an iron-sulfur containing ferredoxin and P450. Electrons are relayed from NADH to P450 to catalyze the hydroxylation of D-camphor. Due to its unique physiological substrate, *P. putida* P450 has been commonly known as P450cam. Moreover, the water solubility of P450cam advanced the P450 research and P450cam has become a model system of mammalian P450.^[1] In 1985, Poulos reported the first crystal structure of P450cam, which illustrates the unique coordination of a thiolate to a heme iron.^[11] The biophysical and biochemical analysis expanded and P450cam

has become the most extensively characterized P450 family member. By 2013, 109 different structures of P450cam had been deposited in protein data bank.

P450cam catalytic cycle

Hydroxylation of camphor is part of a metabolic process in *Pseudomonas putida* to harvest carbon and obtain energy. Utilizing an oxygen molecule, P450cam catalyzes regio- and stereo-specific hydroxylation of D-camphor and generates 5-exo-hydroxycamphor.^[10] As shown in Figure 2, the enzymatic activity of P450cam proceeds through the series of the catalytic events: i) substrate binding; ii) the first electron transfer (ET1); iii) oxygen binding; iv) the second electron transfer (ET2); v) proton transfer; vi) oxygen activation and hydroxylation reaction; vii) product release.

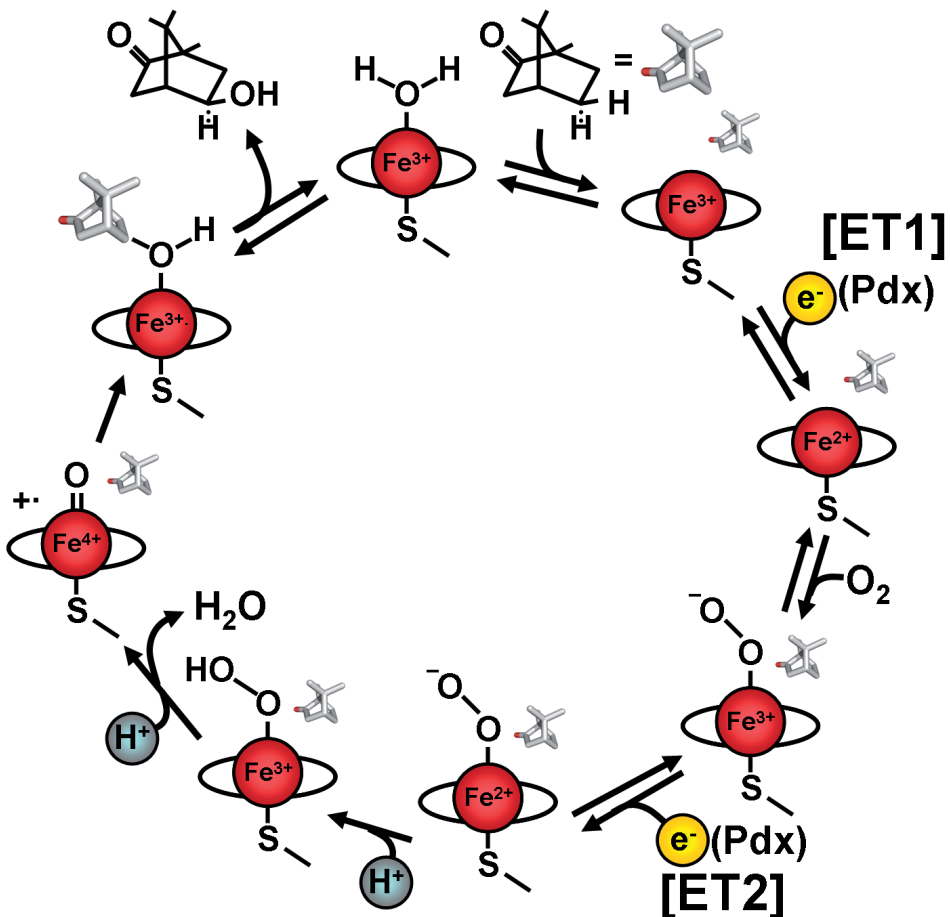


Figure 2. Catalytic cycle of P450cam.^[12]

In the resting state of P450cam, the heme iron is coordinated by a water molecule as the sixth ligand. The substrate-free form of P450cam has been shown to exhibit an "open" conformation to allow the substrate to access to the active site.^[13] The reaction cycle is initiated by binding of substrate, camphor. Camphor binding changes the spin state of heme iron from low spin to high spin. It was well documented that the transition of spin state is accompanied by the change of redox potential.^[11] In the resting state, the substrate-free form of P450cam exhibits a redox potential of -300 mV.^[14] However, upon binding of camphor, redox potential is elevated to -170 mV,^[14] which promotes the first ET event.^[11] The ferric state (Fe^{3+}) of P450cam accepts the first electron from the physiological ET partner protein, putidaredoxin (Pdx). Recent results of mutagenesis and kinetics studies suggested that this ET event is the rate-limiting step for catalytic turnover (41 s^{-1}).^[15] Upon binding of an oxygen molecule, the ferrous heme iron (Fe^{2+}) binds O_2 to form oxygenated P450cam.^[12] In the second ET event, Pdx has two roles; ET and effector activity. The binding of Pdx to oxygenated P450cam results in some structural change in the P450cam. This conformation shift facilitates the ET2 as well as enables the following events of the oxygen activation and product formation.^[16] The underlining mechanism of the Pdx effector activity is still under debate. However, the stringent requirement of Pdx for the ET2 process indicates that there is a drastic difference between ET1 and ET2.^[15] The second electron is delivered to the ferrous iron and activates the O-O bond. After the protonation of the activated oxygen molecule, the oxenoid-iron ($\text{Fe}^{4+}=\text{O}$), also known as compound I, is formed by displacement of a water molecule. The oxenoid-iron reacts with the camphor molecule to produce 5-*exo*-hydroxycamphor. The dissociation of the product from active site is accompanied by repositioning a water molecule as the axial ligand of the heme iron and reaction cycle in complete.^[12]

P450cam structural properties

P450cam consists of 414 amino acid residues with a molecular weight of 46.6 kDa. As an archetypical P450 enzyme, its type b heme iron is coordinated by an axial thiolate ligand of Cys357 (Figure 3).^[17]

The secondary structure elements of P450cam comprise thirteen α -helices and five β -sheets. The nomenclatures of the A–L helices and β 1–5 sheets are based on their order in the P450cam amino acid sequence (Figure 4). The B' helix has been added to the system by Poulos and co-workers after they found the additional α -helix in high-resolution crystal structure.^[19] The proximal and distal sides of P450cam have distinct functions. It has been reported that Pdx binds to the proximal side of P450cam while the distal side allows substrate access to the active site.

The unique appearance of the Soret band at 450 nm is attributed to the reduction of the heme iron and the concomitant binding of carbon monoxide.^[12] Besides CO and camphor, P450cam can accommodate a variety of compounds in the substrate

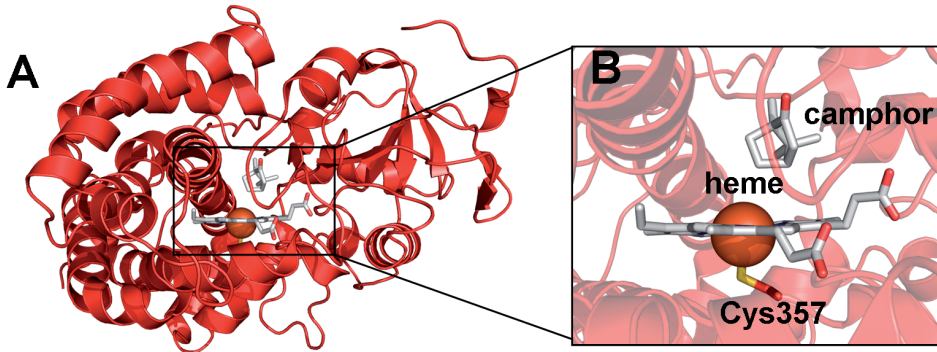


Figure 3. Crystal structure of P450cam bound to camphor (PDB entry, 1DZ4^[17]). (A) ribbon representation of P450cam. (B) Zoom in view of active site of P450cam. The brown sphere represents the heme iron.

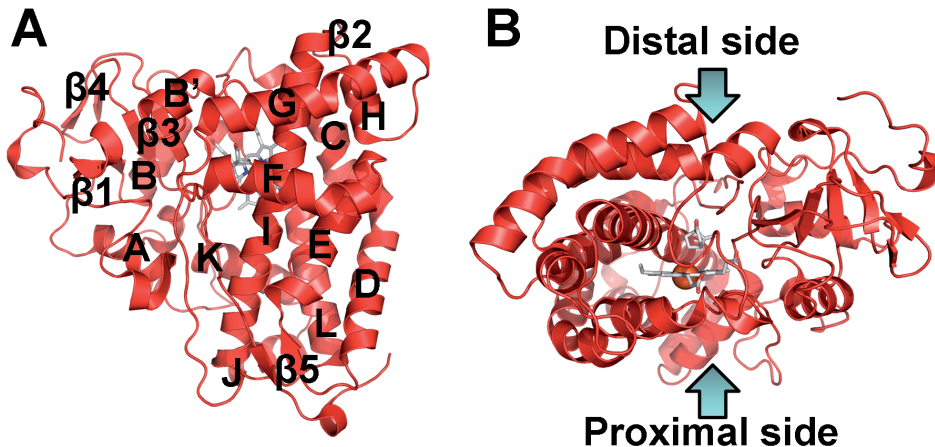


Figure 4. Ribbon representation of P450cam structures (PDB entry 1DZ4^[17]). (A) Nomenclature of the secondary structure elements of P450cam, facing the distal side (B) Arrows indicate the proximal and distal sides of the protein.

binding site. For instance, P450cam binds small molecules such as cyanide, imidazole, cysteine, DTT as well as substrate analogues such as adamantane-derivatives.^[12] The binding of these molecules influences the coordination sphere of the iron, which can result in transitions of the spin state of ferric iron between high and low.^[12] Although a number of ligands were known to interact with P450cam, the process of substrate binding had puzzled researchers for decades because atomic resolution structures of P450cam show that there is no channel present on the protein surface to allow a substrate to access the active site. In 2001, Dunn *et al.* demonstrated the opening of

substrate access channel of P450cam by crystallizing P450cam bound to ruthenium sensitizer-linked substrates (Figure 5).^[18] The adamantane moiety of the complex binds to the active site of P450cam and its ruthenium tethered linker protrudes toward the protein surface, thereby forcing the access channel to be in the open conformation. In 2010, Lee *et al.* solved the crystal structure of substrate-free form, which showed the location of the access channel beyond any doubts.^[13]

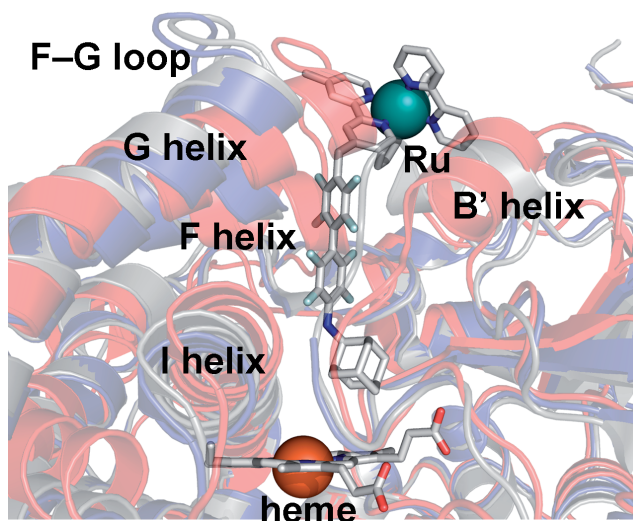


Figure 5. Cartoon representation of the overlaid P450cam structures. Red, gray and blue represent P450cam bound to camphor (PDB entry 1DZ4^[17]), ruthenium complex (1K2O^[18]) and substrate-free (3L61^[13]), respectively. The sticks chelating to the green sphere illustrate ruthenium sensitizer-linked substrate.

The helices B', F, G and I as well as the F-G loop have been found to be involved in the conformation change between the open and closed state of the substrate access channel.^[13, 18] It has been speculated that the synergistic movement of the B', F and G helices optimizes the efficiency of the substrate uptake as well as the catalytic reaction.^[13] The potassium ion binding site is another key feature of B' helix.^[19] It has been reported that the binding affinity of the substrate is dependent of the concentration of potassium ions. At a high concentration of potassium (> 50 mM), the stability of closed conformation increases, thereby decreasing the dissociation rate of the substrate.^[20, 21] Mutagenesis demonstrated that the I helix residues, Asp251 and Thr252, facilitate the proton transfer to the activated oxygen molecule in the active site.^[22] To further investigate the structure dynamics and the catalytic mechanism of P450cam, Pochapsky and co-workers studied the P450cam structure in solution state by NMR spectroscopy.^[23, 24] Their NMR results indicated that the active site of P450cam

is more mobile than previously described.^[24] In particular, significant dynamics was observed for the B' helix.^[23] It was speculated that the plasticity of the active site contributes to the ability of P450cam to accommodate a wide variety of substrates as well as inhibitors.

Putidaredoxin

Putidaredoxin (Pdx), a [2Fe-2S] cluster containing ferredoxin, acts as a physiological electron transfer partner of P450cam in *Pseudomonas putida*. It shuttles two electrons from putidaredoxin reductase to P450cam during the camphor hydroxylation reaction.^[25]

The redox center of Pdx consists of two iron atoms (Fe1 and Fe2), both of which are coordinated to the two sulfide ions as well as two thiol groups of the cysteine residues. Atom Fe1 is positioned in close proximity of the protein surface (Figure 6). Therefore, it is believed to play a major role in the electron transfer process.

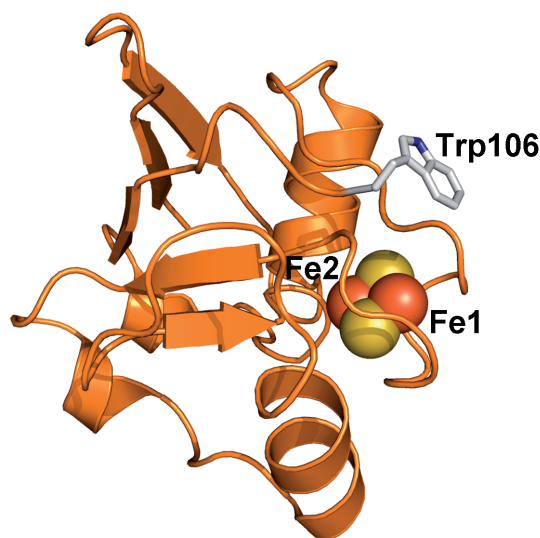


Figure 6. Ribbon representation of Pdx (PDB entry, 1XLP^[26]). Sticks and spheres illustrate the side chain of Trp106 and [2Fe-2S] cluster, respectively.

Over the decades, the [2Fe-2S] cluster of Pdx had hindered the structural studies of the protein. In NMR studies, vital information about the active site of the protein cannot be determined due to the significant broadening effect caused by high-spin state of iron atoms. Pochapsky and co-workers challenged the problem by replacing two irons by gallium ions.^[27] However, the substitution of the redox center leads to a structure change in Pdx. The crystallization of Pdx was also very challenging. At high concentrations of the protein, the progressive loss of the iron sulfur cluster from the

protein was observed. The identification of surface exposed cysteine residues led to a breakthrough in Pdx crystallization. Pdx contains six endogenous cysteine residues, four of which are the ligands for the two irons. It was found that the substitution of Cys73 and Cys85 greatly enhances the stability of the iron sulfur cluster.^[28] In 2003, Sevioukova *et al.* solved the crystal structures of Pdx C73S and Pdx C73S/C85S variants.^[28] With the exception of the residues in the active site, the structures obtained by X-ray crystallography and NMR were in good agreement. The structural analysis indicated that the oxidized state of Pdx exhibits more dynamic than the reduced state.^[26, 29] The regions nearby the [2Fe-2S] cluster (Tyr33, Asp34, His49 and Tyr51) as well as the C-terminus (Val74–Asn82 and Pro102–Trp106), in particular, were found to be mobile in the oxidized Pdx.^[29] These residues play key roles in the recognition of the partners PdR and P450cam.

Pdx comprises of 106 amino acid residues of which single tryptophan is present at the C-terminus. Despite the hydrophobic nature of the side chain, Trp106 of Pdx is fully exposed on protein surface and exhibits rotational freedom on the timescale of nanoseconds to sub-nanoseconds.^[29] Early mutagenesis studies demonstrated that Trp106 primarily functions as a recognition motif for the partners.^[30] The binding affinity and electron transfer rates dramatically reduced when Trp106 is either substituted or deleted from Pdx WT.^[15, 30] The most intriguing feature of Pdx function is the effector activity, in which Pdx binding induces a conformation change in P450cam to start the catalytic action of the camphor hydroxylation reaction.^[25] However, the underlying mechanism of the effector activity is poorly understood. Currently, two contradictory mechanisms have been proposed. According to Pochapsky and co-workers, Pdx acts as an effector by inducing a conformation change in oxy-P450cam.^[31] A structural change in the Pdx binding site mechanically transmits to remote regions of P450cam. The isomerization of Ile88–Pro89 amide bond has been reported to be the key feature of the conformation change.^[32] According to this study Pdx binding converts the *trans* conformer of the peptide bond into the *cis* conformer, which leads to the reorientation of the substrate in the active site as well as the closure of the substrate access channel. The substrate is thereby trapped in the active site of P450cam, which minimizes the solvation of the substrate and the escape of harmful peroxide intermediates.^[31, 33]

The recently determined crystal structure of Pdx-bound P450cam exhibits the open configuration and the substrate and/or product can freely access to the active site (structure details are discussed in the Chapter 3). Based on this observation, Poulos and co-workers proposed that the effector role of Pdx is to cause P450cam to open up the substrate access channel.^[34] Opening of the substrate access channel allows the catalytic water molecule to enter the active site. It was speculated that this water mediates the hydrogen bonded networks required for the proton transfer.^[34] Another key residue, Asp251, is freed from the salt bridge during the conformational shift to the open state. Together with the adjacent residue, Thr252, Asp251 plays a vital role in the proton transfer for O–O bond heterolysis.^[34] The opening is thought also to

cause a change in the iron spin state and such a spin state shift has been observed in a resonance Raman spectroscopy study.^[35] Champion and co-workers reported that Pdx binding produces a low spin state of heme iron, reflecting the open conformation of P450cam.^[35] A recent study using double electron-electron resonance (DEER) spectroscopy indicated that the conformation change of P450cam is dependent on the oxidation states of Pdx.^[21] In line with the suggestions of the previous studies, the authors report that binding of oxidized state of Pdx induces P450cam to be in open conformation. However, reduced and CO-bound P450cam remains in the closed conformation in the complex with the reduced state of Pdx.^[21] Thus, not all studies paint a consistent picture of the mechanism of the effector function of Pdx binding. This phenomenon remains to be elucidated.

Putidaredoxin reductase

Putidaredoxin reductase (PdR) is an FAD-containing flavoprotein (Figure 7). To reduce an oxygen molecule, P450cam requires two electrons. PdR transfers two electrons from NADH to Pdx which in turn shuttles them to P450cam. PdR consists of 421 amino acid residues and possesses FAD and NAD binding domains.^[25]

The interaction of PdR with Pdx is often compared with the complex formation of adrenodoxin reductase (AdR) and adrenodoxin (Adx), which are the homologue of

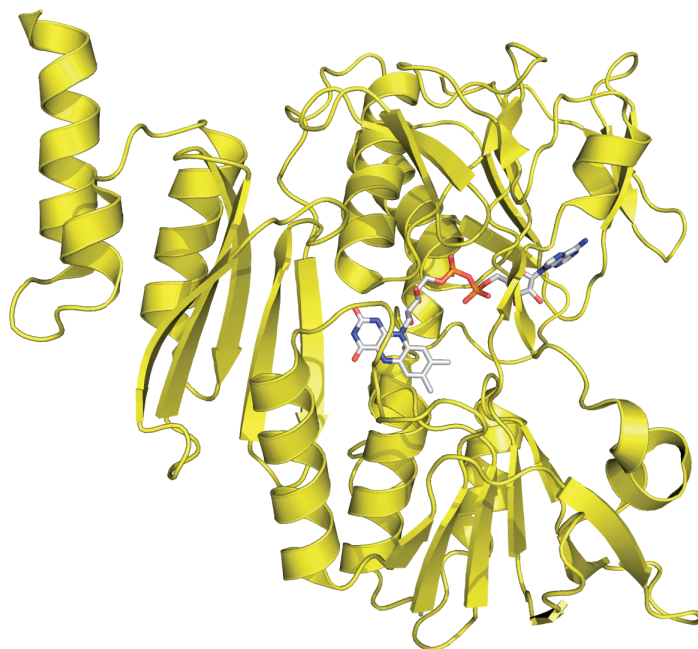


Figure 7. Ribbon representation of PdR (PDB entry, 1Q1R^[36]). FAD is shown in sticks.

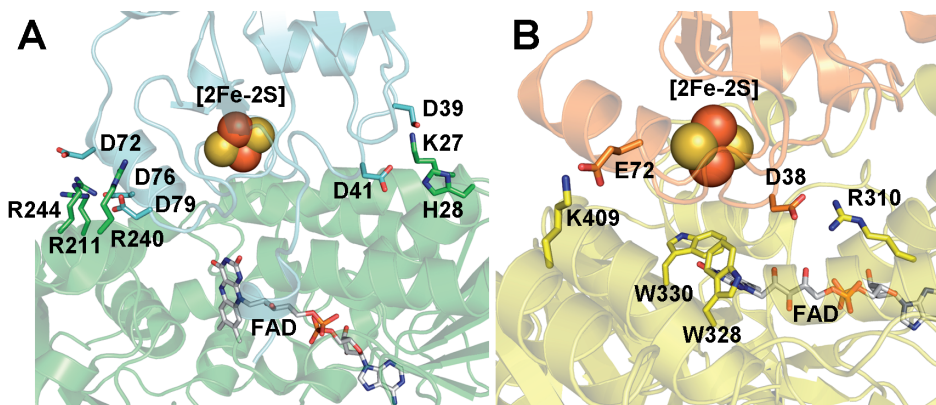


Figure 8. Cartoon representation of AdR-Adx and PdR-Pdx complexes. Sticks represent the side chains of the interaction residues and FAD. (A) Green and light blue represent AdR and Adx, respectively (PDB entry 1E6E^[37]). (B) Yellow and orange represent PdR and Pdx, respectively (PDB entry 1Q1R^[36]).

human proteins. The crystal structures of PdR-Pdx and AdR-Adx complexes highlighted the difference of binding modes in two systems (Figure 8).^[25] The interaction of AdR-Adx complex is primarily driven by electrostatic interactions. The acidic patches on the Adx surface interact with the basic concave FAD-binding site of AdR.

PdR-Pdx binding, on the other hand, primarily involves hydrophobic contacts and polar interactions. Trp328 and Trp330 of PdR are key components of the complex formation and part of the electron transfer pathway between PdR and Pdx. The experimentally obtained ET rate from PdR to Pdx is 235 s^{-1} while theoretical maximal ET rate is estimated to be $2.7 \times 10^5 \text{ s}^{-1}$. The difference of three orders of magnitude has been attributed to the reorganization energy of Pdx reduction.^[25]

Protein-protein interactions

During protein complex formation, the proteins undergo at least an intermediate step (illustrated in Figure 9).^[38] First, the proteins form an encounter complex in which one protein searches for the docking surface of the other and then the well-defined, final complex is formed. It has been speculated that the long-range electrostatic interaction drives the transient state of protein-protein interaction.^[39-41] However, the recent results of paramagnetic NMR analysis suggested that hydrophobic interactions also play an important role.^[42, 43] The primary role of the encounter state is to minimize the dimensionality search of optimal binding, and thus to enhance the number of productive collisions. In classic textbooks, the dynamic encounter state is assumed to exist only transiently and to rapidly form the final well-defined complex. However, the latest NMR spectroscopy data have indicated that the encounter complex represents a significant population in weak protein-protein complexes (e.g. electron transfer

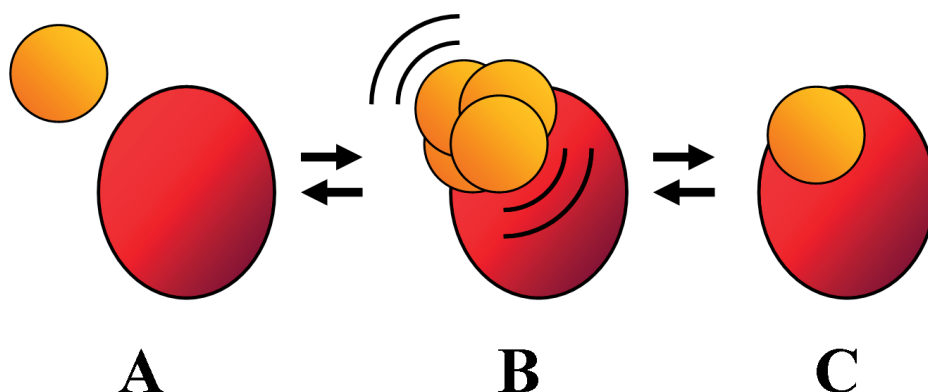


Figure 9. Model of transient protein complex formation. A) Two proteins come close together by diffusion. B) The encounter complex: proteins sample each other's surface in multiple orientations. C) A single, well-defined complex is formed.

protein complexes).^[38, 44] Kinetic data analysis also suggested that some proteins achieve electron-transfer active states in the encounter complex rather than in a single well-defined complex.^[39, 40, 45-48]

Paramagnetic NMR probes

A variety of paramagnetic NMR techniques have been rapidly developed in the last few decades. They enable protein chemists to analyze not only structural information of protein interfaces but also kinetics, binding affinity and transient intermediates of protein interactions.^[49, 50] The presence of unpaired electrons causes paramagnetic effects in NMR spectra, which includes "line broadening" and "line shifts". Line broadening is the consequence of enhanced relaxation by unpaired electrons. Since the effect is proportional to the sixth power of distance between the electrons and observed nuclei, it has been used as a sensitive tool of distance measurement in proteins.^[51] Line shifts in NMR spectra can be categorized as contact shifts and pseudocontact shifts. Contact shifts are caused by the delocalization of unpaired electrons onto observed nuclei and can be observed only up to several bonds away from the paramagnetic center. Pseudocontact shifts (PCS) result from dipolar interactions between the electron(s) and nuclei. The magnitude of a pseudocontact shift depends on the anisotropy of the magnetic susceptibility described by the $\Delta\chi$ tensors and is proportional to the third power of the distance between electron and nucleus.^[51] Strongly paramagnetic metal ions can possess a large $\Delta\chi$ tensor, enabling the observation of pseudocontact shifts for nuclei far from the unpaired electron.^[52] Pseudocontact shifts, thereby, provide restraints to refine structures of macromolecules.^[50]

Lanthanoid ions (Ln^{3+}) are known to be excellent paramagnetic groups that possess unpaired electrons in the 4f orbitals. Different lanthanoids share similar ionic radii and geometries but exhibit a broad range of magnitudes of paramagnetic effects. For instance, lanthanum (La^{3+}) and lutetium (Lu^{3+}) ions are diamagnetic whereas dysprosium (Dy^{3+}), thulium (Tm^{3+}) and ytterbium (Yb^{3+}) ions are strongly paramagnetic.^[52, 53] Therefore, lanthanoid ions are widely used for paramagnetic NMR studies.

The lanthanoid tags offer several distinctive advantages over conventional bivalent ion (Mn^{2+} , Co^{2+} etc.) probes. First of all, the substitution of different lanthanoid ions allows for a wide range of paramagnetic effects, providing a number of $\Delta\chi$ tensor values with the same probe. Secondly, some lanthanoids possessing a high anisotropy magnetic tensor are able to align slightly to the external magnetic field. Therefore, those lanthanoid-labeled proteins and protein complexes achieve partial molecular alignments in the absence of alignment media. Residual dipolar couplings can be therefore measured under the same conditions between unaligned sample and partially aligned sample. Since the alignment induced by a paramagnetic ion will not be limited by molecular size, lanthanoid tags are an attractive tool for RDC measurements in macromolecules as well as in the study of intermolecular interactions.^[54]

Many kinds of lanthanoid tags have been published over recent years, including protein fusions with lanthanoid-binding peptides^[55, 56] as well as lanthanoid-binding peptide that are attached via a disulfide bond.^[57] Caged lanthanoid NMR probe version 7, CLaNP-7, is a synthetic lanthanoid chelating molecule developed for the

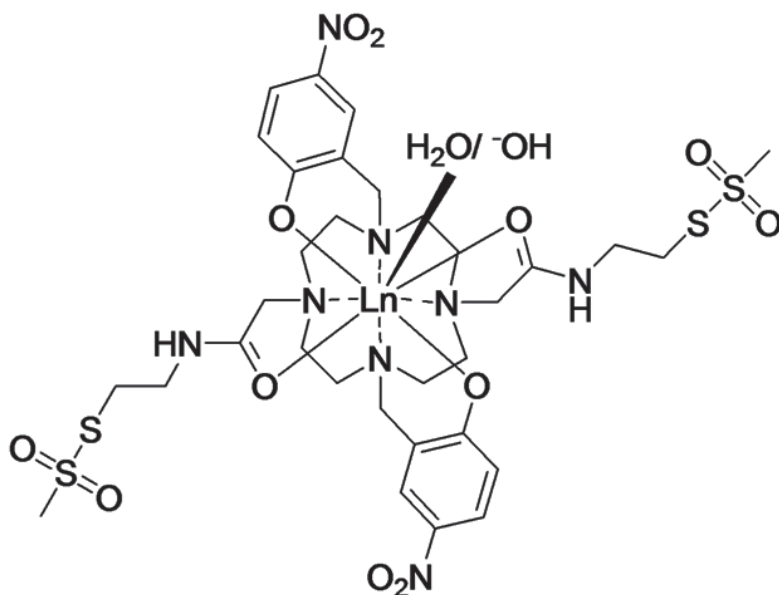


Figure 10. Caged lanthanoid NMR probe version 7, CLaNP-7.

attachment of lanthanoid atoms on protein surfaces (Figure 10).^[58] It has been designed to fulfill the following criteria: i) the probe is capable of accommodating different lanthanoid atoms, allowing to observe a range of paramagnetic effects; ii) two thiol “arms” of the probe covalently binds to two cysteine residues on a protein surface. The “two-point attachment” restricts the flexibility of the probe movement, preventing averaging effects. The resonance averaging effect becomes detrimental when the magnitudes of the paramagnetic effects are strongly dependent on the distance between paramagnetic center and observed nuclei. It also reduces the degree of residual dipolar coupling (RDC) when the probe is used to induce partial alignment in a magnetic field.^[59] With Tm^{3+} as a paramagnetic ion, CLaNP-7 showed PCS for nuclei as far as 60 Å distance from the lanthanoid. Tm^{3+} loaded CLaNP-7 induces RDC of about 20 Hz at 14 T (600 MHz) magnetic field strength.^[58] Furthermore, paramagnetic relaxation enhancement caused by the gadolinium ion (Gd^{3+}) contained in CLaNP-7 is also a useful tool for macromolecular structure determination, with distances up to 45 Å measured accurately (Chapter 3).^[60]

Pseudocontact shift

Pseudocontact shifts (PCSs) provide long-range distance restraints (in the range of 10–60 Å) as well as relative orientations on the basis of the anisotropy of the magnetic susceptibility of paramagnetic metals.^[61] PCSs offer opportunities to determine structures of proteins and protein-protein complexes. The PCS results from the dipolar coupling between the time averaged magnetic moment of the unpaired electron(s) of lanthanoid ion (Ln^{3+}) and that of a given nucleus. Figure 11 illustrates the $\Delta\chi$ tensor of Ln^{3+} -CLaNP-7 on a given protein surface.

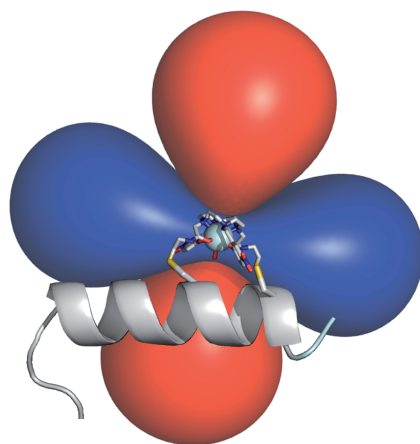


Figure 11. Cartoon representation of anisotropy of magnetic susceptibility of Yb^{3+} -CLaNP-7. Sticks and ribbon show a model of CLaNP-7 on α -helix of a protein. Blue and red isosurfaces represent a nucleus with a PCS of a -1 and $+1$ ppm, respectively.

PCS can be described by the following equation:

$$\text{PCS} = \frac{1}{12\pi r^3} \left[\Delta\chi_{\text{ax}} (3\cos^2\theta - 1) + \frac{3}{2} \Delta\chi_{\text{rh}} (\sin^2\theta \cos 2\Omega) \right]$$

where θ and Ω are angles of position vectors of a given nucleus with respect to the reference frame of magnetic susceptibility tensor. r represents the distance between the unpaired electron of Ln^{3+} and a given nucleus (Figure 12).^[61] The magnitude of the PCS is proportional to the inverse third power of the distance, which allows for obtaining long-range distance information compared to relaxation, which scales with r^6 . The anisotropy of magnetic susceptibility is described by axial ($\Delta\chi_{\text{ax}}$) and rhombic ($\Delta\chi_{\text{rh}}$) components.

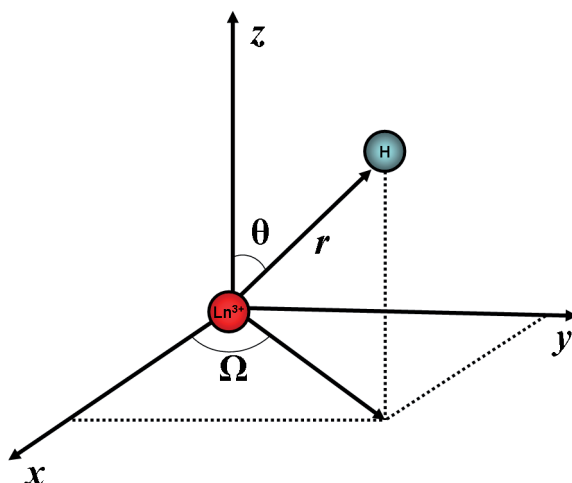


Figure 12. Coordinate system describing PCS. Red and blue spheres represent a paramagnetic metal and an observed nucleus, respectively.

Residual dipolar coupling

Residual dipolar couplings (RDCs) were initially recognized as a useful NMR tool to provide distance independent orientation restraints for structure refinement. Nowadays, the application of RDC has been expanded to structure determination of protein-protein complexes.^[61] RDC also offers valuable information about dynamics in proteins and protein-protein interactions.^[62]

The RDC can be detected when tumbling of proteins is not completely isotropic but partially aligned with the external magnetic field. This is often achieved by addition of external alignment media to protein samples. Alternatively, paramagnetic metals, either natural present^[63] or artificially introduced, to the protein of interest.^[61] Partial

alignment of biomolecules leads to incomplete averaging of dipole-dipole interaction between two spins. The resulting residual dipolar couplings provide information about the orientation of the protein relative to the external magnetic field.^[61]

Paramagnetic relaxation enhancement

Paramagnetic relaxation enhancement (PRE) was originally considered to be deleterious or at least a nuisance effect when metalloenzymes were investigated by NMR spectroscopy. Essential information about the active site was lost due to the fact that resonances of nuclei close to the metal were broadened out beyond detection. PRE arises from the dipole-dipole interactions of an unpaired electron in the paramagnetic center with nuclei in the proximity. PRE effect is dependent on the inverse sixth power of distance between an unpaired electron and a given nucleus.^[44, 64] In comparison with the NOE effect, which yields measurable distances up to 6 Å, PRE causes effects over distances up to 20 Å and in some cases even up to 45 Å.^[60, 64] The deleterious effect of line broadening by PRE was soon turned into a useful tool for NMR experiments. By artificially introducing an unpaired electron in a paramagnetic center into protein samples, PRE can be used as a molecular ruler, due to the strong distance dependency.^[44] PRE is also extremely sensitive to lowly populated states of protein conformations and protein complexes.^[64-67] Nowadays, PRE is the most common paramagnetic NMR experiment to determine distance restraints for structure determination of proteins and transient protein-protein complexes.^[44, 61]

Thesis outline

At the start of this research in 2009, a model of Pdx-P450cam complex was available.^[68] This model was generated on the basis of a series of NMR data and showed good correlations with earlier mutagenesis results. To test the validity of this model and further characterize the dynamics of Pdx-P450cam interaction, we decided to carry out paramagnetic NMR analysis. In Chapter 2, the attachment of a paramagnetic NMR probe, CLaNP-7, is evaluated at multiple sites of Pdx and P450cam. The $\Delta\chi$ tensors of Ln^{3+} -CLaNP-7 were experimentally determined by PCS analysis. These results form the prelude for the intermolecular paramagnetic NMR experiments to study the Pdx-P450cam complex discussed in Chapter 3. To calculate the structure of the Pdx-P450cam complex, 446 inter-protein distance and orientation restraints were used on the basis of the PCS, RDC and PRE experiments. After the structure had been determined by paramagnetic NMR analysis, our collaborator, Dr. Nojiri and co-workers in Osaka University (Japan) solved the crystal structure of the complex at a resolution of 2.5 Å. The crystal structure is identical to the solution structure within the variation of the ensemble. Compared with the previous model, the orientation of Pdx is rotated by 90° perpendicular to the axis of P450cam heme. The structural analysis of the binding interface revealed potential ET transfer pathways and important interactions between

Pdx Asp38 and P450cam Arg112 as well as hydrophobic contacts between Trp106 and P450cam Ala113. Moreover, several polar residues are found in the interface that had not been recognized to be relevant for binding before. In Chapter 4, site-directed mutagenesis and kinetic measurements were employed to probe the energetic importance and role of the polar residues in the Pdx-P450cam interaction. The results of the paramagnetic NMR analysis used for the structure calculations of the complex suggested the presence of an encounter state in the Pdx-P450cam complex. To characterize this lowly populated state, Gd³⁺ loaded CLaNP-7 as well as an MTSL spin labels were attached at six different positions on Pdx and P450cam surfaces and inter-protein PRE analysis was performed (Chapter 5). Dynamics in the P450cam enzyme is observed not only for the protein-protein interaction but also for the substrate binding process. Most of the crystal structures of P450cam exhibit a closed conformation in which there is no channel large enough for substrate to access the active site. In Chapter 6, using paramagnetic substrate analogues, the substrate access channel of P450cam was investigated by X-ray crystallography and paramagnetic NMR analysis. Finally, in the concluding remarks, the results from these chapters are discussed in relation to recent studies of the effector role of Pdx in the P450cam catalytic system.

References

1. T. Omura *Proc Jpn Acad Ser B Phys Biol Sci.* **2011**, *87*, 617-640.
2. R. W. Estabrook, D. Y. Cooper, O. Rosenthal *Biochem Z.* **1963**, *338*, 741-755.
3. D. Y. Cooper, S. Levin, S. Narasimhulu, O. Rosenthal *Science.* **1965**, *147*, 400-402.
4. T. Sakaki *Biol Pharm Bull.* **2012**, *35*, 844-849.
5. D. R. Nelson, D. C. Zeldin, S. M. Hoffman, L. J. Maltais, H. M. Wain, D. W. Nebert *Pharmacogenetics.* **2004**, *14*, 1-18.
6. D. W. Nebert, M. Adesnik, M. J. Coon, R. W. Estabrook, F. J. Gonzalez, F. P. Guengerich, I. C. Gunsalus, E. F. Johnson, B. Kemper, W. Levin, et al. *DNA.* **1987**, *6*, 1-11.
7. D. H. Peterson, H. C. Murray *J Am Chem Soc.* **1952**, *74*, 1871-1872.
8. S. B. Mahato, S. Garai *Steroids.* **1997**, *62*, 332-345.
9. Y. Katsumoto, M. Fukuchi-Mizutani, Y. Fukui, F. Brugliera, T. A. Holton, M. Karan, N. Nakamura, K. Yonekura-Sakakibara, J. Togami, A. Pigeaire, G. Q. Tao, N. S. Nehra, C. Y. Lu, B. K. Dyson, S. Tsuda, T. Ashikari, T. Kusumi, J. G. Mason, Y. Tanaka *Plant Cell Physiol.* **2007**, *48*, 1589-1600.
10. M. Katagiri, B. N. Ganguli, I. C. Gunsalus *J Biol Chem.* **1968**, *243*, 3543-3546.
11. T. L. Poulos, B. C. Finzel, I. C. Gunsalus, G. C. Wagner, J. Kraut *J Biol Chem.* **1985**, *260*, 16122-16130.
12. O. Pylypenko, I. Schlichting *Annu Rev Biochem.* **2004**, *73*, 991-1018.
13. Y. T. Lee, R. F. Wilson, I. Rupniewski, D. B. Goodin *Biochemistry.* **2010**, *49*, 3412-3419.
14. S. G. Sligar, I. C. Gunsalus *Proc Natl Acad Sci U S A.* **1976**, *73*, 1078-1082.
15. V. Y. Kuznetsov, T. L. Poulos, I. F. Sevrioukova *Biochemistry.* **2006**, *45*, 11934-11944.
16. I. F. Sevrioukova, T. L. Poulos *Arch Biochem Biophys.* **2011**, *507*, 66-74.
17. I. Schlichting, J. Berendzen, K. Chu, A. M. Stock, S. A. Maves, D. E. Benson, R. M. Sweet, D. Ringe, G. A. Petsko, S. G. Sligar *Science.* **2000**, *287*, 1615-1622.
18. A. R. Dunn, I. J. Dmochowski, A. M. Bilwes, H. B. Gray, B. R. Crane *Proc Natl Acad Sci U S A.* **2001**, *98*, 12420-12425.
19. T. L. Poulos *Biochem Bioph Res Co.* **2003**, *312*, 35-39.

20. B. OuYang, S. S. Pochapsky, G. M. Pagani, T. C. Pochapsky *Biochemistry*. **2006**, *45*, 14379-14388.
21. W. K. Myers, Y. T. Lee, R. D. Britt, D. B. Goodin *J Am Chem Soc*. **2013**, *135*, 11732-11735.
22. S. Nagano, T. L. Poulos *J Biol Chem*. **2005**, *280*, 31659-31663.
23. E. K. Ascitutto, M. Dang, S. S. Pochapsky, J. D. Madura, T. C. Pochapsky *Biochemistry*. **2011**, *50*, 1664-1671.
24. E. K. Ascitutto, M. J. Young, J. Madura, S. S. Pochapsky, T. C. Pochapsky *Biochemistry*. **2012**, *51*, 3383-3393.
25. I. F. Sevrioukova, T. L. Poulos *J Biol Chem*. **2012**, *287*, 3510-3517.
26. I. F. Sevrioukova *J Mol Biol*. **2005**, *347*, 607-621.
27. T. C. Pochapsky, M. Kuti, S. Kazanis *J Biomol NMR*. **1998**, *12*, 407-415.
28. I. F. Sevrioukova, C. Garcia, H. Li, B. Bhaskar, T. L. Poulos *J Mol Biol*. **2003**, *333*, 377-392.
29. N. Sari, M. J. Holden, M. P. Mayhew, V. L. Vilker, B. Coxon *Biochemistry*. **1999**, *38*, 9862-9871.
30. S. G. Sligar, P. G. Debrunner, J. D. Lipscomb, M. J. Namtvedt, I. C. Gunsalus *Proc Natl Acad Sci U S A*. **1974**, *71*, 3906-3910.
31. E. K. Ascitutto, J. D. Madura, S. S. Pochapsky, B. OuYang, T. C. Pochapsky *J Mol Biol*. **2009**, *388*, 801-814.
32. B. OuYang, S. S. Pochapsky, M. Dang, T. C. Pochapsky *Structure*. **2008**, *16*, 916-923.
33. L. Rui, S. S. Pochapsky, T. C. Pochapsky *Biochemistry*. **2006**, *45*, 3887-3897.
34. S. Tripathi, H. Li, T. L. Poulos *Science*. **2013**, *340*, 1227-1230.
35. M. Unno, J. F. Christian, D. E. Benson, N. C. Gerber, S. G. Sligar, P. M. Champion *J Am Chem Soc*. **1997**, *119*, 6614-6620.
36. I. F. Sevrioukova, H. Li, T. L. Poulos *J Mol Biol*. **2004**, *336*, 889-902.
37. J. J. Muller, A. Lapko, G. Bourenkov, K. Ruckpaul, U. Heinemann *J Biol Chem*. **2001**, *276*, 2786-2789.
38. J. Schilder, M. Ubbink *Curr Opin Struct Biol*. **2013**, *23*, 911-918.
39. Z. X. Liang, I. V. Kurnikov, J. M. Nocek, A. G. Mauk, D. N. Beratan, B. M. Hoffman *J Am Chem Soc*. **2004**, *126*, 2785-2798.
40. Z. X. Liang, J. M. Nocek, K. Huang, R. T. Hayes, I. V. Kurnikov, D. N. Beratan, B. M. Hoffman *J Am Chem Soc*. **2002**, *124*, 6849-6859.
41. Q. Bashir, A. N. Volkov, G. M. Ullmann, M. Ubbink *J Am Chem Soc*. **2010**, *132*, 241-247.
42. Y. C. Kim, C. Tang, G. M. Clore, G. Hummer *Proc Natl Acad Sci U S A*. **2008**, *105*, 12855-12860.
43. S. Scanu, J. M. Foerster, G. M. Ullmann, M. Ubbink *J Am Chem Soc*. **2013**, *135*, 7681-7692.
44. M. Ubbink *Febs Lett*. **2009**, *583*, 1060-1066.
45. X. Xu, W. Reinle, F. Hannemann, P. V. Konarev, D. I. Svergun, R. Bernhardt, M. Ubbink *J Am Chem Soc*. **2008**, *130*, 6395-6403.
46. Z. X. Liang, M. Jiang, Q. Ning, B. M. Hoffman *J Biol Inorg Chem*. **2002**, *7*, 580-588.
47. K. E. Wheeler, J. M. Nocek, D. A. Cull, L. A. Yatsunyk, A. C. Rosenzweig, B. M. Hoffman *J Am Chem Soc*. **2007**, *129*, 3906-3917.
48. B. M. Hoffman, L. M. Celis, D. A. Cull, A. D. Patel, J. L. Seifert, K. E. Wheeler, J. Wang, J. Yao, I. V. Kurnikov, J. M. Nocek *Proc Natl Acad Sci U S A*. **2005**, *102*, 3564-3569.
49. L. B. Banci, I.; Eltis, L. D.; Felli, I. C.; Kastrau, D. H.; Luchinat, C.; Piccioli, M.; Pierattelli, R.; Smith, M. *Eur J Biochem*. **1994**, *225*, 715-725.
50. I. D. Bertini, A.; Jimenez, B.; Luchinat, C.; Parigi, G.; Piccioli, M.; Poggi, L. *J Biomol NMR*. **2001**, *21*, 85-98.
51. I. L. Bertini, C.; Parigi, G. *Elsevier, Amsterdam*. **2001**.
52. I. Bertini, M. B. Janik, Y. M. Lee, C. Luchinat, A. Rosato *J Am Chem Soc*. **2001**, *123*, 4181-4188.
53. R. Barbieri, I. Bertini, G. Cavallaro, Y. M. Lee, C. Luchinat, A. Rosato *J Am Chem Soc*. **2002**, *124*, 5581-5587.
54. X. C. Su, K. McAndrew, T. Huber, G. Otting *J Am Chem Soc*. **2008**, *130*, 1681-1687.
55. L. J. Martin, M. J. Hahnke, M. Nitz, J. Wohnert, N. R. Silvggi, K. N. Allen, H.

- Schwalbe, B. Imperiali *J Am Chem Soc.* **2007**, *129*, 7106-7113.
56. C. O. Ma, S. J. *J Magn Reson.* **2000**, *146*, 381-384.
57. X. C. Su, T. Huber, N. E. Dixon, G. Otting *Chembiochem.* **2006**, *7*, 1599-1604.
58. W. M. Liu, P. H. Keizers, M. A. Hass, A. Blok, M. Timmer, A. J. Sarris, M. Overhand, M. Ubbink *J Am Chem Soc.* **2012**, *134*, 17306-17313.
59. M. Prudencio, J. Rohovec, J. A. Peters, E. Tocheva, M. J. Boulanger, M. E. Murphy, H. J. Hupkes, W. Kusters, A. Impagliazzo, M. Ubbink *Chem Eur J.* **2004**, *10*, 3252-3260.
60. Y. Hiruma, M. A. Hass, Y. Kikui, W. M. Liu, B. Olmez, S. P. Skinner, A. Blok, A. Kloosterman, H. Koteishi, F. Lohr, H. Schwalbe, M. Nojiri, M. Ubbink *J Mol Biol.* **2013**, *425*, 4353-4365.
61. P. H. Keizers, M. Ubbink *Prog Nucl Magn Reson Spectrosc.* **2011**, *58*, 88-96.
62. J. R. Tolman, K. Ruan *Chem Rev.* **2006**, *106*, 1720-1736.
63. J. R. Tolman, J. M. Flanagan, M. A. Kennedy, J. H. Prestegard *Proc Natl Acad Sci U S A.* **1995**, *92*, 9279-9283.
64. Q. Bashir, S. Scanu, M. Ubbink *Febs J.* **2011**, *278*, 1391-1400.
65. G. M. Clore, J. Iwahara *Chem Rev.* **2009**, *109*, 4108-4139.
66. C. Tang, J. Iwahara, G. M. Clore *Nature.* **2006**, *444*, 383-386.
67. J. Y. Suh, C. Tang, G. M. Clore *J Am Chem Soc.* **2007**, *129*, 12954-12955.
68. W. Zhang, S. S. Pochapsky, T. C. Pochapsky, N. U. Jain *J Mol Biol.* **2008**, *384*, 349-363.

CHAPTER 2

Validation and characterization of lanthanoid tags for P450cam by paramagnetic NMR spectroscopy

Part of this chapter was published as Hiruma, Y.; Hass, M.A.; Kikui, Y.; Liu, W.M.; Olmez, B.; Skinner, S.P.; Blok, A.; Kloosterman, A.; Koteishi, H.; Löhr, F.; Schwalbe, H.; Nojiri, M.; Ubbink, M. (2013) The Structure of the Cytochrome P450cam-Putidaredoxin Complex Determined by Paramagnetic NMR Spectroscopy and Crystallography, *J Mol Biol* 425, 4353–4365.

Abstract

Paramagnetic NMR techniques have opened up new possibilities to obtain molecular details of large proteins and/or protein complexes. With the use of lanthanoid (Ln^{3+}) tags, structural information can be retrieved from simple 2D TROSY/HSQC experiments. Recently, Liu *et al.* developed a novel Ln^{3+} probe, CLaNP-7, which has been shown to provide valuable paramagnetic NMR effects on proteins. In this study, CLaNP-7 was applied to two proteins, cytochrome P450cam (P450cam) and its electron transfer partner protein, putidaredoxin (Pdx) to determine the structure of their complex in solution. The tag was attached at multiple sites to find the best positions for this purpose. The size and orientation of $\Delta\chi$ tensors of Ln^{3+} -CLaNP-7 and the metal positions were experimentally determined by pseudocontact shift (PCS) analysis. Moreover, using the distance restraints derived from PCSs, the conformational change of P450cam was examined upon binding of Pdx. In contrast to the recent report by Tripathi *et al.*, the distinct conformational shift of P450cam from closed to open state was not detected. These results thus form the prelude parameters for the intermolecular paramagnetic NMR experiments to study Pdx-P450cam complex discussed in chapter 3. At the same time the work gives insight in the efficiency of lanthanoid tagging as a means for structure determination.

Introduction

Recent paramagnetic NMR techniques have advanced the possibilities for structure determination of protein complexes in solution.^[1] By attaching artificially synthesized lanthanoid tags to protein surfaces, long-range distance information can be retrieved from simple NMR experiments,^[2] which is radically different from conventional nuclear Overhauser experiments. Moreover, by utilizing different lanthanoid ions, either pseudocontact shift (PCS) or paramagnetic relaxation enhancement (PRE) can be measured.^[2] A prerequisite for reliable paramagnetic NMR experiments is the use of a rigid lanthanoid tag. The paramagnetic tag used in this work is a caged lanthanoid NMR probe (CLaNP), version 7,^[3] which binds covalently to two Cys residues that are in close proximity. The two-point attachment of CLaNP-7 ensures a low mobility of the probe on the protein surface, and minimal averaging of the paramagnetic effects.^[3-4] In this study, a series of double Cys mutants of Pdx and P450cam were produced. The attachment of CLaNP-7 was validated by assessing the intramolecular paramagnetic NMR effects, which is illustrated in Figure 1.

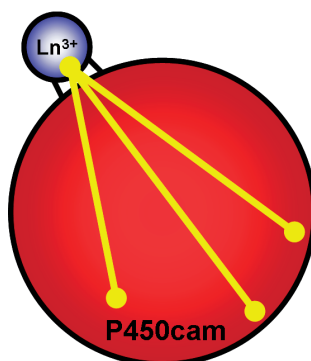


Figure 1. Schematic representation of the intramolecular PCS analysis used in this study. Ln^{3+} -CLaNP-7 was linked to isotopically labeled proteins. The observed PCS is dependent on the orientation of the $\Delta\chi$ tensor and the distance between Ln^{3+} and the given nuclei.

[^{15}N] labeled proteins were tagged with CLaNP-7 and PCS of amide protons were measured. To allow for comparison with previously reported magnetic susceptibility anisotropy tensors ($\Delta\chi$ tensor),^[3] ytterbium (Yb^{3+}) and thulium (Tm^{3+}) were used in this study. The orientations and anisotropy of the $\Delta\chi$ tensor of a series of CLaNP-7 labeled Pdx and P450cam mutants were determined. Assessment of intramolecular PCS provides not only validation of the probe attachment, but also the fraction of the protein that is labeled with a probe. It can be also used to calculate the position of Ln^{3+} ion, which is essential for the interpretation of intermolecular paramagnetic NMR experiments (chapter 3). In addition, the PCSs from paramagnetic tags at

multiple locations helped the NMR assignment of P450cam amide groups. Finally, the intramolecular PCS experiments were used to obtain information on the conformational change in P450cam upon binding of Pdx. In contrast to the recently proposed model of Pdx effector activity,^[5] the result of PCS analysis indicates that P450cam does not undergo significant conformation change upon the binding of Pdx.

Results

Protein production

Most pairs of surface exposed cysteine residues were introduced at the proximal region of P450cam where Pdx has been reported to interact with P450cam.^[6] Nevertheless, a control mutant was also created at the distal region of P450cam, E195C/A199C/C334A (mutant D). The locations of the tag in Pdx were selected close to the proposed Pdx-P450cam binding interface. To avoid interference, exposed Cys residues at positions 334 on P450cam and positions 73 and 85 on Pdx were substituted. These substitutions have been used in other studies.^[7-8] Other Cys residues are present in both proteins, some of which are partially exposed on the protein surfaces. However, the results of size-exclusion chromatography and mass spectrometry analysis indicated that these were found neither to induce oligomerization nor interfere with the tagging. The P450cam and Pdx constructs are summarized in the Table 1.

Out of twelve P450cam constructs, six P450cam mutants (A–F) were over-expressed and purified. The average protein yields of these variants exceeded over 50 mg per liter of culture with [¹⁵N] isotopically enriched minimal media. The other six constructs (mutant G–M) yielded very little protein (less than 1 mg / L) and therefore, it was decided not to use them for CLaNP-7 labeling. For Pdx constructs, Pdx mutant II and III did not yield correctly folded proteins due to the extensive loss of iron-sulfur cluster. Pdx mutant I, on the other hand, showed the identical absorption spectrum as wild type and the protein yield reached 10 mg / L of culture with [¹⁵N] minimal media. Low yield of P450cam constructs was attributed to the inability to incorporate the heme group correctly and stably as indicated by the observation of a Soret peak at 420 nm in their absorption spectra. The reason for the difficulty of gene expression of Pdx variants can be similar. The coordination of [2Fe-2S] cluster can be disturbed by double Cys mutations, which leads to instable or incorrectly folded protein.

Probe attachment and characterization

Isolated P450cam (mutant A–F) and Pdx (mutant I) were labeled with CLaNP-7 and ¹⁵N-¹H HSQC spectra were recorded. Figure 2 shows a section of the overlaid HSQC spectra of Pdx mutant I.

As illustrated in Figure 2, the PCS is defined as the difference in the chemical shifts between paramagnetic Yb³⁺/Tm³⁺ samples and diamagnetic Lu³⁺ sample. By comparing the intensities of PCS peaks against those of the residual peaks, the fraction of CLaNP-7 labeling can be determined (Figure 3). For instance, if there is almost no

Table 1. Summary of P450cam and Pdx constructs prepared in this study. Most of the double cysteine mutations were designed to be in the vicinity of the proposed binding interface of Pdx-P450cam complex.^[6] Some constructs yielded very little protein or P420 species, which are indicated by "Unsuccessful".

P450cam	Mutations	Probe positions	CLaNP-7 attachment
Mutant A	K126C/R130C/C334A	Proximal side	Yb ³⁺ & Tm ³⁺
Mutant B	A333C/H337C/C334A	Proximal side	Yb ³⁺ & Tm ³⁺
Mutant C	Q272C/E276C/C334A	Proximal side	Tm ³⁺
Mutant D	E195C/A199C/C334A	Distal side	Yb ³⁺ & Tm ³⁺
Mutant E	A113C/Q117C/C334A	Proximal side	Yb ³⁺
Mutant F	A113C/N116C/C334A	Proximal side	Yb ³⁺
Mutant G	E40C/V44C/C334A	Proximal side	Unsuccessful
Mutant H	Q69C/R72C/C334A	Proximal side	Unsuccessful
Mutant J	Q69C/E73C/C334	Proximal side	Unsuccessful
Mutant K	Q227C/N229C/C334A	Proximal side	Unsuccessful
Mutant L	R277C/R280C/C334A	Proximal side	Unsuccessful
Mutant M	Q388C/N390C/C334A	Proximal side	Unsuccessful

Pdx	Mutations	CLaNP-7 attachment
Mutant I	V6C/R12C/C73S/C85S	Yb ³⁺ & Tm ³⁺
Mutant II	K79C/N81C/C73S/C85S	Unsuccessful
Mutant III	E93C/D95C/C73S/C85S	Unsuccessful

attachment of CLaNP-7, a single peak would be observed at the chemical shift for a given residue. In contrast, if half of the sample were labeled with Yb³⁺/Tm³⁺-CLaNP-7, two peaks would appear in the NMR spectrum for a given residue, with 1:1 intensity ratio. And lastly, if almost all of the protein is labeled, the intensity of the residual peak would become very small.

For Pdx mutant I, no peaks of untagged Pdx were observed. By estimating the maximum intensity using the noise level, it is estimated at least 95% of the Pdx was labeled with CLaNP-7. The attachment of CLaNP-7 was also confirmed by mass spectrometry analysis. The theoretical molecular mass of 100% [¹⁵N] labeled Pdx mutant I was calculated to be 11528.8 and that of Yb³⁺-CLaNP-7 complex would be 12407.6 (from online ExpASY-Compute pl/Mw; http://www.expasy.ch/tools/pi_tool.html). The observed molecular weight was 12400.2, which differed by 7 Da from the expected Yb³⁺-CLaNP-7 labeled Pdx. The difference can be attributed to the efficiency of the enrichment of [¹⁵N] isotope in the protein production. In the case of P450cam mutants, low intensities of residual peaks were present. By measuring the height of paramagnetic peaks, we concluded that 80–90% of the protein was labeled with CLaNP-7 in all cases.

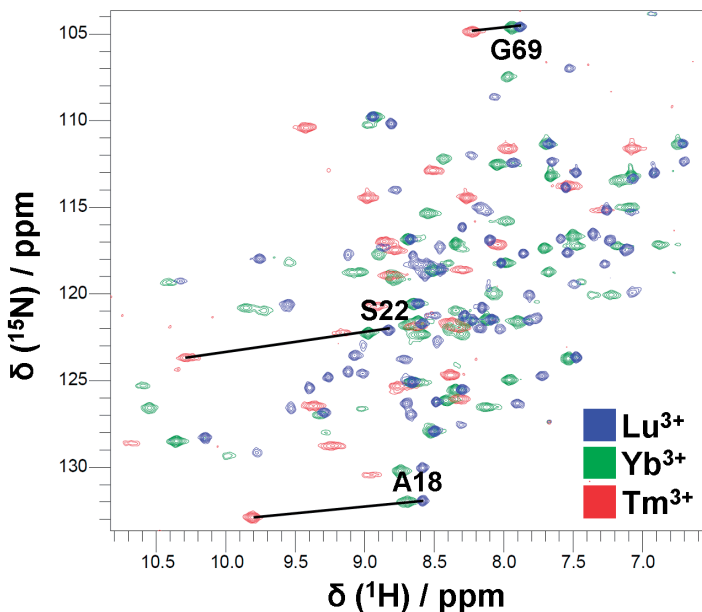


Figure 2. Overlay of the HSQC spectra of Ln^{3+} -CLaNP-7 labeled Pdx. Blue, green and red peaks represent Lu^{3+} , Yb^{3+} and Tm^{3+} containing samples, respectively. The PCSs are illustrated for several residues by a solid lines.

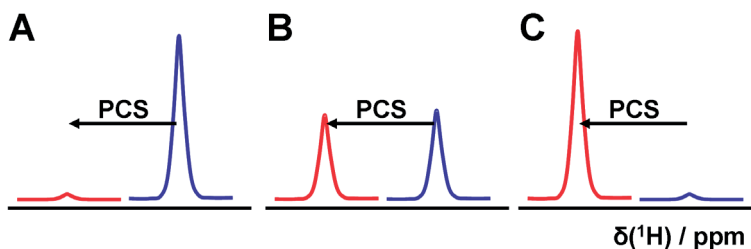


Figure 3. Schematic representation of determination of CLaNP-7 labeling in NMR spectrum. Blue and red peaks represent untagged and tagged protein, respectively. (A) almost 0% CLaNP-7 labeling. (B) 50% CLaNP-7 labeling. (C) >95% CLaNP-7 labeling.

The extension of the assignment of P450cam nuclei by PCS data

PCS depends on the orientation and anisotropy of $\Delta\chi$ tensors of lanthanoids.^[9] $\Delta\chi$ tensors can be represented by their axial ($\Delta\chi_{ax}$) and rhombic ($\Delta\chi_{rh}$) components, both of which were characterized for $\text{Yb}^{3+}/\text{Tm}^{3+}$ -CLaNP-7 previously.^[3] The assignments for amide resonances of oxidized Pdx were based on previous work.^[10] The amide resonances of oxidized, camphor bound P450cam were kindly provided by Dr. Mathias Hass (Leiden University).

For Yb^{3+} -CLaNP-7 labeled P450cam mutant A, B, D, E and F, the number of PCS measured were 133, 117, 158, 133 and 129, respectively. Due to the broadening caused by relaxation enhancement of Tm^{3+} , the number of PCS measured for Tm^{3+} -CLaNP-7 samples were smaller (97, 97, 109, and 109 for mutant A, B, C and D, respectively). To illustrate the regions experiencing PCS from different positions of Ln^{3+} , PCSs caused by $\text{Yb}^{3+}/\text{Tm}^{3+}$ were plotted against P450cam residue number (Figure 4).

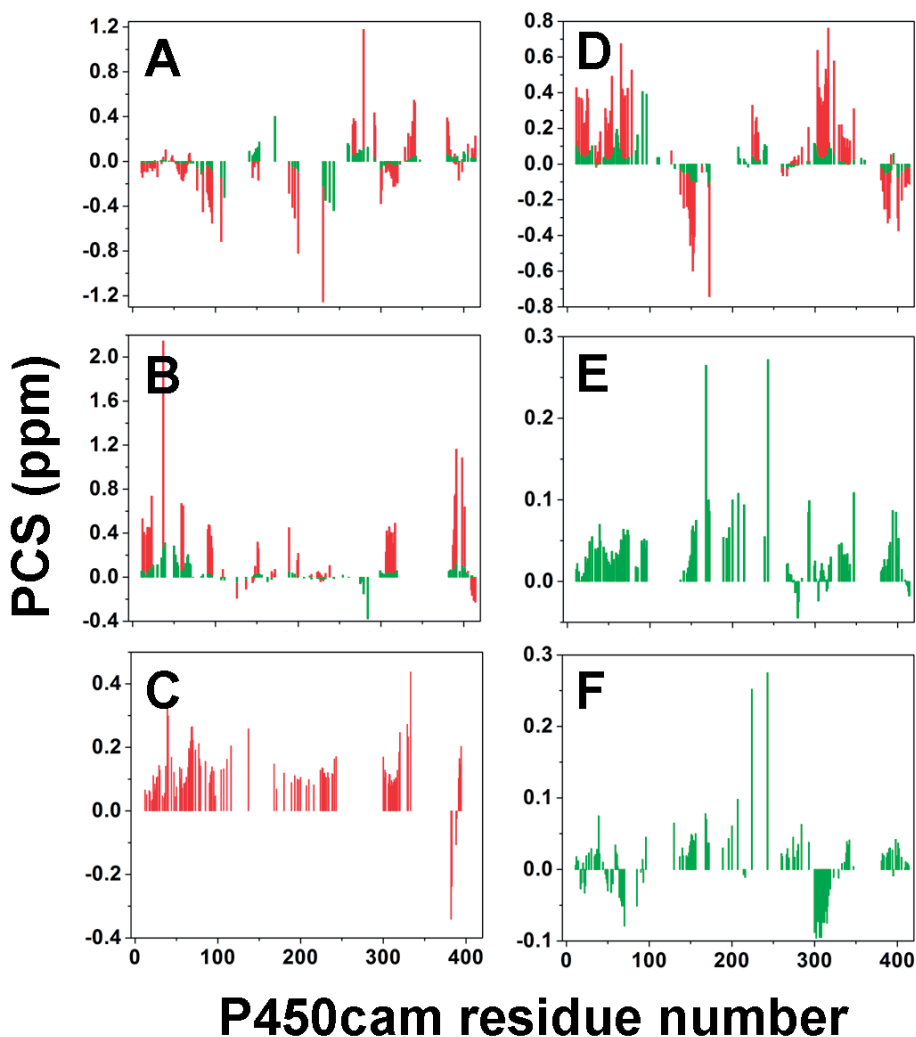


Figure 4. Experimentally observed PCSs were plotted against the P450cam residue number. The panel A, B, C, D, E and F represent P450cam mutant A, B, C, D, E and F, respectively. Green columns are for Yb^{3+} and red columns for Tm^{3+} data. For the mutant E and F, only Yb^{3+} data sets were available due to the limited amount of sample. In case of mutant C, only the Tm^{3+} data were analyzed for the same reason.

The PCS measurements of the six different positions cover 45% (188/414) of the residues for the entire protein. It is worth noting that the regions nearby heme (248–252 and 350–360) were hardly accessible. The loss of NMR signals is attributed to the relaxation enhancement from the heme iron. In the presence of substrate, camphor, the heme iron becomes high spin, which causes the line broadening of the resonances of nuclei within 8 Å of the iron.^[11] Some residual peaks previously assigned by multiple 3D NMR experiments^[6, 11–13] were corrected according to the back-calculated and experimentally observed PCS values.

In case of Pdx mutant I, the number of PCS measured for Yb³⁺ and Tm³⁺ were 37 and 15, respectively. To illustrate the accuracy of the PCS measurement, back-calculated PCS was plotted against experimentally obtained PCS. Figure 5 shows the scatter plot of Yb³⁺/Tm³⁺-CLaNP-7 labeled Pdx mutant I.

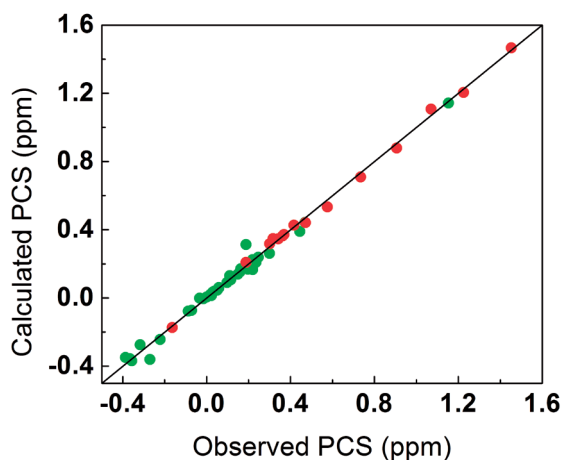


Figure 5. Plot of back-calculated PCS versus experimentally observed PCS of Pdx mutant I. Green and red points represent the Yb³⁺ and Tm³⁺ samples, respectively. The ideal correlation is indicated by the solid line.

Most of the data points exhibit good correlations between the back-calculated and observed PCS. The back-predicted PCSs were calculated from the crystal structures of Pdx C73S and P450cam C334A (PDB entries, 1XLP^[14] and 1DZ4,^[15] respectively). If Cys substitutions or the attachment of paramagnetic tag significantly perturb the structures of the proteins, deviations would be detected between the observed and back-calculated PCS. The agreement of observed and back-calculated PCS provides a validation of CLaNP-7 attachment as well as the integrity of the 3D structure. $\Delta\chi_{ax}$ and $\Delta\chi_{rh}$ values were estimated by program Numbat.^[9] The list of $\Delta\chi$ tensors and associating quality (Q) factors were summarized in the Table 2. See Materials and Methods for the Q factor definition.

Table 2. Intramolecular PCS experiments.

Sample	CLaNP-7	# assignments	$\Delta\chi$ (10^{-32} m ³)	Q
[¹⁵ N] P450cam mutant A (K126C/R130C/C334A)	Yb ³⁺	133	$\Delta\chi_{\text{ax}} = 6.3 \pm 0.3$ $\Delta\chi_{\text{rh}} = 8.5 \pm 0.5$	0.04
	Tm ³⁺	97	$\Delta\chi_{\text{ax}} = 54.6 \pm 2.6$ $\Delta\chi_{\text{rh}} = 16.9 \pm 0.8$	0.04
[¹⁵ N] P450cam mutant B (A333C/H337C/C334A)	Yb ³⁺	117	$\Delta\chi_{\text{ax}} = 5.9 \pm 0.4$ $\Delta\chi_{\text{rh}} = 6.7 \pm 0.4$	0.06
	Tm ³⁺	97	$\Delta\chi_{\text{ax}} = 56.9 \pm 1.2$ $\Delta\chi_{\text{rh}} = 13.0 \pm 0.8$	0.04
[¹⁵ N] P450cam mutant C (Q272C/Q276C/C334A)	Tm ³⁺	109	$\Delta\chi_{\text{ax}} = 44.7 \pm 2.0$ $\Delta\chi_{\text{rh}} = 8.0 \pm 2.0$	0.07
[¹⁵ N] P450cam mutant D (E195C/A199C/C334A)	Yb ³⁺	158	$\Delta\chi_{\text{ax}} = 6.7 \pm 0.3$ $\Delta\chi_{\text{rh}} = 6.3 \pm 0.4$	0.07
	Tm ³⁺	109	$\Delta\chi_{\text{ax}} = 44.7 \pm 0.8$ $\Delta\chi_{\text{rh}} = 21.3 \pm 1.1$	0.04
[¹⁵ N] P450cam mutant E (A113C/Q117C/C334A)	Yb ³⁺	133	$\Delta\chi_{\text{ax}} = 7.4 \pm 0.4$ $\Delta\chi_{\text{rh}} = 7.6 \pm 0.6$	0.06
[¹⁵ N] P450cam mutant F (A113C/N116C/C334A)	Yb ³⁺	129	$\Delta\chi_{\text{ax}} = 5.1 \pm 0.1$ $\Delta\chi_{\text{rh}} = 7.2 \pm 0.4$	0.14
[¹⁵ N] Pdx mutant I (V6C/R12C/C73S/C85S)	Yb ³⁺	37	$\Delta\chi_{\text{ax}} = 6.4 \pm 0.7$ $\Delta\chi_{\text{rh}} = 8.6 \pm 1.3$	0.06
	Tm ³⁺	15	$\Delta\chi_{\text{ax}} = 49.0 \pm 0.5$ $\Delta\chi_{\text{rh}} = 15.7 \pm 1.2$	0.02

The $\Delta\chi$ tensors derived from PCS analysis were comparable to those found in the model proteins in a previous study.^[3] Q factor analysis indicates that the back-predicted PCSs agree well with the experimentally obtained PCSs. Also, in line with the suggestions with a previous study,^[16] the positions of Ln³⁺ were found to be 8 ± 2 Å distance away from the alpha carbons of two substituted Cys residues. In the case of P450cam mutant F, however, the distances between Ln³⁺ and the alpha carbons of C113 and C116 were measured to be 8 Å and 12 Å, respectively (Figure 6). The calculated position cannot be achieved if CLaNP-7 were anchored at A113C/N116C via two disulfide bridges. It is concluded that CLaNP-7 was attached to Cys113 via a single arm.

Previously, it had been shown that single point attachment of CLaNP significantly reduces the observed $\Delta\chi$ tensors.^[17] This is due to the mobility of the probe on protein surface averaging out PCSs. For mutant F, a slightly smaller $\Delta\chi_{\text{ax}}$ and larger Q factor were found as compared to the other mutants. However, the overall change was not as significant as the previously reported.^[17] It is speculated that the mobility of CLaNP-7

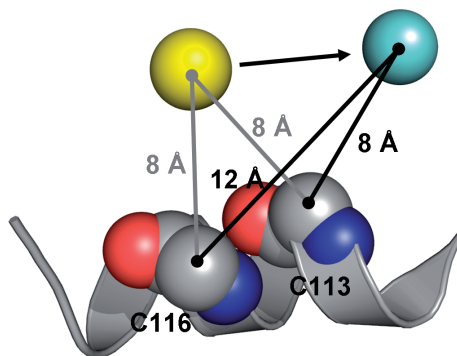


Figure 6. Cartoon representation of the position of Ln^{3+} on P450cam mutant F. Yellow and cyan spheres illustrate the initially predicted and experimentally derived positions of Ln^{3+} , respectively. Gray, red and blue spheres in the ribbon represent the substituted residues C113 and C116 of P450cam.

for mutant F was restricted by the interactions of the residues closeby. The problem of single-arm attachment was circumvented by a change of the mutation site from N116 to the adjacent residue, Q117 (mutant E).

Intramolecular paramagnetic NMR of [^{13}C , ^{15}N] P450cam in the presence of Pdx

The PCS measurements above were obtained by two-dimensional ^{15}N - ^1H TROSY/HSQC experiments. To further extend the PCS analysis, P450cam mutant A was enriched with [^{13}C , ^{15}N] isotopes. An HNCOC experiment was recorded with $\text{Lu}^{3+}/\text{Tm}^{3+}$ -CLaNP-7 labeled samples. The $\Delta\chi_{\text{ax}}$ and $\Delta\chi_{\text{rh}}$ calculated from experimentally obtained PCS were compatible to previously determined values. Due to the limited availability of the sample, the total number of PCS measured for 3D experiment was 95, which is slightly smaller than for the 2D experiment (Table 1). The calculations of $\Delta\chi$ tensors and 2D/3D NMR assignment of P450cam allows to study dynamics of the conformational states of P450cam by PCS measurements. Recently, Tripathi *et al.* proposed the effector role of Pdx on the basis of the crystal structures of the Pdx-P450cam complex, to consist of a conformation change in P450cam, opening up its substrate access channel.^[5] According to their model, P450cam adopts a closed conformation in the absence of Pdx while it assumes the open conformation when it is bound to Pdx. To assess the dynamics of P450cam upon Pdx binding, the intramolecular PCS of P450cam were determined in the absence and presence of Pdx. P450cam mutant A was enriched with [^{13}C] and [^{15}N] isotopes and labeled with $\text{Lu}^{3+}/\text{Tm}^{3+}$ -CLaNP-7. Subsequently, excess oxidized Pdx was added to the NMR samples and a series of three dimensional HNCOC spectra were acquired. In case of the diamagnetic dataset (Lu^{3+}), chemical shift perturbations ($\text{CSP}_{\text{binding}}$) were observed nearby the Pdx binding site in accord with a previous report.^[11] The chemical shift perturbation ($\Delta\delta^{\text{Tm}}$) measured in the Pdx bound

sample reflects the contributions of Pdx binding (CSP_{binding}) and a change in the PCS (ΔPCS) due to a conformation change in P450cam as shown in the following equations:

$$\Delta\delta^{\text{Tm}} = CSP_{\text{(binding)}} + \Delta\text{PCS} \quad [1]$$

$$\Delta\delta^{\text{Lu}} = CSP_{\text{(binding)}} \quad [2]$$

$$\Delta\text{PCS} = \Delta\delta^{\text{Tm}} - \Delta\delta^{\text{Lu}} \quad [3]$$

The contribution of Pdx binding can thus be subtracted, using the chemical shift changes in the diamagnetic sample. The ΔPCS attributed to the conformation change was derived by the comparison of PCS between Pdx-free and Pdx-bound samples.

The observed ΔPCS were plotted against P450cam residue number and color-coded on the P450cam surface (Figure 7).

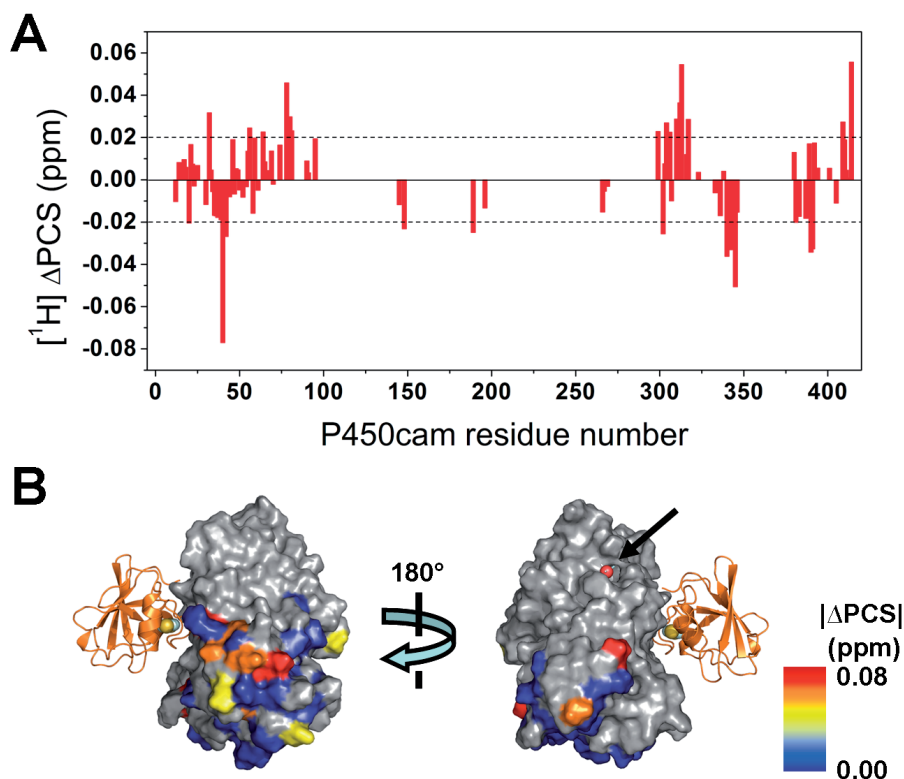


Figure 7. Effect of Pdx binding on PCS in P450cam mutant A. (A) The differences in PCS (ΔPCS) are plotted against the P450cam residue number. (B) Surface representation of P450cam, color coded for the residues with $|\Delta\text{PCS}| \geq 0.030$, red; $0.030 > |\Delta\text{PCS}| \geq 0.025$, orange; $0.025 > |\Delta\text{PCS}| \geq 0.020$, yellow; $0.020 > |\Delta\text{PCS}|$, blue and no data, gray. Pdx as found in the complex (chapter 3) is shown in ribbons.

The changes of the PCS were not only observed at the Pdx binding site but also in other regions of P450cam. The residues Glu40, Leu312, Lys313 and Val414, experiencing the largest change of PCS, are located at the A helix, β 4 sheet and C-terminal loop. In our current study, the predicted Δ PCSs were not calculated for the open conformation of P450cam. Therefore, it is hard to quantify the extent of Δ PCSs for those residues upon the conformation change. However, the overall magnitude of PCS change is close to the experimental errors. It suggests that those residues undergo minor structural change upon binding of Pdx. It should be noted that not the entire surface of P450cam was sampled for Δ PCS due to the interference of the large broadening effect of Tm³⁺-CLaNP-7. Currently, further intramolecular PCS measurements are undertaken to clarify the effect of Pdx binding on P450cam. P450cam mutant D is selectively enriched with [¹⁵N] Leu and labeled with Yb³⁺/Lu³⁺-CLaNP-7. The preliminary results also indicate that P450cam does not undergo significant conformation change upon binding of Pdx, which is in the line with the suggestions of the current study (Dr. Simon Skinner, personal communication).

Discussion

Determination of $\Delta\chi$ tensors

One of the most important results presented here was obtained by analysis of the intramolecular PCS data for the respective mutants. Using this approach, we were able to demonstrate the attachment of CLaNP-7 to the proteins and derive the positions of the Ln³⁺ ions and the orientations of the $\Delta\chi$ tensors. Our finding of $\Delta\chi$ tensors was in accord with the results for the model protein, pseudoazurin, and was not dependent on pH as described by Liu *et al.* for cytochrome *c*.^[3] Characteristically, the $\Delta\chi$ tensor of Yb³⁺-CLaNP-7 exhibits rather a large rhombicity compared to Yb³⁺-CLaNP-5. It can be attributed to the change of the coordination system of Yb³⁺ and overall charge of Yb³⁺-CLaNP-7. However, for Tm³⁺, the $\Delta\chi_{th}$ is similar for both CLaNPs. CLaNP-7 was recently synthesized in our group to reduce the overall charge of CLaNP from 3+ to 1+.^[3] Interestingly, the different properties of CLaNP-7 opened up the possibility to apply paramagnetic NMR experiments to P450cam. When Ln³⁺-CLaNP-5 was added to wild type P450cam, it led to the formation of a large amount of aggregated protein. On the other hand, P450cam showed much more tolerance toward Ln³⁺-CLaNP-7 incubation. The formation of oligomers was significantly less than with CLaNP-5 treatment. The hydrophobicity of CLaNP-7 enables the enrichment of probe-labeled P450cam. Standard ion-exchange chromatography and/or size-exclusion chromatography often result in the insufficient separation of probe-free and probe-labeled proteins. The attachment of CLaNP-7 creates a hydrophobic patch on a protein surface that changes its elution point in the affinity to hydrophobic interaction chromatography (HiTrap Phenyl FF hydrophobic column).

The $\Delta\chi$ tensors derived from the experimentally obtained PCS suggested that all of the mutants were labeled with CLaNP-7 via two arms, except for P450cam mutant F (A113C/N116C). Fitting of the Ln^{3+} position based on the PCS showed that CLaNP-7 was anchored at P450cam mutant F via a single disulfide bond. A plausible explanation is that the side chain of the second mutation site, N116C, was orientated away from the protein surface and was inaccessible for the formation of a disulfide bridge. Single point attachment can generate significant rotational freedom to CLaNP-7, reducing the magnitude of PCS due to the averaging effect as was seen for CLaNP-5.^[17] However, the reduction in $\Delta\chi$ tensor values was rather limited in the present case. The problem of single-arm attachment was overcome by a change of the mutation site to the adjacent residue Q117. It was demonstrated that the $\Delta\chi$ tensor and metal location of P450cam mutant E (A113C/Q117C) agree well with the expected tensor, both in size and orientation. The study of P450cam mutant F highlighted a methodology for finding double-point attachment of CLaNP based on $\Delta\chi$ tensor analysis of intramolecular PCS.

One of the essential parameters for the analysis of paramagnetic NMR experiments is the fraction of probe labeled protein. Different techniques were applied to estimate the efficiency of labeling on proteins. Atomic absorption spectroscopy showed the presence of Ln^{3+} and heme iron in P450cam samples. However, it did not allow us to determine the fraction of labeling. The reliability of the data was limited by the formation of aggregated proteins during sample preparation. Alternatively, the labeling efficiency can be calculated from the fraction of free thiol on protein surface. The determination of free thiol content was performed by using Ellman's reagent.^[18] P450cam comprises eight endogenous cysteine residues, of which one surface exposed Cys was substituted to Ala. Unfortunately, however, it was not possible to calculate the amount of Ellman's reagent on proteins, since its absorption heavily overlaps with that of the P450cam Soret band. The absorbance of camphor bound P450cam, with $\epsilon_{391\text{nm}} = 108 \text{ mM}^{-1}\text{cm}^{-1}$, dwarfs that of Ellman's reagent with $\epsilon_{412\text{nm}} = 14.2 \text{ mM}^{-1}\text{cm}^{-1}$.^[19] Another conventional way to determine probe labeling on proteins is mass spectrometry (MS). The limited mass range of the MS available to us, only enabled us to measure molecular weights of less than 30 kDa. Since the molecular mass of P450cam is 47 kDa, MS analysis could not be performed. For Pdx (12 kDa), the MS data confirmed the complete labeling with CLaNP-7. It is worth noting that the fraction of probe labeling drops when Pdx was stored at -80°C . The disulfide bonds that connect CLaNP-7 and Pdx become susceptible to reduction during rapid thawing of the samples at room temperature. To estimate the fraction of probe labeling in P450cam, we decided to utilize the peak intensities in the NMR spectra. By measuring the height of paramagnetic peaks, we concluded that more than 80–90% of P450cam was labeled with CLaNP-7. It should be noted that these values represent the samples after purification. Due to the formation of oligomers and presence of probe-free P450cam, the yield of Ln^{3+} -CLaNP-7 labeled P450cam immediately after the reaction

was usually less than 20%. Another quick and easy estimation of fraction of CLaNP-7 labeling can be obtained from absorption spectra recorded on the NMR samples. CLaNP-7 gives maximum absorption peak at the wavelength of 390 nm due to the presence of nitro-phenyl group. Absorption spectrum analysis revealed that the ratio of $A_{390\text{nm}}/A_{280\text{nm}}$ increases from 1.4 to ≥ 2.1 when P450cam is labeled to 80–90%. For Pdx with complete labeling, the ratio of $A_{400\text{nm}}/A_{280\text{nm}}$ exceeds 1.95.

The extension of NMR assignments by PCS analysis

The determination of $\Delta\chi$ tensors of Ln^{3+} at multiple positions on the protein surface aided in the extension of the assignment of P450cam NMR spectra. Due to the relatively large size of the protein, conventional 3D NMR experiments require long acquisition time as well as a high concentration of protein. Furthermore, in order to obtain high resolution spectra, it is necessary to isotopically enrich proteins with ^2H , ^{15}N and ^{13}C . The production of such isotopically labeled proteins was expensive due to a low protein yield. In this study, it was demonstrated that with the use of PCS data, the preparations and experiments of NMR can be simplified. P450cam samples used in this report were enriched solely with ^{15}N , which yielded as much as 50 mg per a liter of culture. In addition, simple 2D HSQC spectra were recorded with a protein concentration of merely 100 μM (equivalent to 2–3 mg of protein per sample).

The six series of PCS data yielded assignments for 45% of the residues of the entire protein. The regions where PCS were not measured were the distal side of P450cam and the active site nearby the heme. The PCS measurement of the distal side nuclei can be achieved by extending the mutation sites of probe attachment. Here, most of the CLaNP-7 labeling sites were designed at the proximal side of the protein to study the interaction of Pdx-P450cam complex. The spin state of the heme iron influences the NMR peaks of the residues in close vicinity. When heme iron is high spin, those peaks broaden out beyond detection.^[11] The problem of the line broadening can be eliminated by the replacement of substrate with substrate analogues. Phenylimidazole is one of the substrate analogues that is known to associate with heme iron and act as a sixth ligand.^[20] The coordination of a strong sixth ligand changes the spin state of the iron and reduces the line broadening. Since information of the active site helps to reveal the nature of the catalytic reaction of P450cam, further assignments by paramagnetic NMR analysis in that region are desirable.^[21]

Intramolecular paramagnetic NMR effects upon Pdx binding

To evaluate the effects of Pdx binding, isotopically enriched P450cam was labeled with CLaNP-7 and the changes in PCSs were measured upon addition of Pdx. Due to the limited availability of the sample as well as the interference of broadening effect of Tm^{3+} , only 95 peaks were analyzed, which represents only a limited region of P450cam. The results of the PCS analysis indicated that P450cam undergoes a minor conformational change upon the binding of Pdx. These results are in contrast

to the proposed model of the effector activity of Pdx by Tripathi *et al.* in which Pdx binding causes the conformation change of P450cam to adapt open conformation.^[5] Goodin and co-workers examined the conformational shift of P450cam by double electron-electron resonance (DEER) spectroscopy.^[22] The results of DEER suggested that it is dependent on the oxidation state of Pdx. The binding of oxidized Pdx induces the conformational transition to open state while reduced Pdx favors the closed conformation. The discrepancy of the results can be attributed to the experimental conditions. Tripathi *et al.* drew the conclusion on the basis of the crystal structures of Pdx-P450cam complex. However, the formation of the crystals of Pdx-P450cam complex was only observed under conditions that favor P450cam to be in the open conformation.

The changes of the specificity and selectivity of electron transfer partner between the first and second ET play a key role in the regulation of the catalytic reaction of P450cam. To study the second ET complex, the paramagnetic NMR experiments were repeated with dithionite reduced states of Pdx and carbon monoxide bound P450cam. However, the disulfide bridges between CLaNP-7 and P450cam were vulnerable to the reducing environment. The reduced state of P450cam was also prepared in the reconstituted system of Pdx-P450cam in the presence of a catalytic amount of PdR. However, the NMR spectra indicated that the paramagnetic NMR effect was still lost due to the loss of CLaNP-7. The detachment of the probe under reducing conditions has recently been overcome by the modification of CLaNP molecule. The two methyl thiosulfate groups of CLaNP arms were substituted with bromide groups. This novel probe, called CLaNP-9, reacts with cysteine residues to form covalent thioether bridges via two-point attachment. Preliminary data suggested that CLaNP-9 labeled P450cam remains intact even in the presence of strongly reducing agents such as dithionite. As a future perspective, the effector activity of Pdx in the second ET could be investigated by intramolecular paramagnetic NMR experiments.

Material and Methods

Chemicals

Ln³⁺-CLaNP-7 was kindly provided by Dr. Wei-Min Liu. The plasmids harboring the cDNA of Pdx and P450cam were generous gift from Prof. Stephen G. Sligar, University of Illinois at Urbana-Champaign, U.S.^[12] The genes were subcloned into the pET28a expression vectors using NcoI and XhoI restriction enzymes by Anneloes Blok (Leiden University), without use of the His tag sequence. Column material was obtained from GE Healthcare, Munich, Germany.

Mutagenesis

Site-directed mutagenesis was performed using QuikChange protocol (Stratagene, La Jolla, CA).

Protein production

Isotopically enriched P450cam variants were produced as previously described.^[23] The pET28a plasmid containing P450cam gene was transformed into BL21 pLysS strain. Single colonies were picked and inoculated into 5 mL LB medium with 50 µg/mL kanamycin at 37°C for 4 hours. 20 µL of the pre-culture was transferred to 100 mL [¹⁵N] M9 minimal medium with 50 µg/mL kanamycin overnight at 37°C. 10 mL of M9 pre-culture was transferred into 500 mL of [¹⁵N] M9 minimal media with 50 µg/mL kanamycin and grown at 37°C until $A_{600\text{nm}} = 0.4\text{--}0.6$. Gene expression was induced by adding 0.5 mM IPTG, 0.2 mM 5-aminolevulinic acid, 1 mM camphor (1% MeOH) and 100 µM FeCl₃·6H₂O. The cultures were allowed to grow at 22°C for 70–80 hours. Cells were resuspended in a KP_i buffer (20 mM KP_i, pH 7.4, 50 mM KCl, 1 mM camphor, 1% MeOH, 1 mM DTT, 1 mM PMSF and 1 mM DNase). Samples were flash frozen in N₂ (l) and stored at –80°C.

The resuspended cells were defrosted rapidly at room temperature. A few mg of crystal of lysozyme crystals were added and the sample was stirred for 30 minutes at 22°C. The lysate was further disrupted by French-press and sonication. Following centrifugation at 35000 r.p.m. for 30 minutes at 4°C, protamine sulfate was added to a lysate with 10 mg/g of cell pellet and incubated in cold room for 30 minutes. The sample was then centrifuged with 35000 r.p.m. for 30 minutes at 4°C. The pH of the supernatant was adjusted to around 7.4 by addition of a few drops of KOH. Ammonium sulfate powder was added slowly to the sample to achieve 70% (w/v). The sample was then stirred in cold room for 30 minutes. Following centrifugation at 35000 r.p.m. for 30 minutes at 4°C, the pellet was resuspended with KP_i buffer A (20 mM KP_i, pH 7.4, 1 mM camphor, 1% MeOH, 1 mM DTT) and dialyzed overnight in 4 L of KP_i buffer B (20 mM KP_i, pH 7.4, 50 mM KCl, 1 mM camphor 1% MeOH, 1 mM DTT). The dialysate was loaded on a HiTrap Q sepharose FF anion-exchange column (60 mL). The protein was eluted with a linear gradient of 0.1–0.4 M KCl in KP_i buffer A and the brown fractions were collected. The fractions were pooled and concentrated by ultrafiltration using a Centricon 3K (Millipore) and injected into a Superose 12 size exclusion column pre-equilibrated with KP_i buffer C (20 mM KP_i, pH 7.4, 150 mM KCl, 1 mM camphor, 1% MeOH, 1 mM DTT). Ammonium sulfate crystals were added (30% w/v) to the pooled fractions and the sample was stirred for 20 minutes at 4°C. Subsequently, the sample was centrifuged for 20 minutes to remove precipitation and the supernatant was applied to a HiTrap Phenyl FF hydrophobic column (10 mL). The brown fractions containing P450cam were collected after elution with a linear gradient 30–0% ammonium sulfate in KP_i buffer A. Then the fractions were dialyzed overnight in 4 L of KP_i buffer B. The dialysate was loaded on a HiTrap Q sepharose HP anion-exchange column (10 mL). The protein was eluted with a linear gradient of 0.1 – 0.3 M KCl in KP_i buffer A. The fractions with the $A_{391\text{nm}}/A_{280\text{nm}}$ value greater than 1.2 were collected. Approximately, 50 mg of P450cam was obtained from 1 L of culture.

The [^{15}N] enriched Pdx mutant was produced and purified as previously described.^[23] The concentration of Pdx was determined with $\epsilon_{412\text{nm}} = 11.0 \text{ mM}^{-1} \text{ cm}^{-1}$. Approximately 5 mg of Pdx was obtained from 1 L of culture.

Ln^{3+} -CLaNP-7 labeling

Purified double-cysteine P450cam and Pdx samples were incubated with 5 mM DTT in 20 mM KPi , pH 7.4, 50 mM KCl, 1 mM camphor, 1% MeOH for 30 minutes on ice. DTT was removed by using a PD-10 column. The protein solution was mixed with seven molar equivalents of Ln^{3+} -CLaNP-7 and gently stirred overnight at 4°C in argon degassed KPi buffer B (without DTT). Unlabeled protein, protein oligomers and surplus of Ln^{3+} -CLaNP-7 were removed by three chromatography steps, on a HiTrap Q HP anion-exchange column, a HiTrap Phenyl FF hydrophobic column and a Superose 12 size exclusion column. The Ln^{3+} -CLaNP-7 incubated sample was filtered and loaded on a HiTrap Q sepharose HP anion-exchange column (10 mL). The protein was eluted with a linear gradient of 0.1-0.4 M KCl in KPi buffer A (without DTT) and the first peak fractions were collected. Ammonium sulfate crystals were added (30% w/v) to the pooled fractions and the sample was stirred for 20 minutes at 22°C . Subsequently, the sample was centrifuged for 20 minutes to remove precipitation and the supernatant was applied to a HiTrap Phenyl FF hydrophobic column (2 mL). The brown fractions containing P450cam were collected after elution with a linear gradient 30–0% ammonium sulfate in KPi buffer A (without DTT). Finally, the pooled fractions were briefly buffer-exchanged and concentrated by ultrafiltration using a Centricon 10K (Millipore) and injected into a Superose 12 size exclusion column pre-equilibrated with 50 mM Tris-HCl, pH 7.4, 100 mM KCl and 1 mM camphor, 1% MeOH, 6% D_2O . The fractions with $A_{391\text{nm}}/A_{280\text{nm}}$ larger than 2.1 were pooled and concentrated. Approximately, 80–90% of proteins were lost during the labeling procedure possibly due to oligomerization and probe-free protein.

NMR samples and experiments

NMR samples contained 50–170 μM [^{15}N] Pdx or [^{15}N] P450cam variants labeled with Ln^{3+} -CLaNP-7, in 50 mM Tris-HCl, pH 7.4, 100 mM KCl, 1 mM camphor and 6% D_2O . 2D ^{15}N - ^1H HSQC and ^{15}N - ^1H TROSY spectra^[24] were recorded at 298 K on a Bruker Avance III 600 MHz spectrometer equipped with a TCI-Z-GRAD cryoprobe. In case of 3D HNC0 experiments, NMR samples contained 70–100 μM [^{13}C , ^{15}N] P450cam mutant A labeled with $\text{Tm}^{3+}/\text{Lu}^{3+}$ -CLaNP-7 with three molar equivalents of Pdx (C73S).

NMR assignment

All NMR data were processed in NmrPipe^[25] and analyzed in CCPNMR.^[26] The assignments for oxidized Pdx amide resonances were based on previous work.^[10] The partial assignments of the amide resonances for oxidized P450cam were kindly provided by Dr. Mathias Hass through personal contact.

PCS analysis

PCS measurements were carried out as previously described.^[4] The crystal structures of P450cam (PDB entry 1DZ4^[15]) and Pdx (PDB entry 1XLP^[14]) were used to fit the experimentally obtained PCS data. The position of the lanthanoid and the $\Delta\chi$ tensor describing the anisotropy of the paramagnetic effect were calculated using Numbat.^[9]

The correlations between observed and back calculated PCS were expressed in a quality factors (Q). It is defined as the ratio of the rmsd between experimentally observed and back-calculated data and the rms of the sum of them (Eq. 4).

$$Q = \frac{\sqrt{\sum_i \{\Delta\delta_{\text{PCS}}^{\text{obs}}(i) - \Delta\delta_{\text{PCS}}^{\text{sim}}(i)\}^2}}{\sqrt{\sum_i \{|\Delta\delta_{\text{PCS}}^{\text{obs}}(i)| + |\Delta\delta_{\text{PCS}}^{\text{sim}}(i)|\}^2}} \quad [4]$$

References

1. M. Ubbink, *Biochem Soc Trans*, **2012**, *40*, 415-418.
2. P. H. Keizers, B. Mersinli, W. Reinle, J. Donauer, Y. Hiruma, F. Hannemann, M. Overhand, R. Bernhardt, M. Ubbink, *Biochemistry*, **2010**, *49*, 6846-6855.
3. W. M. Liu, P. H. Keizers, M. A. Hass, A. Blok, M. Timmer, A. J. Sarris, M. Overhand, M. Ubbink, *J Am Chem Soc*, **2012**, *134*, 17306-17313.
4. M. A. Hass, P. H. Keizers, A. Blok, Y. Hiruma, M. Ubbink, *J Am Chem Soc*, **2010**, *132*, 9952-9953.
5. S. Tripathi, H. Li, T. L. Poulos, *Science*, **2013**, *340*, 1227-1230.
6. W. Zhang, S. S. Pochapsky, T. C. Pochapsky, N. U. Jain, *J Mol Biol*, **2008**, *384*, 349-363.
7. D. P. Nickerson, L. L. Wong, *Protein Eng*, **1997**, *10*, 1357-1361.
8. I. F. Sevrioukova, C. Garcia, H. Li, B. Bhaskar, T. L. Poulos, *J Mol Biol*, **2003**, *333*, 377-392.
9. C. Schmitz, M. J. Stanton-Cook, X. C. Su, G. Otting, T. Huber, *J Biomol NMR*, **2008**, *41*, 179-189.
10. T. A. Lyons, G. Ratnaswamy, T. C. Pochapsky, *Protein Sci*, **1996**, *5*, 627-639.
11. S. S. Pochapsky, T. C. Pochapsky, J. W. Wei, *Biochemistry*, **2003**, *42*, 5649-5656.
12. B. P. Unger, I. C. Gunsalus, S. G. Sligar, *J Biol Chem*, **1986**, *261*, 1158-1163.
13. N. U. Jain, E. Tjioe, A. Savidor, J. Boulie, *Biochemistry*, **2005**, *44*, 9067-9078.
14. I. F. Sevrioukova, *J Mol Biol*, **2005**, *347*, 607-621.
15. I. Schlichting, J. Berendzen, K. Chu, A. M. Stock, S. A. Maves, D. E. Benson, R. M. Sweet, D. Ringe, G. A. Petsko, S. G. Sligar, *Science*, **2000**, *287*, 1615-1622.
16. P. H. Keizers, A. Saragliadis, Y. Hiruma, M. Overhand, M. Ubbink, *J Am Chem Soc*, **2008**, *130*, 14802-14812.
17. P. H. Keizers, J. F. Desreux, M. Overhand, M. Ubbink, *J Am Chem Soc*, **2007**, *129*, 9292-9293.
18. G. L. Ellman, *Arch Biochem Biophys*, **1959**, *82*, 70-77.
19. P. W. Riddles, R. L. Blakeley, B. Zerner, *Methods Enzymol*, **1983**, *91*, 49-60.
20. T. L. Poulos, A. J. Howard, *Biochemistry*, **1987**, *26*, 8165-8174.
21. S. P. Skinner, M. Moshev, M. A. Hass, P. H. Keizers, M. Ubbink, *J Biomol NMR*, **2013**, *56*, 401.
22. W. K. Myers, Y. T. Lee, R. D. Britt, D. B. Goodin, *J Am Chem Soc*, **2013**, *135*, 11732-11735.

23. Y. Hiruma, M. A. Hass, Y. Kikui, W. M. Liu, B. Olmez, S. P. Skinner, A. Blok, A. Kloosterman, H. Koteishi, F. Lohr, H. Schwalbe, M. Nojiri, M. Ubbink, *J Mol Biol*, **2013**, *425*, 4353-4365.
24. K. Pervushin, R. Riek, G. Wider, K. Wuthrich, *Proc Natl Acad Sci U S A*, **1997**, *94*, 12366-12371.
25. F. Delaglio, S. Grzesiek, G. W. Vuister, G. Zhu, J. Pfeifer, A. Bax, *J Biomol NMR*, **1995**, *6*, 277-293.
26. W. F. Vranken, W. Boucher, T. J. Stevens, R. H. Fogh, A. Pajon, M. Llinas, E. L. Ulrich, J. L. Markley, J. Ionides, E. D. Laue, *Proteins*, **2005**, *59*, 687-696.

CHAPTER 3

The structure of the cytochrome P450cam-putidaredoxin complex determined by paramagnetic NMR spectroscopy and crystallography

Part of this chapter was published as Hiruma, Y.; Hass, M.A.; Kikui, Y.; Liu, W.M.; Olmez, B.; Skinner, S.P.; Blok, A.; Kloosterman, A.; Koteishi, H.; Löhr, F.; Schwalbe, H.; Nojiri, M.; Ubbink, M. (2013) The Structure of the Cytochrome P450cam-Putidaredoxin Complex Determined by Paramagnetic NMR Spectroscopy and Crystallography, *J Mol Biol* **425**, 4353–4365.

Abstract

Cytochrome P450cam catalyzes the hydroxylation of camphor in a complex process involving two electron transfers from the iron sulfur protein putidaredoxin. The enzymatic control of the successive steps of catalysis is critical for a highly efficient reaction. The injection of the successive electrons is part of the control system. To understand the molecular interactions between putidaredoxin and cytochrome P450cam the structure of the complex was determined both in solution and in the crystal state. Paramagnetic NMR spectroscopy using lanthanoid tags yielded 446 structural restraints that were used to determine the solution structure. An ensemble of 10 structures with an RMSD of 1.3 Å was obtained. The crystal structure of the complex was solved, showing a position of putidaredoxin that is identical to the one in the solution structure. The NMR data further demonstrate the presence of a minor state or set of states of the complex in solution, which is attributed to the presence of an encounter complex. The structure of the major state shows a small binding interface and a metal-to-metal distance of 16 Å, with two pathways that provide strong electronic coupling of the redox centers. The interpretation of these results is discussed in the context of electron transfer. The structure indicates that the electron transfer rate can be much faster than the reported value, suggesting that the process may be gated.

Introduction

Cytochromes P450 (CYP) are heme-containing monooxygenases, catalyzing hydroxylation reactions of a variety of aromatic and aliphatic compounds.^[1] The CYP superfamily is one of the most extensively studied groups of metalloenzymes, because of its importance, for example in steroidal hormone biosynthesis, drug metabolism and degradation of xenobiotic compounds in human beings. Approximately four thousands CYP genes have been identified and at least fifty seven CYPs have been reported in humans.^[2] Cytochrome P450cam (P450cam, also called CYP101A1) from *Pseudomonas putida* is the best characterized CYP family member, providing a paradigm for CYP structure and function.^[3] P450cam catalyzes the regio- and stereo-specific hydroxylation of D-camphor by using molecular oxygen and two electrons from NADH. Putidaredoxin reductase (Pdr) oxidizes NADH and transfers the electrons to putidaredoxin (Pdx), which shuttles them to P450cam.^[3] The two electron transfers from Pdx, to the ferric and oxy-forms of P450cam, respectively, differ.^[4-5] Ferric P450cam is able to accept an electron from diverse reducing agents, whereas oxy-P450cam is highly specific for Pdx. With other reductants, such as dithionite, oxy-P450cam generates less than 5% of the maximum amount of hydroxylated camphor.^[6-7] It has been suggested that in the second electron transfer step Pdx serves as an effector molecule for P450cam as well as an electron donor.^[6, 8] Thus, understanding the interactions between Pdx and P450cam at the atomic level can help to understand the catalytic mechanism of this enzyme. Site-directed mutagenesis and calorimetric and spectroscopic methods have been applied to study the complex.^[4, 9-14] The structures of Pdx and P450cam separately have been elucidated.^[15-16] For P450cam many structures in the closed form have been reported, with various ligands in the cavity near the heme but with no obvious substrate access channel. With very large ligands, the channel is forced open, as was shown in several crystal structures.^[17-18] Recently, also the crystal structure of the substrate free form in the open state was solved, showing a clear access channel to the active site.^[19]

Solving the structure of the complex with conventional NMR structure determination of the complex is challenging, due to its size (58 kDa), as well as the paramagnetic nature of the heme and the iron-sulfur cluster, which broadens out many NMR signals. Zhang *et al.* proposed a model of the oxidized Pdx-P450cam complex based on NMR restraints. In combination with NMR chemical shift perturbations, they used paramagnetic relaxation enhancements (PRE) and residual dipolar couplings (RDC) to determine the distances and orientations of the complex.^[14] This model has been optimized *in silico* in several studies and used to predict the mechanism of electron transfer from Pdx to P450cam.^[20-22] It cannot, however, account for all mutagenesis results.^[23] For instance, it has been reported that the substitution of Arg66 of Pdx significantly alters the affinity for P450cam. This residue has been proposed to be the key residue to participate in salt bridge formation in the binding interface,^[23] which is not observed in the model.

Paramagnetic NMR techniques offer a new, alternative method for structure determination of protein complexes.^[20, 24-25] In particular lanthanoid tags provide very useful paramagnetic centers. The introduction of such tags at specific sites on the protein surface causes paramagnetic effects on the NMR signals of surrounding nuclei, both in the same protein and in a bound partner. Due to the very large magnetic moment of unpaired electrons, more than 600 times larger than that of protons, the interactions with nuclear spins extend to tens of Å, yielding well-defined, long-range restraints that can be used for structure determination. The paramagnetic effects used in this study are pseudocontact shifts (PCS), PRE and RDC induced by partial alignment by the anisotropy of the magnetic susceptibility of the lanthanoid. To obtain a high resolution structure, the position of the paramagnetic center needs to be rigid and well-defined relative to the protein. It has been demonstrated that double-armed lanthanoid tags provide such rigid attachment, which is reflected in large PCS and RDC.^[26-27]

Here, we report the structure of the oxidized Pdx-P450cam complex based on a set of 446 restraints for structure calculation obtained by using three double-armed paramagnetic lanthanoid tags attached to Pdx and P450cam. After the structure had been determined, we also solved the crystal structure of the complex. The solution structure based on paramagnetic restraints is represented by an ensemble of ten structures with an average RMSD from the mean of 1.3 Å for the position of Pdx. The crystal structure is identical to the solution structure within the variation of the ensemble. These results demonstrate the accuracy of the paramagnetic approach for structure determination. The structure shows the details of the molecular interaction and suggests two pathways for the electronic coupling between the metal centers. The NMR data also provide evidence for a minor state or set of states in solution, which could represent the encounter complex.

Results

Protein tagging with lanthanoid probes

To determine the structure of the Pdx-P450cam complex in solution, a set of intermolecular distance and orientation restraints were obtained from the effects of paramagnetic tags attached to both proteins. The tags were attached to Cys residues. To avoid interference, exposed Cys residues at positions 334 on P450cam and positions 73 and 85 on Pdx were substituted. These substitutions have been used in other studies.^[28-29] Other Cys residues are present in both proteins, but these were found not to interfere with the tagging. The tag used in this work is a caged lanthanoid NMR probe (CLaNP), version 7,^[30] which binds covalently to two Cys residues that are in close proximity. The two-point attachment of CLaNP-7 ensures a low mobility of the probe on the protein surface, and minimal averaging of the paramagnetic effects. Pairs of surface exposed cysteine residues were introduced at the proximal side of P450cam,

namely K126C/R130C/C334A (mutant A), and A333C/C334A/H337C (mutant B), as well as on Pdx, V6C/R12C/C73S/C85S (mutant I). Mutant I is located at the back of Pdx, relative to the iron-sulfur cluster but the positions A and B on P450cam are in proximity of the potential binding site for Pdx, so to determine whether CLaNP-7 attached to these sites affects the binding, the dissociation constants for the complex with Pdx were determined using calorimetry and were found to be very similar to the one for Pdx and WT P450cam (Figure 1), indicating that the CLaNP tag does not interfere with complex formation at these locations.

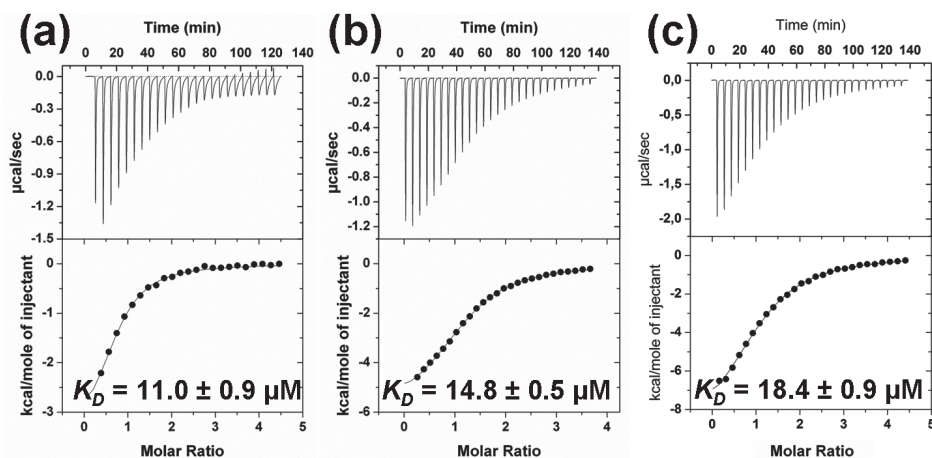


Figure 1. Isothermal titration calorimetry (ITC). The top panels of each graph represent the heat release upon titration of Pdx into a solution of P450cam. The bottom panels show the integrated areas for the individual peaks plotted against the Pdx / P450cam molar ratios. The errors of K_D represent the SD derived from the curve fits. (a) Tm^{3+} -CLaNP-7 P450cam mutant A sample. (b) Tm^{3+} -CLaNP-7 P450cam mutant B sample. (c) WT P450cam sample.

Intramolecular PCS were measured for P450cam and Pdx linked to CLaNP-7 loaded with Yb^{3+} , and used to determine the location of the lanthanoid ion and the orientation of principal components of the anisotropy of the magnetic susceptibility ($\Delta\chi$) tensor (see Chapter 2 for details). This information is required in order to use the intermolecular PCS as accurate restraints for structure determination. To obtain the restraints, the proteins were isotopically labeled with ^{15}N and the resonances of backbone amide groups were observed in standard two-dimensional heteronuclear correlation spectra. Thus, all NMR restraints are between the tags and backbone amide groups. Pdx was also perdeuterated to improve the spectral quality of the Pdx bound to P450cam. Assignments for Pdx were based on published data^[31] and for P450cam the assignments of the oxidized, camphor-bound form were based partly on published assignments^[32] and extended by comparison with assignments of other forms of P450cam available in

the lab (kindly provided by Simon Skinner at Leiden University) and the intramolecular PCS measured with Yb³⁺-CLaNP-7 (see Chapter 2 for details).

Intermolecular paramagnetic effects

Three types of interprotein paramagnetic effects were measured; PRE, PCS and RDC. P450cam carrying a CLaNP-7 loaded with a gadolinium ion (Gd³⁺) induces PRE on isotope labeled Pdx. As a control, an identical sample was used with CLaNP-7 loaded with a lutetium ion (Lu³⁺), a diamagnetic lanthanoid. The PRE depends on the inverse sixth power of the distance between the Gd³⁺ and the nucleus, providing sensitive intermolecular distance restraints.

Thulium (Tm³⁺) containing CLaNP-7 induces PCS that depend on the position of the nucleus within the frame defined by the $\Delta\chi$ tensor of the lanthanoid. Tm³⁺ also partially aligns the protein complex in solution causing residual dipolar couplings (RDC) that report on the orientation of the protein relative to the $\Delta\chi$ tensor. Representative data of these three paramagnetic effects are shown in Figure 2. For mutants A, B and I in total 509 intermolecular restraints were obtained (Table 1).

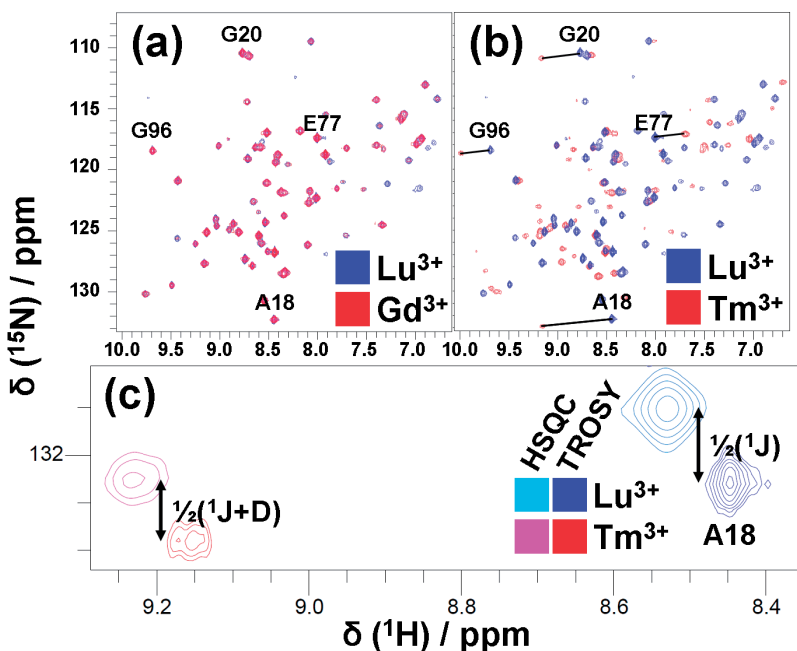


Figure 2. Intermolecular paramagnetic effects. ¹H-¹⁵N correlation spectra of ¹⁵N-labeled, perdeuterated Pdx in complex with P450cam mutant A tagged with CLaNP-7 containing either Lu³⁺, Gd³⁺ or Tm³⁺ illustrate intermolecular PRE (a), PCS (b) and RDC (c). In (b) several PCS are indicated by lines. Panel (c) illustrates how the ¹H-¹⁵N RDC is determined by comparison of HSQC and TROSY spectra. The difference in the ¹⁵N resonance position between the spectra is half the *J*-coupling for the diamagnetic sample and half the *J*-coupling plus half the RDC for the paramagnetic sample.^[33] Spectra were acquired at 14 T (600 MHz).

Table 1. Intermolecular paramagnetic NMR restraints. The correlations between observed and back-calculated data were assessed with Q (Eq. 2).

Sample	CLaNP-7	Inter-NMR	# restraints	Q (closed)	Q (open)
P450cam mutant A (K126C/R130C/C334A)	Gd ³⁺	PRE	60	0.25	0.22
	Tm ³⁺	PCS	54	0.03	0.04
		RDC	48	0.14	0.15
P450cam mutant B (A333C/H337C/C334A)	Gd ³⁺	PRE	(63)*	0.58	0.44
	Tm ³⁺	PCS	43	0.07	0.12
		RDC	37	0.34	0.32
Pdx mutant I (V6C/R12C/C73S/C85S)	Tm ³⁺	PCS	103	0.08	0.08
		RDC	101	0.28	0.36
Total			446		

*Left out in the calculation of the final ensemble, because these data were strongly affected by a minor state (see text).

Structure calculation

The structure calculation of the Pdx-P450cam complex was carried out by Dr. Mathias Hass (Leiden University). The top ten lowest energy solutions represent an ensemble with an average backbone RMSD of 1.3 (SD = 0.6) Å relative to the mean (Figure 3, panel i). A comparison of experimental (red symbols) and back-calculated restraints from the ensemble of structures (blue lines in Figure 3a-f for Pdx and Figure 3g-h for P450cam) shows that almost all of the PCS and RDC restraints are satisfied. Also the PRE-derived distances of mutant A agree well with the experimental data. Only mutant B tagged with Gd³⁺ shows poor correlations between back-calculated and experimentally obtained distances (Figure 3, panel f).

For several stretches of residues stronger PRE were measured than were predicted from the ensemble, and these effects are well outside the error margins. The residual PREs and their distribution over the Pdx surface are illustrated in Figure 4.

The PRE is known to be extraordinarily sensitive to lowly populated states for cases in which this state experiences a much higher PRE than the ground state. We conclude that the determined ensemble represents the major state that occasionally visits other conformations where Pdx is closer to the Gd³⁺-tag at P450cam residues 333 and 337. It is well established that in electron transfer complexes of weak to moderate affinity the encounter state is significantly populated.^[34] Thus, we attribute the observed dynamics within the Pdx-P450cam complex to an equilibrium between the well-defined, ET active state and the encounter state, similar to what was described for the ET complex of cytochrome c peroxidase and cytochrome c.^[35] It cannot be excluded that the CLaNP attached to mutant B in some way induces such a minor state. Further research is required to exclude this possibility and to map

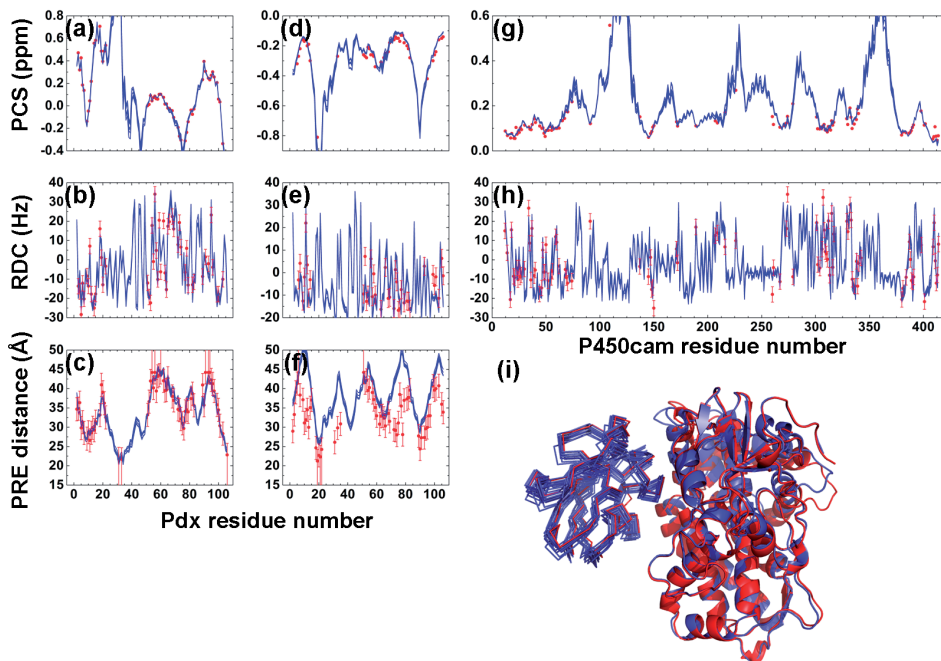


Figure 3. Violation analysis and solution ensemble of the Pdx-P450cam complex. The PCS (a, d, g), RDC (b, e, h) and PRE derived distances (c, f) are plotted against Pdx (a-f) and P450cam (g, h) residue numbers. Red circles and blue lines represent experimental and back-calculated effects for the ten lowest energy solutions, respectively. For PCS, the error bars are within the circular symbols. The panel (a), (b) and (c) represent mutant A, (d), (e) and (f) show the data for mutant B and (g) and (h) are for mutant I. The PCS and RDC data were obtained with CLaNP-7 loaded with Tm^{3+} and the PRE data using Gd^{3+} -CLaNP-7. (i) The crystal structure (red) and the top 10 lowest energy solution structures (blue) of the oxidized Pdx-P450cam complex are shown in a ribbon representation. The Pdx molecules are shown in C α traces. The overlaid structures represent an ensemble with an average backbone RMSD of 1.3 ± 0.6 Å relative to the mean.

the area sampled by Pdx in this encounter state. The final ensemble of the complex was calculated without the PRE restraints from mutant B, because they are strongly influenced by the minor state.

Crystal structure determination

Then, the crystal structure was solved to a resolution of 2.5 Å using mutant A of P450cam and Pdx C73S by Dr. Nojiri and co-workers (Osaka University, Japan). Curiously, P450cam is present with the access channel to the heme in the open state, similar to the substrate free structure of P450cam described by Lee *et al.*^[19] It is thought that camphor binding induces P450cam to close the channel,^[19] and thus the open state is probably due to the absence of camphor and not to presence of Pdx in our structure. In the catalytic cycle, Pdx donates an electron to the camphor

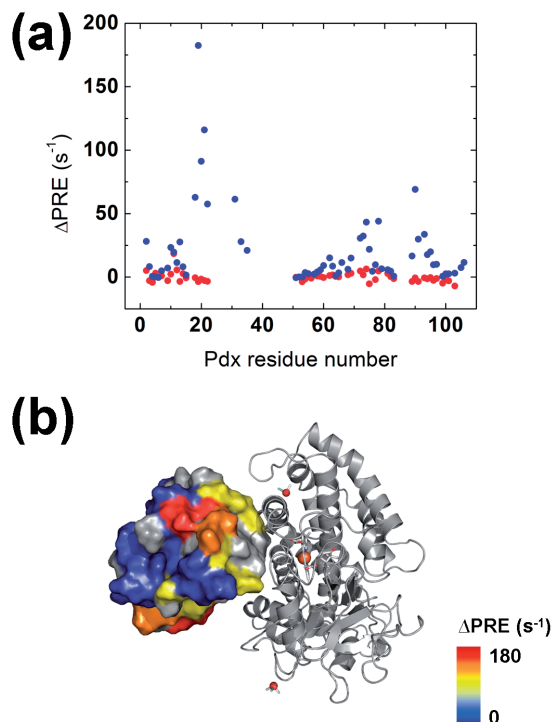


Figure 4. PRE residuals (Δ PRE) were derived by subtracting the back-calculated PREs from the experimentally obtained PREs. (a) Δ PRE were plotted against Pdx residue number. Red and blue points represent mutant A and mutant B, respectively. (b) Surface representation of Pdx, showing the residues affected by Gd^{3+} attached to mutant B. Pdx residues were color coded according to Δ PRE with ≥ 30 , red; 20-30, orange; 5-20, yellow; $< 5 \text{ s}^{-1}$, blue. Unobserved residues are in gray.

bound state only,^[23] so it appears counter intuitive that Pdx would induce opening at the same time. This point is discussed further at the end of the Discussion session. A careful comparison of the Pdx structure in the complex with the reduced and oxidized forms of Pdx,^[15] suggests that Pdx is in the reduced state in the crystal, which would indicate it was reduced by synchrotron radiation, as has been reported for free Pdx before.^[15]

Pdx is bound at the proximal side of the heme, in the same orientation as found in the solution structure (Figure 5a). An overlay of the backbone of Pdx observed in the crystal structure (in red) with those in the solution model (blue) after superposition of the P450cam molecules is shown in Figure 3i. It can be seen that the position of Pdx in the crystal structure falls within the ensemble observed in solution. The average RMSD for the $C\alpha$ atoms between the mean of the solution structures and the crystal structure is 1.7 \AA , which is indeed within the variation of the solution ensemble.

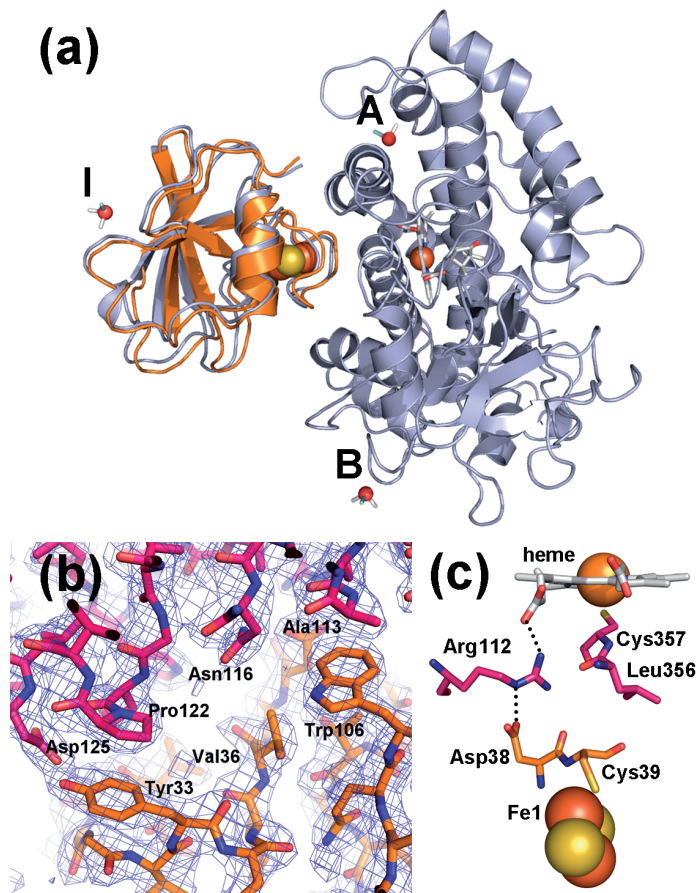


Figure 5. (a) The crystal structure (orange) and the solution structure closest to the mean (gray) of the oxidized Pdx-P450cam complex are shown in a ribbon representation with the P450cam structures aligned. The positions of Ln^{3+} ions, $\Delta\chi$ tensors and redox centers of Pdx and P450cam are depicted in sticks and spheres. (b) Detail of the interface showing a σ_A -weighted $2F_o - F_c$ map contoured at 1.0σ . P450cam and Pdx are shown with pink and orange carbons, respectively. (c) Detail of the interface showing residues that provide strong electronic coupling between the redox centers.

Description of the structure

The backbone structure of Pdx is essentially unchanged upon binding P450cam. The orientations of the side chains are expected to be most reliable in the crystal structure, because the NMR restraints used in this study were derived from backbone amide protons only. However, most of them are in very similar positions and conformations. The most striking difference is the orientation of Pdx Tyr33, which is far from P450cam in the solution complex, whereas in the crystal structure it makes contact with Asp125 of P450cam (Figure 5b) and the pyrrolidine ring of Pro122 of P450cam lies parallel

to the aromatic ring of Tyr33. Kinetic studies have shown the importance of this Tyr residue for the complex formation.^[23] Tyr33 is known to be flexible. It is positioned in different orientations in the various structures of Pdx^[15] and in solution it shows dynamics on the μ s-ms timescale in oxidized Pdx.^[36]

In previous studies, it was suggested that the formation of a salt bridge between Pdx Asp38 and P450cam Arg112 plays a vital role in the binding and electron transfer in the Pdx-P450cam complex.^[9, 13, 37] In the crystal and solution structures the residues are very close and a H bond can be formed between Asp38O δ 1 and Arg112N ϵ (2.73 Å, Figure 5c). The Arg residue is also H bonded to one of the heme propionates. On the basis of the model of the complex by Zhang *et al.* Pdx Trp106 has been proposed to function as a recognition site in the Pdx-P450cam interaction.^[14] In the crystal structure, this residue is close to the interface, interaction mostly with P450cam Ala113 (Figure 5b). A key residue that seems to stabilize the Pdx-P450cam complex is Pdx Arg66, which interacts with P450cam Glu76 by a salt bridge (Table 2). In addition to the prominent electrostatic interactions, Pdx-P450cam complex is predominantly stabilized by hydrophobic and van der Waals interactions. Table 2 summarizes those residues forming close contacts to the neighboring atoms with less than 4 Å apart. Val28 of Pdx is positioned in the proximity of Met121 and His361 of P450cam. The part of the Pdx [2Fe-2S] cluster loop including Asp38, Cys39, Gly40, Ser42 and Ser44 interacts with heme-binding loop of P450cam. Another residue suggested to be important by the previous study^[23] is P450cam Arg109 which forms a van der Waals interaction with Pdx Met70.

Table 2. Summary of interacting residues in the Pdx-P450cam binding interface (< 4 Å).

	Pdx	P450cam
Electrostatic interactions / H-bonds	Tyr33 (O η)	Asp125 (O δ)
	Asp38 (O δ)	Arg112 (N ϵ)
	Arg66 (N η)	Glu76 (O)
Van der Waals interactions	Val28	Met121, His361
	Tyr33	Pro122
	Asp38	Leu358
	Cys39	Leu356
	Gly40	Gln360
	Ser42	His352
	Ser44	Gly353
	Met70	Arg109
	Trp106	Ala113

Discussion

Here, we conducted three different paramagnetic NMR experiments to obtain 446 restraints for structural calculations, namely, PCS, PRE and RDC. Tm^{3+} containing CLaNP-7 induces PCS and RDC while Gd^{3+} containing CLaNP-7 causes PRE. Due to the difference in the distance dependency, PRE is known to be more sensitive to detect lowly populated states of protein conformations than PCS and RDC.^[38] As illustrated in the mutant B, the back-predicted PCS agree well with experiment and also the distances derived from the crystal structure matched those derived from the observed PCS within error, suggesting that PCS data mostly represent the major form of the complex. On the other hand, most Pdx residues experienced significantly larger PRE than predicted by the major form of the complex. The additional PRE is attributed to a minor state or ensemble of states in which Pdx visits sites much closer to the location B on the surface of P450cam. The existence of such encounter states has been well-documented for complexes of redox enzymes and electron carrier proteins.^[34] It is thought they facilitate ET by reducing the dimensionality of the search for the binding site.^[34] For mutant A and mutant I no additional PRE was detected, suggesting that in the encounter state Pdx mostly faces P450cam with the same face found in the final structure is located towards the site of mutation B, but not A.

A NMR based model of the complex has been reported before by Zhang *et al.*^[14] (no PDB entry). The most notable difference between our structure and the model proposed by Zhang *et al.* is the orientation of Pdx with the respect of P450cam. Our structure is rotated by about 90° around an axis roughly perpendicular to the P450cam heme. As a result, the major part of the interaction network in the binding interface differs from the previous model, with the prominent interaction between Pdx Asp38 and P450cam Arg112 being a notable exception. Zhang *et al.* derived their model by the combination of 23 RDC orientational restraints and seven PRE distances originating from Pdx labeled with a nitroxide spin label at Pdx Cys73.^[14] The experimental distances between Cys73 and the seven amide groups of P450cam were reported and could be compared and a good match was found (Table 3), given the uncertainty in the location of the radical due to the considerable rotational freedom of the MTSL spin label.

As predicted in the previous studies, extensive hydrophobic interaction networks dominate the binding interface.^[14] Site-directed mutagenesis studies have highlighted the importance of Pdx Trp106 for the complex formation.^[11] In our crystal structure, the indole ring of Trp106 is located in a hydrophobic pocket formed by carbon atoms from Arg106, Arg112, Ala113 and Asn116 of P450cam. Ala113 appears to be the prominent interaction residue. It allows the bulky side chain of Trp106 to be inserted in the binding interface. Tyr33 of Pdx is another key residue being responsible for the complex formation. Notably, NMR studies demonstrated that both Tyr33 and Trp106 are highly mobile when Pdx is free in solution.^[25] The dynamic nature of these residues

Table 3. Comparisons of PRE derived distance restraint.

P450cam residue #	Model of Zhang <i>et al.</i>		Our structure
	(experimental, Å) ^a	(back-calculated, Å) ^a	(back-calculated, Å) ^b
230	16.3	14.8	15.4
228	19.2	16.8	16.3
226	17.4	17.2	21.6
85	21.0	21.1	17.8
77	17.7	17.4	13.1
70	21.3	22.9	23.2
67	23.4	26.6	25.9

^a Previously reported.¹¹⁴¹ ^b Distances are reported from the nitrogen atom of the lysine side chain that was substituted by Cys for MTSL attachment to the backbone amide hydrogen of the given residue in Pdx.

has also been observed in X-ray crystallography and fluorescence measurements.^{115, 391} Presumably, when Pdx binds to P450cam, they play a role as recognition motifs and facilitate binding that is optimal for ET.

The shortest distance between the [2Fe-2S] cluster and heme iron in the ensemble of solution structures is 15.7 ± 0.4 Å and 16.3 Å in the crystal structure. To establish which amino acids contribute most to enhancing the electron transfer between the iron-sulfur cluster and the heme, the program HARLEM⁴⁰¹ was used. The results from HARLEM suggest two coupling pathways (Figure 5c) involving the Fe1 of the [2Fe-2S] cluster and ligand Cys39 of Pdx, and then either via P450cam Leu356 and Cys357 to the heme Fe or via Pdx Asp38 and P450cam Arg112 and the heme propionate to the conjugated heme ring. The latter route is in line with suggestions in previous studies.^{21, 23, 371} The rate of ET to oxidized P450cam has been reported to be 41 ± 1 s⁻¹ at 20°C.²³¹ With the given distance, the maximum, activationless rate is estimated by HARLEM to be much larger, on the order of 10⁵ s⁻¹. This implies that the measured rate can only represent true electron transfer if the reorganization energy is large (>1.3 eV), suggesting that the transfer could be gated. It remains unclear what conformational change could represent the gate.

It is interesting to compare the structures of the Pdx-P450cam complex with that of Pdx bound to its other partner, PdR (PDB entry 3LB8⁴¹¹). The total buried surface area for the PdR-Pdx complex is 1520 Å², larger than that of the Pdx-P450cam complex (1157 Å²). It has been suggested that PdR-Pdx complex formation is driven by one central PdR Arg310-Pdx Asp38 salt bridge and extensive hydrophobic interactions. An important electron transfer coupling pathway between the FAD group in PdR and the [2Fe-2S] cluster in Pdx has been predicted⁴¹¹ to involve a contact between PdR Trp330 and Pdx Cys39, analogous to the Pdx Cys39-P450cam Leu356 contact in the

Pdx-P450cam complex. Together, these results suggest that Pdx shuttles electrons from PdR to P450cam using the same electron entry and exit patch and with very similar interaction modes.

While this manuscript was under review, Tripathi *et al.* published the crystal structure of the Pdx-P450cam complex that was obtained via cross-linking of the two proteins.^[42] It is interesting to compare our complex with those reported in that study. Tripathi *et al.* found a position and orientation of Pdx relative to P450cam that is essentially identical to ours. Table 4 lists the interface characteristics of the different structures.

Table 4. Interface properties^a.

	Buried surface area (Å ²)	Gap volume index ^b	Fraction non-polar atoms
NMR ensemble (PDB entry 2M56) ^c	1107 ± 101	6.6 ± 0.9	0.37 ± 0.05
Crystal structure (PDB entry 3W9C) ^c	1266	5.1	0.33
Crystal structure (PDB entry 4JX1) ^d	1323 ± 15	5.4 ± 0.3	0.30 ± 0.03

^a determined with 2P21db^[43]; ^b Gap volume/Buried surface area; measure of the surface complementarity;

^c This work; ^d average of four models in the asymmetric unit.^[42]

The larger variation in the data for the NMR ensemble probably represents the uncertainty in the side chain positions, due to the absence of side chain restraints. The orientation of some residues in the interface differs between the two structures. In particular, P450cam residues Arg109, Asn116 and Leu358 are oriented differently (Figure 6).

In their structure of the reduced complex 2 (PDB entry 4JX1) Arg109 and Asn116 are hydrogen-bonded to Pdx Gln105 and Trp106, respectively, which is not the case in our structure. Arg109 is pointing in another direction, and something similar is seen in the other two structures reported by Tripathi *et al.* (PDB entries 4JWS and 4JWU), so the exact role of those residues in stabilizing the interaction with Pdx via Trp106 need to be established. It may differ for the oxidized and reduced states of the complex. This is important because, as indicated by Tripathi *et al.*, the Arg106 is located in the C-helix, which could act as a relay between the Pdx binding site and the opening of P450cam via the B' and F and G helices. Tripathi *et al.* also found that P450cam is present in a state that resembles the open state of P450cam, similar to our crystal structure. It is not clear whether the open state found in the crystal structures is a consequence of crystal packing. In both cases, contacts of the F or G helices with neighboring molecules in the crystal are observed, which could imply that only the open state of the complex is able to crystallize. We have fitted our NMR data with

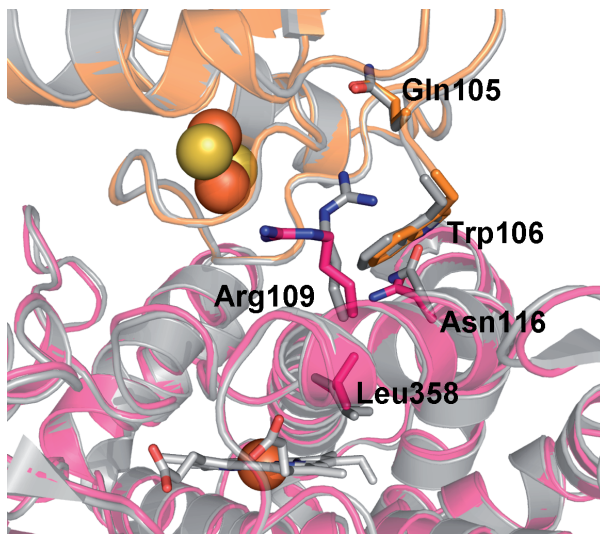


Figure 6. Overlay of the crystal structures of the oxidized Pdx P450cam complex (pink and orange, PDB entry 3W9C) and the reduced state (gray, PDB entry 4JX1).^[42]

the open and closed states of P450cam, leading to the same position and orientation of Pdx relative to P450cam and the quality of the fit was similar (see Table 1). Further NMR experiments that are able to distinguish between the open and closed states of P450cam in the complex are required to establish whether Pdx binding causes the opening of P450cam also in solution.

In conclusion, this work has shown that paramagnetic NMR spectroscopy is able to produce accurate structures of protein complexes in solution. In this case, the backbone structure of the free protein was used and treated as a rigid body. Allowing for backbone rearrangement upon binding is possible in principle with a more extensive dataset. Paramagnetic effects on side chains could also be added to determine details of the interface. The advantage of the approach is that the paramagnetic effects in the complex can be determined rapidly, using only sensitive two-dimensional experiments, such as HSQC and TROSY spectra. This allows application to dilute samples, which is especially relevant for complexes of large proteins.

Experimental Section

Chemicals

CLaNP-7 was synthesized and chelated to Lu^{3+} , Gd^{3+} and Tm^{3+} ions as reported previously.^[30] The plasmids harboring the cDNA of Pdx and P450cam were generous gift from Prof. Stephen G. Sligar, University of Illinois at Urbana–Champaign, U.S.^[44] The genes were subcloned into the pET28a expression vectors using NcoI and XhoI

restriction enzymes, without use of the His tag sequence. Column material was obtained from GE Healthcare, Munich, Germany.

Mutagenesis

Site-directed mutagenesis was performed using QuikChange protocol (Stratagene, La Jolla, CA).

Protein production

^{15}N , ^2H enriched Pdx was produced and purified as previously described^[8] with an additional purification step. The resuspended cells (20 mM KPi , pH 8.0, 50 mM KCl, 1 mM DNase, 1 mM PMSF) were disrupted by French-press. Following centrifugation at 35000 r.p.m. for 30 minutes at 4°C, the sample was loaded on a HiTrap DEAE sepharose FF anion-exchange column. The protein was eluted with a linear gradient of 0.1–0.4 M KCl in 20 mM KPi , pH 8.0 and the brown fractions were collected. Ammonium sulfate crystals were added (30% w/v) and the solution was stirred for 20 minutes at 4°C. Subsequently, the sample was centrifuged for 20 minutes to remove precipitation and the supernatant was applied to a HiTrap Phenyl FF hydrophobic column. The brown fractions containing Pdx were collected after elution with a linear gradient 30–0 % ammonium sulfate in 20 mM KPi , pH 8.0. Finally, the pooled fractions were briefly buffer-exchanged and concentrated by ultrafiltration using a Centricon (Millipore) and injected into a Sephadex G75 size exclusion column pre-equilibrated with 50 mM Tris-HCl, pH 7.4, 100 mM KCl and 1 mM camphor. The fractions with $A_{325\text{nm}}/A_{280\text{nm}}$ larger than 0.68 were pooled and concentrated. The concentration of Pdx was determined with $\epsilon_{412\text{nm}} = 11.0 \text{ mM}^{-1}\text{cm}^{-1}$.^[45] Approximately 12 mg of Pdx was obtained from 1 L of culture. Isotopically enriched P450cam variants were produced and purified as previously described for the wild type protein.^[46] In addition to the established purification protocol, a HiTrap Phenyl FF hydrophobic column was used at the end of purification procedure to obtain a $A_{391\text{nm}}/A_{280\text{nm}}$ value greater than 1.40. Approximately, 50 mg of P450cam was obtained from 1 L of culture.

Ln^{3+} -CLaNP-7 labeling

Purified double-cysteine P450cam and Pdx samples were incubated with 5 mM DTT in 20 mM KPi , pH 7.4, 150 mM KCl, 1 mM camphor, for 1 hour on ice. DTT was removed by using a PD-10 column. The protein solution was mixed with seven molar equivalents of Ln^{3+} -CLaNP-7 and incubated overnight at 4°C. Unlabeled protein, protein oligomers and surplus of Ln^{3+} -CLaNP-7 were removed by three chromatography steps, on a HiTrap Q HP anion-exchange column, a HiTrap Phenyl FF hydrophobic column and a Superose 12 size exclusion column.

NMR samples and experiments

NMR samples contained 50–100 μM [^2H , ^{15}N] Pdx (WT) or [^2H , ^{15}N] P450cam (C334A) with three molar equivalents of Ln^{3+} -CLaNP-7 labeled P450cam or Pdx mutants,

respectively, in 50 mM Tris-HCl, pH 7.4, 100 mM KCl, 1 mM camphor and 6% D₂O. 2D ¹⁵N-¹H HSQC and ¹⁵N-¹H TROSY spectra^[47] were recorded at 290 K on a Bruker Avance III 600 MHz spectrometer equipped with a TCI-Z-GRAD cryoprobe. NMR data were processed in NmrPipe^[48] and analyzed in CCPNMR.^[49]

NMR assignment

The assignments for oxidized Pdx amide resonances were based on previous work.^[31] For P450cam the assignments of the oxidized, camphor-bound form were based partly on published assignments^[32] and extended by comparison with assignments of other forms of P450cam available in the lab (kindly provided by Dr. Simon Skinner at Leiden University) and the intramolecular PCS measured with Yb³⁺-CLaNP-7 (see Chapter 2 for details).

Restraint analysis

Gd³⁺-induced intermolecular PRE ($R_{2,para}$) were determined as described by Battiste and Wagner^[50] and converted to restraints as published.^[35] The ratios of the peak height, I_{para}/I_{dia} , of amide signals in the presence of Gd³⁺-CLaNP-7 labeled binding partner (I_{para}) and the corresponding Lu³⁺-CLaNP-7 labeled protein (I_{dia}) were normalized by dividing them by the averaged values of the ten largest I_{para}/I_{dia} ratios (0.96, 1.09 and 0.94 for P450cam mutant A, P450cam mutant B and Pdx mutant I samples, respectively). PRE ($R_{2,para}$) were converted into distances using Eq. 1:

$$r = \sqrt[6]{\frac{f_{bound} \cdot f_{labeled}}{R_{2,para}} \frac{\gamma^2 g^2 \beta^2 \mu_0^2 (S+1) S}{240\pi^2} \left(4\tau_c + \frac{3\tau_c}{1 + \omega_h^2 \tau_c^2} \right)} \quad [1]$$

where r is the distance between Gd³⁺ ion and a given amide proton; f_{bound} is the fraction of the bound ¹⁵N protein ($f_{bound} = 0.9$); $f_{labeled}$ is the fraction of the CLaNP-7 labeled protein ($f_{labeled} = 0.8-0.9$); γ is the gyromagnetic ratio of proton; g is the electronic g factor; β is the Bohr magneton; ω_h is the Larmor frequency of protons; μ_0 is vacuum permeability; S is spin quantum number for Gd³⁺ ($S = 7/2$); τ_c is the rotational correlational time of Gd³⁺-proton vector. τ_c was estimated to be 30 ns using HYDRONMR^[51] for the Pdx-P450cam complex. The intermolecular distances were calculated according to Eq. 1 and divided in three classes of restraints: i) residues with resonance peaks that completely broaden out in the paramagnetic spectrum. For these residues, only an upper limit of the distance was calculated. ii) residues with resonances visible in the paramagnetic spectrum and with $R_{2,para} \geq 3.0 \text{ s}^{-1}$. Error margins were set to $\pm 3 \text{ \AA}$ to accommodate for experimental errors. iii) residues with $R_{2,para} < 3.0 \text{ s}^{-1}$. These residues were considered to be too remote from the Gd³⁺ ion to cause a significant PRE and therefore only the lower limit was calculated and found to be 44 Å for mutant A.

The quality of fit between observed (O^{obs}) and back-predicted (O^{sim}) observables (PRE, PCS, RDC) was expressed in a Q values, Eq. 2. Note that the sum of observable

and back-predicted values is used in the denominator because this makes the Q insensitive to the phenomenon that small O^{obs} with large O^{sim} give larger Q values than the other way around, unlike the standard Q with only O^{obs} in the denominator.

$$Q = \sqrt{\frac{\sum_i \{O^{\text{obs}}(i) - O^{\text{sim}}(i)\}^2}{\sum_i \{|O^{\text{obs}}(i)| + |O^{\text{sim}}(i)|\}^2}} \quad [2]$$

Isothermal titration calorimetry

Calorimetric measurements were performed on a VP-ITC (MicroCal). The sample cell contained 50 μM of CLaNP-7 labeled P450cam mutants and the injection syringe 1 mM of WT Pdx in 50 mM Tris-HCl, pH 7.4, 100 mM KCl, 1 mM camphor. Titration experiments were carried out at 290 K with 30 injections of 10 μL with 20 sec duration and 350 sec between each injection. The sample was mixed at 351 r.p.m.

Interface calculation

The buried surface areas were calculated using naccess^[52] and ASA.py,^[53] with similar results. For the Pdx-Pdx complex (PDB entry 3LB8), the interface area found by us is much larger than the small area reported,^[41] for reasons that are unclear.

X-ray crystallography

Cocrystallization, data collection and processing of Pdx-P450cam complex were performed by Dr. Nojiri and co-workers (Osaka University, Japan).

Note: The atomic coordinates of the solution structures and the NMR restraints as well as atomic coordinates and structure factors of the crystal structure have been deposited in the Protein Data Bank, www.pdb.org (PDB ID codes 2M56 and 3W9C, respectively).

References

1. T. L. Poulos, *Biochem Biophys Res Co*, **2005**, 338, 337-345.
2. N. Strushkevich, F. MacKenzie, T. Cherkesova, I. Grabovec, S. Usanov, H. W. Park, *Proc Natl Acad Sci U S A*, **2011**, 108, 10139-10143.
3. I. F. Sevrioukova, T. L. Poulos, *Arch Biochem Biophys*, **2011**, 507, 66-74.
4. C. B. Brewer, J. A. Peterson, *J Biol Chem*, **1988**, 263, 791-798.
5. M. Unno, H. Shimada, Y. Toba, R. Makino, Y. Ishimura, *J Biol Chem*, **1996**, 271, 17869-17874.
6. J. D. Lipscomb, S. G. Sligar, M. J. Namtvedt, I. C. Gunsalus, *The Journal of biological chemistry*, **1976**, 251, 1116-1124.
7. T. Tosha, S. Yoshioka, K. Ishimori, I. Morishima, *J Biol Chem*, **2004**, 279, 42836-42843.
8. S. S. Pochapsky, T. C. Pochapsky, J. W. Wei, *Biochemistry*, **2003**, 42, 5649-5656.
9. M. Holden, M. Mayhew, D. Bunk, A. Roitberg, V. Vilker, *J Biol Chem*, **1997**, 272, 21720-21725.
10. H. Shimada, S. Nagano, Y. Ariga, M. Unno, T. Egawa, T. Hishiki, Y. Ishimura, *J Biol Chem*, **1999**, 274, 9363-9369.
11. S. G. Sligar, Debrunne.Pg, J. D. Lipscomb, M. J. Namtvedt, I. C. Gunsalus, *Proc Natl Acad Sci U S A*, **1974**, 71, 3906-3910.
12. T. C. Pochapsky, G. Ratnaswamy, A. Patera, *Biochemistry*, **1994**, 33, 6433-6441.

13. M. J. Hintz, D. M. Mock, L. L. Peterson, K. Tuttle, J. A. Peterson, *J Biol Chem*, **1982**, *257*, 14324-14332.
14. W. Zhang, S. S. Pochapsky, T. C. Pochapsky, N. U. Jain, *J Mol Biol*, **2008**, *384*, 349-363.
15. I. F. Sevrioukova, *J Mol Biol*, **2005**, *347*, 607-621.
16. I. Schlichting, J. Berendzen, K. Chu, A. M. Stock, S. A. Maves, D. E. Benson, R. M. Sweet, D. Ringe, G. A. Petsko, S. G. Sligar, *Science*, **2000**, *287*, 1615-1622.
17. Y. T. Lee, E. C. Glazer, R. F. Wilson, C. D. Stout, D. B. Goodin, *Biochemistry*, **2011**, *50*, 693-703.
18. A. R. Dunn, I. J. Dmochowski, A. M. Bilwes, H. B. Gray, B. R. Crane, *Proc Natl Acad Sci U S A*, **2001**, *98*, 12420-12425.
19. Y. T. Lee, R. F. Wilson, I. Rupniewski, D. B. Goodin, *Biochemistry*, **2010**, *49*, 3412-3419.
20. G. Otting, *Annu Rev Biophys*, **2010**, *39*, 387-405.
21. F. Wallrapp, D. Masone, V. Guallar, *J Phys Chem A*, **2008**, *112*, 12989-12994.
22. M. Freindorf, Y. Shao, J. Kong, T. R. Furlani, *J Inorg Biochem*, **2008**, *102*, 427-432.
23. V. Y. Kuznetsov, T. L. Poulos, I. F. Sevrioukova, *Biochemistry*, **2006**, *45*, 11934-11944.
24. P. H. Keizers, M. Ubbink, *Prog Nucl Magn Reson Spectrosc*, **2011**, *58*, 88-96.
25. J. Koehler, J. Meiler, *Prog Nucl Magn Reson Spectrosc*, **2011**, *59*, 360-389.
26. P. H. Keizers, J. F. Desreux, M. Overhand, M. Ubbink, *J Am Chem Soc*, **2007**, *129*, 9292-9293.
27. P. H. Keizers, A. Saragliadis, Y. Hiruma, M. Overhand, M. Ubbink, *J Am Chem Soc*, **2008**, *130*, 14802-14812.
28. D. P. Nickerson, L. L. Wong, *Protein Eng*, **1997**, *10*, 1357-1361.
29. I. F. Sevrioukova, C. Garcia, H. Li, B. Bhaskar, T. L. Poulos, *J Mol Biol*, **2003**, *333*, 377-392.
30. W. M. Liu, P. H. Keizers, M. A. Hass, A. Blok, M. Timmer, A. J. Sarris, M. Overhand, M. Ubbink, *J Am Chem Soc*, **2012**, *134*, 17306-17313.
31. T. A. Lyons, G. Ratnaswamy, T. C. Pochapsky, *Protein Sci*, **1996**, *5*, 627-639.
32. B. OuYang, S. S. Pochapsky, M. Dang, T. C. Pochapsky, *Structure*, **2008**, *16*, 916-923.
33. G. Kontaxis, G. M. Clore, A. Bax, *J Magn Reson*, **2000**, *143*, 184-196.
34. M. Ubbink, *Biochem Soc Trans*, **2012**, *40*, 415-418.
35. A. N. Volkov, J. A. Worrall, E. Holtzmann, M. Ubbink, **2006**, *103*, 18945-18950.
36. N. Sari, M. J. Holden, M. P. Mayhew, V. L. Vilker, B. Coxon, *Biochemistry*, **1999**, *38*, 9862-9871.
37. H. Koga, Y. Sagara, T. Yaoi, M. Tsujimura, K. Nakamura, K. Sekimizu, R. Makino, H. Shimada, Y. Ishimura, K. Yura, et al., *Febs Lett*, **1993**, *331*, 109-113.
38. S. Scanu, J. Forster, M. G. Finiguerra, M. H. Shabestari, M. Huber, M. Ubbink, *Chembiochem*, **2012**, *13*, 1312-1318.
39. P. S. Stayton, S. G. Sligar, *Biochemistry*, **1991**, *30*, 1845-1851.
40. I. Kurnikov, **2000**.
41. I. F. Sevrioukova, T. L. Poulos, I. Y. Churbanova, *J Biol Chem*, **2010**, *285*, 13616-13620.
42. S. Tripathi, H. Li, T. L. Poulos, *Science*, **2013**, *340*, 1227-1230.
43. M. J. Basse, S. Betzi, R. Bourgeas, S. Bouzidi, B. Chetrit, V. Hamon, X. Morelli, P. Roche, *Nucleic Acids Res*, **2013**, *41*, D824-827.
44. B. P. Unger, I. C. Gunsalus, S. G. Sligar, *J Biol Chem*, **1986**, *261*, 1158-1163.
45. I. C. Gunsalus, G. C. Wagner, *Methods Enzymol*, **1978**, *52*, 166-188.
46. L. Rui, S. S. Pochapsky, T. C. Pochapsky, *Biochemistry*, **2006**, *45*, 3887-3897.
47. K. Pervushin, R. Riek, G. Wider, K. Wuthrich, *Proc Natl Acad Sci U S A*, **1997**, *94*, 12366-12371.
48. F. Delaglio, S. Grzesiek, G. W. Vuister, G. Zhu, J. Pfeifer, A. Bax, *J Biomol NMR*, **1995**, *6*, 277-293.
49. W. F. Vranken, W. Boucher, T. J. Stevens, R. H. Fogh, A. Pajon, M. Llinas, E. L. Ulrich, J. L. Markley, J. Ionides, E. D. Laue, *Proteins*, **2005**, *59*, 687-696.
50. J. L. Battiste, G. Wagner, *Biochemistry*, **2000**, *39*, 5355-5365.
51. J. Garcia de la Torre, M. L. Huertas, B. Carrasco, *J Magn Reson*, **2000**, *147*, 138-146.
52. S. J. Hubbard, J. M. Thornton, **1993**.
53. B. K. Ho, **2007**.

CHAPTER 4

Hot spot residues in the cytochrome P450cam- putidaredoxin binding interface

Part of this chapter was published as Hiruma, Y.; Gupta, A.; Kloosterman, A.; Olijve, C.; Olmez, B.; Hass, M.A.; Ubbink, M. (2014) Hot Spot Residues in the Cytochrome P450cam-Putidaredoxin Binding Interface, ChemBioChem 15, 80-86

Abstract

Cytochrome P450cam (P450cam) is a heme containing monooxygenase that catalyzes hydroxylation of D-camphor to produce 5-exo-hydroxycamphor. The catalytic cycle of P450cam requires two electrons, both of which are donated by a [2Fe-2S] cluster containing ferredoxin, putidaredoxin (Pdx). Recently, atomic resolution structures of the Pdx-P450cam complex have been solved by X-ray crystallography as well as paramagnetic NMR spectroscopy. The binding interface revealed the potential electron transfer pathways and interactions between Pdx Asp38 and P450cam Arg112 as well as hydrophobic contacts between Pdx Trp106 and P450cam residues. Several polar residues are found in the interface that had not been recognized to be relevant for binding before. In this study, site-directed mutagenesis, kinetic measurements and NMR studies were employed to probe the energetic importance and role of the polar residues in the Pdx-P450cam interaction. A double mutant cycle (DMC) analysis of kinetic data shows that favorable interactions exist between Pdx Tyr33 and P450cam Asp125 as well as Pdx Ser42 and P450cam His352. The results show that alanine substitutions of these residues and several others do not influence the rates of electron transfer. It is concluded that these polar interactions contribute to partner recognition rather than electronic coupling of the redox centers.

Introduction

Cytochrome P450 (P450) is a superfamily of heme-containing monooxygenases that participate in a variety of biological metabolisms. From bacteria to humans, P450 members are found in all kingdoms and at least 15,000 P450 genes have been currently reported.^[1] The most common reaction that P450 enzymes catalyze is the insertion of oxygen atom into a chemically inert organic substrate ($R-H + O_2 + 2H^+ + 2e \leftrightarrow R-OH + H_2O$). Due to their specificities and efficiencies, P450 enzymes are widely applied in industrial fields including bioconversion, bioremediation and biosensors.^[2] One of the most extensively characterized P450 family members is P450cam (CYP101A1). P450cam from *Pseudomonas putida* catalyzes the regio- and stereo-specific hydroxylation of D-camphor. The activation and cleavage of the oxygen molecule in the P450cam catalytic cycle is accompanied with two electron transfers (ETs) from the physiological ET partner protein, putidaredoxin (Pdx). Pdx shuttles electrons between the FAD-containing putidaredoxin reductase (Pdr) and the monooxygenase, P450cam.^[3] Interestingly, ferric P450cam can accept the first electron from diverse chemical reductants and Pdx homologues (ET1), but the second (ET2) requires Pdx as donor. The stringent requirement for Pdx in ET2 has been explained by the effector activity. Pdx not only provides the electron but also causes the start of the catalytic reaction.^[4-6] However, the underlying mechanism of the effector role of Pdx remains under debate. Recently, X-ray crystallography and NMR have uncovered the three dimensional structures of Pdx-P450cam complex (see chapter 3 for the details).^[7, 8] Pdx binds to the proximal surface of P450cam in which the intermolecular distance between iron sulfur cluster and heme iron is approximately 16 Å. Compared with the previously proposed model of Zhang *et al.*,^[9] Pdx is rotated nearly 90° relative to P450cam. The crystal structures of the Pdx-P450cam complex show which residues constitute the interface.^[7, 8] The functional role of Pdx Trp106 had been recognized as early as the 1970's.^[5] In the complex it is in contact with Ala113 of P450cam.^[7] Another key interaction, between Pdx Asp38 and P450cam Arg112, was confirmed by the atomic resolution structures. The potential hydrogen bond between the side chains of these residues is thought to be essential for one of the electron transfer coupling pathways.^[8, 10] Moreover, several other polar residues are found in the interface that had not been recognized to be relevant for binding before. For instance, in the crystal structures, Pdx Ser42 and Ser44 are positioned in the close proximity to P450cam His352 (less than 5 Å). Another potentially important residue, P450cam His361 is located at the core of the binding interface. The imidazole side chain of P450cam His361 is pointed towards the [2Fe-2S] cluster of Pdx and had previously been proposed to be the part of the ET2 pathway.^[11] The flexibility of Pdx Tyr33 is vital to the interaction of Pdr-Pdx complex. Upon binding to P450cam, the side chain of Pdx Tyr33 adapts a rigid configuration and forms a hydrogen bond to P450cam Asp125. In this study, site-directed mutagenesis, kinetics and NMR studies were employed

to further probe energetic importance and role of the polar residues involved in Pdx-P450cam interaction. Our experimental results indicated that turnover rates of ET remain intact upon the substitution of these residues by alanine. However, the mutations influence the dissociation rates and binding affinities of the Pdx-P450cam complex. The relevance of the work for understanding the effector activity of Pdx binding will be addressed in discussion.

Results

Previous mutagenesis studies highlighted that the key residues in the formation of the Pdx-P450cam complex and ET include Pdx Asp38, Arg66, Trp106 and P450cam Arg109 and Arg112.^[11, 12] The crystal structures of Pdx-P450cam complex revealed a number of other residues that exhibit close contacts ($< 4\text{\AA}$) in the interface and participate in polar interactions.^[7, 8] To characterize the contributions of residues, Pdx Ser42 and Ser44 and P450cam His352 and His361 were substituted to alanine. In addition, Pdx Y33A and P450cam D125A constructs were prepared. These residues are not found in the core but on the rim of the binding interface, yet were predicted to be important in partner recognition.^[8, 11] Figure 1 illustrates the mutation sites used in this study.

To investigate the effects of the mutations on the ET1 reaction, pre-steady state kinetics were studied by stopped-flow spectrophotometry. As described in the early studies,^[13, 14] the rate of ET1 can be derived from the rate of formation of carbon

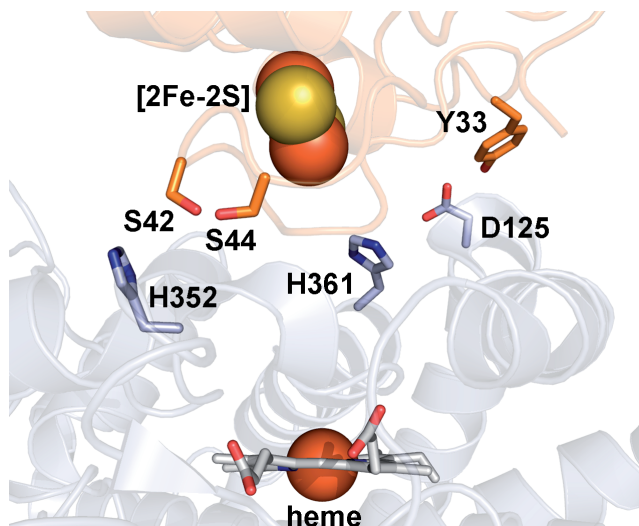
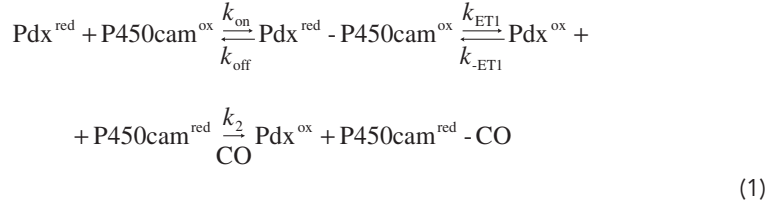


Figure 1. The crystal structure of the Pdx-P450cam complex (PDB entry, 3W9C)^[8] is shown in a ribbon representation. The residues substituted by alanine and the heme are labeled and shown in sticks. The [2Fe-2S] cluster is represented in spacefill.

monoxide (CO) bound ferrous P450cam (P450cam^{red}-CO). Equation 1 shows the model of the formation of P450cam^{red}-CO species.



The Soret absorption maximum at 447 nm of P450cam^{red}-CO was monitored for reactions with increasing concentrations of reduced Pdx (Pdx^{red}). The reverse ET reaction of Pdx is neglected because $k_2[\text{CO}] \gg k_{\text{-ET1}}$.^[14] The reaction can be described by a rapidly established binding/dissociation equilibrium and a slow ET reaction. Thus, ten milliseconds after mixing, a steady state condition is valid for Pdx^{red}-P450cam^{ox}, and its concentration can be taken to be constant. The data are then described by the rate constant k_{obs} .^[15]

$$k_{\text{obs}} = \frac{k_{\text{ET1}} \cdot k_{\text{on}} \cdot [\text{Pdx}]}{k_{\text{off}} + k_{\text{ET1}} + k_{\text{on}} \cdot [\text{Pdx}]} \quad (2)$$

Because $k_{\text{ET1}} \ll k_{\text{off}}, k_{\text{on}} \cdot [\text{Pdx}]$, equation (2) can be written as:

$$k_{\text{obs}} = k_{\text{ET1}} \frac{[\text{Pdx}]}{K_D + [\text{Pdx}]} \quad (3)$$

By varying the [Pdx], K_D and k_{ET1} can be fitted. The first points of the stopped-flow curves, before the steady state of the intermediate is established, contain information about the rate of formation of the Pdx^{red}-P450cam^{ox} complex. Therefore the reaction curves were simulated numerically to extract the values of k_{ET1} , K_D and k_{off} (Figure 2).

The circles in Figure 2A represent the experimental datasets of P450cam H352A for a range of concentrations of Pdx^{red}. The curves were simulated globally to extract the kinetic parameters. Figure 2B shows the simulated concentrations for all species as function of reaction time for [Pdx] = 2.5 μM , as an example. Note the subtle biphasic behavior representing the pre-steady state and steady state phases of the reaction. The k_{off} values are derived from the first few time points, limiting their precision, whereas those of k_{ET1} and K_D are derived from the steady state phase and are better defined. The k_{on} was calculated from the K_D and k_{off} values ($K_D = k_{\text{off}} / k_{\text{on}}$). Table 1 summarizes k_{ET1} , K_D , k_{on} and k_{off} for the WT and mutant complexes.

Figure 2C shows the simulated k_{obs} values, obtained from an exponential fit of the simulated [P450cam^{red}-CO] as a function of time to present the results in a familiar way. An advantage of the numerical simulation is that no steady-state assumption is

made. With this assumption the binding and dissociation are taken to be so fast that a steady state is reached for the $\text{Pdx}^{\text{red}}\text{-P450cam}^{\text{ox}}$ species within the dead time of the stopped-flow apparatus. In that case, the absorption changes for the formation of the $\text{P450cam}^{\text{red}}\text{-CO}$ species obey simple exponential behavior, yielding the classical k_{obs} . For low Pdx concentrations, the simulated k_{obs} values deviate from this k_{obs} . Also no pseudo first-order assumption ($[\text{Pdx}] \gg [\text{P450cam}]$) needs to be made. The simulations show that for low $[\text{Pdx}]$ this condition is not met, which slightly influences the rates obtained.

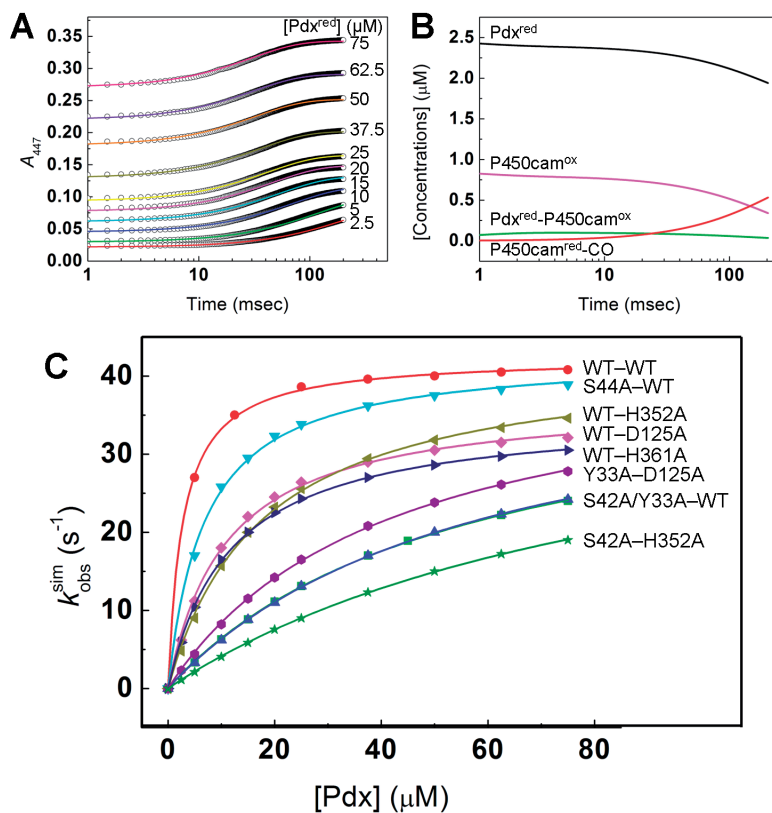


Figure 2. Analysis of ET1 reaction by stopped-flow spectrophotometry. A) A_{447} is plotted as a function of the reaction time for several Pdx^{red} concentrations. The k_{ET1} curves were simulated numerically to obtain k_{off} and K_{D} . B) The simulated concentrations of all species as function of time for the curve of $[\text{Pdx}] = 2.5 \mu\text{M}$ are plotted. C) $k_{\text{obs}}^{\text{sim}}$ was plotted against concentration of Pdx^{red} for the WT and mutant proteins. The labels indicate the Pdx and P450cam WT or variants, respectively. The simulated k_{obs} values were obtained by an exponential fit of the simulated curves for the $[\text{P450cam}^{\text{red}}\text{-CO}]$, as shown in panel B. The stopped flow measurement was carried out by 1:1 mixing of $2 \mu\text{M}$ $\text{P450cam}^{\text{ox}}$ and 5–150 μM Pdx^{red} at 22°C in CO saturated 50 mM Tris-HCl buffer, pH 7.4, containing 100 mM KCl, 1 mM camphor, 1 mM glucose and an oxygen-scrubbing system.

Table 1. Kinetic parameters of ET1. The reaction conditions were the same as given in the caption of Figure 2.

Pdx	P450cam	k_{ET1} (s ⁻¹)	K_D (μM)	k_{on} (10 ⁷ M ⁻¹ s ⁻¹)	k_{off} (10 ² s ⁻¹)
WT	WT	42 ± 1	2.2 ± 0.2	3.6–11.4	0.8–2.5
Y33A	WT	40 ± 1	50 ± 5	6–8	30–40
S42A	WT	42 ± 2	55 ± 8	5.5–7.5	30–41
S44A	WT	42 ± 1	6 ± 0.5	6.7–11.7	4–7
WT	D125A	36 ± 2	9 ± 0.5	5.6–11.1	5–10
WT	H352A	42 ± 2	16 ± 2	5.6–10.6	10–19
WT	H361A	35 ± 3	11 ± 2	7–13	7–12
Y33A	D125A	42 ± 1	38 ± 2	2.6–5.3	10–20
S42A	H352A	42 ± 2	90 ± 10	2.2–5.6	20–50

The k_{ET1} value of wild type (WT) complex was determined to be $42 \pm 1 \text{ s}^{-1}$, which corresponds to the previously reported value of $41 \pm 1 \text{ s}^{-1}$.^[11] Compared to WT complex, k_{ET1} values of Pdx and P450cam variants remain intact. In contrast, K_D values for Pdx Y33A and S42A mutants were 20–30-fold higher than for WT (see Table 1). The k_{off} values of these variants were one order of magnitude higher, indicating that the substitution of Pdx Tyr33 and Ser42 alter the binding affinity rather than ET1. The mutations of P450cam Asp125 and His352, which form hydrogen bonds to Pdx Tyr33 and Ser42, respectively, result in modest changes of K_D with four to eight fold increase. To investigate the extent of the interaction of Tyr33_(Pdx)-Asp125_(P450cam) and Ser42_(Pdx)-His352_(P450cam), double-mutant cycle (DMC) analysis was performed. The free energy of interaction, $\Delta\Delta G_{int}$ (see Experimental Procedures, eq. 6),^[16] between the residue pairs was calculated to be -4.2 kJ/mol and -3.7 kJ/mol for Tyr33_(Pdx)-Asp125_(P450cam) and Ser42_(Pdx)-His352_(P450cam), respectively. Since the experimental error of $\Delta\Delta G_{int}$ for this system was calculated to be ± 1.0 – 1.7 kJ/mol , both cases indicate significant favorable interactions.

Having established the effect of mutations on the ET1 process, we examined the steady state kinetics of NADH oxidation. Camphor turnover activity of P450cam is known to be tightly coupled with two ET events (ET1 and ET2). Since the ET steps are rate limiting in the P450cam reaction cycle,^[14] the catalytic turnover was measured by the NADH consumption rate in the PdR-Pdx-P450cam reconstituted system as previously described.^[17] In this assay, Pdx is kept in the reduced state by ensuring $[\text{PdR}] \gg [\text{P450cam}]$. The spectral changes at 340 nm, indicative of NADH oxidation, were used to determine the steady state P450cam turnover rate. To minimize the contributions of the binding affinities to the ET rates, the concentration of Pdx was 100 μM, which is above the K_D values determined in the stopped-flow experiments. As shown in Table 3, the catalytic turnover of WT_(Pdx)-WT_(P450cam) complex was found

to be $38.2 \pm 0.2 \text{ s}^{-1}$, which is close to the reported value of $35.9 \pm 1.1 \text{ s}^{-1}$.^[17] Similar values were measured for all mutant complexes (Table 2). On the basis of equation (3), the maximum turnover at $[\text{Pdx}] = 100 \mu\text{M}$ (k_{max}) can be predicted assuming ET1 is the rate limiting step.^[11] The results indicate that the effect of the mutations is solely on binding affinity and that the ET steps are not affected significantly.

Table 2. The steady state turnover activities of P450cam catalytic cycle. NADH consumption rates were monitored at 340 nm at 22°C. The reaction mixture contained 0.05 μM P450cam, 100 μM Pdx, 1.0 μM PdR and 400 μM NADH in 50 mM Tris-HCl buffer, pH 7.4, consisting of 100 mM KCl and 1 mM camphor.

Pdx	P450cam	k_{max}	NADH consumption (s^{-1})	relative to WT-WT (%)
WT	WT	41.1	38.2 ± 0.2	100
Y33A	WT	26.7	34.9 ± 2.5	91
S42A	WT	27.1	34.1 ± 0.7	89
S44A	WT	39.6	37.4 ± 0.6	98
WT	D125A	33.0	40.3 ± 0.7	106
WT	H352A	36.2	36.3 ± 0.6	95
WT	H361A	31.5	34.1 ± 0.4	89
Y33A	D125A	30.4	26.3 ± 0.3	69
S42A	H352A	22.1	17.9 ± 0.6	47

The mutations Y33A and S42A resulted in a large decrease of the affinity of Pdx for P450cam. To address the question of why these mutants significantly perturb the binding mode, NMR ^{15}N HSQC spectra (Figure 3A) were recorded of all the Pdx mutants and compared to the Pdx WT to see if the mutation caused substantial structural changes. The differences of the chemical shifts between Pdx mutants and WT (in absence of P450cam) were evaluated using the average of chemical shift differences ($\Delta\delta_{\text{avg}}$) (Figure 3C–E).

The NMR spectra of both Pdx S42A and S44A variants overlapped well with Pdx WT without significant $\Delta\delta_{\text{avg}}$ (Figure 3A, D, E), indicating that they are not structurally different. It is noted that NMR signals of the amide of residues 36–50 are broadened beyond detection because they are close to the paramagnetic [2Fe–2S] cluster in Pdx (Figure 3C–E). In the NMR spectrum of Pdx Y33A several peaks were shifted when compared to the spectrum of Pdx WT (Figure 3A). The $\Delta\delta_{\text{avg}}$ values shown in Figure 3C were mapped on the crystal structure of Pdx (PDB: 1XLP)^[18], Figure 3B. The large values of $\Delta\delta_{\text{avg}}$ were observed not only the residues directly adjacent to the mutation site but also extended to spatially neighboring residues. Pdx residue Asp103, in particular, was not found in the spectrum, possibly due to its large chemical shift change or its

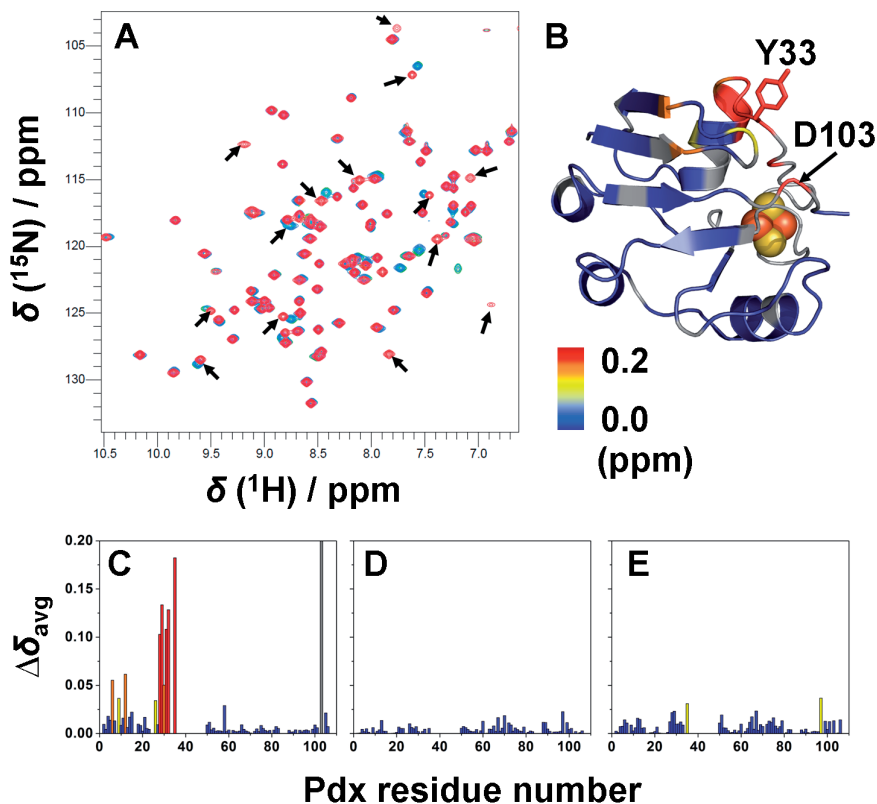


Figure 3. NMR chemical shift perturbation analysis of Pdx mutants. A) Overlaid HSQC spectra. Cyan, red, blue and green resonances represent Pdx WT, Y33A, S42A and S44A variants, respectively. Arrows indicate the largest chemical shift changes observed for Pdx Y33A. B) Ribbon representation of Pdx (PDB entry, 1XLP) colored according to the $\Delta\delta_{\text{avg}}$ values of Y33A with $\Delta\delta_{\text{avg}} \geq 0.10$ and Asp103, red; $0.10 > \Delta\delta_{\text{avg}} \geq 0.05$, orange; $0.05 > \Delta\delta_{\text{avg}} \geq 0.03$, yellow; $0.03 > \Delta\delta_{\text{avg}}$, blue and no data, gray. C–E) $\Delta\delta_{\text{avg}}$ was plotted against Pdx residue number for Pdx Y33A C), Pdx S42A D) and Pdx S44A E).

extensive line broadening. Taken together, we conclude that the structure of Pdx Y33A mutant is likely to be altered by mutation, which may contribute to the reduction of the affinity for P450cam.

Discussion

The structure of the Pdx-P450cam complex provided molecular insight into the ET pathway and effector role of Pdx (see chapter 3 for the details).^[7, 8] In this work, mutagenesis was employed to examine the importance of several polar interface residues highlighted by the structure of the complex. Most of these had not been considered to be important before the structure was available.

Stopped-flow studies indicated that most of the mutations do not influence the rate of ET1 reaction. This is in line with the suggestions in the previous study (chapter 3), where the ET pathways were predicted by the program HARLEM.^[8] None of the residues studied in this report are directly involved in the suggested ET1 pathways. However, Pdx Y33A and S42A substitutions lower the binding affinity by 20–30 fold. Pdx Tyr33 is located at the beginning of the loop region that surrounds the [2Fe-2S] cluster (Figure 3B). An NMR study demonstrated that Tyr33 is mobile on the Pdx surface and occupies several conformational states on the μ s–ms timescale.^[19] The result of our NMR data indicated that the substitution of Tyr33 with alanine changes the structure of the loop region, which transmits to distant residues of Pdx, including Asp103. The functional role of Tyr33 has been recognized in the binding of Pdx both to PdR and P450cam.^[8, 20] The DMC analysis indicated that Pdx Tyr33 has a favorable interaction with P450cam Asp125. As illustrated in the crystal structures of the complex,^[7, 8] Pdx Tyr33 adapts a rigid configuration upon P450cam binding and forms a hydrogen bonding to P450cam Asp125. Pdx Ser42 and Ser44 are positioned adjacent to the [2Fe-2S] cluster (Figure 1) and are part of the polar interactions within the interface. In the DMC analysis, Pdx Ser42 was shown to have a favorable interaction with P450cam His352. The chemical shift perturbation analysis showed that the structure of Pdx S42A mutant is similar to Pdx WT, suggesting that the side chain of Ser42 make a major contribution to the interaction. P450cam His361 is located at the proximal site of heme-binding loop and is in close vicinity to Cys357, the axial ligand of the heme iron. A previous mutagenesis study demonstrated that substitution of the adjacent residue Gln360 with glutamate causes the K_D to increase with 25-fold and the k_{ET1} to decrease with 5-fold.^[12] Moreover, a computational study predicted that along with Gln360, His361 is a part of the ET2 pathway.^[11] The stopped flow measurements on P450cam H361A resulted in the small reduction of the binding affinity and ET1 rate, which suggests that P450cam His361 plays a minor role in ET.

To investigate if the mutations influence the overall ET (ET1+ET2), the catalytic turnover activity of P450cam was monitored by measuring the NADH consumption rate. In accord with the results of the ET1 reaction, all Pdx and P450cam mutants exhibit a turnover rate close to that of WT (considering the higher K_D in some cases). It is concluded that the polar interactions in the Pdx-P450cam interface studied here contribute to the complex formation rather than ET reactions.

In this work, the polar residues that were targeted for the substitution were established on the basis of the crystal structures of Pdx-P450cam complex. In the structures, P450cam is found in open^[7] and semi-open conformation (see chapter 3 for the details).^[8] The authors of reference^[7] interpreted this finding to implicate that Pdx forces P450cam into the open state upon binding and related this to the effector activity. The authors of reference^[8] suggested the open state may be a crystallization effect. A very recent study employing double electron-electron resonance (DEER)

spectroscopy provide evidence showing that P450cam adapts a closed conformation in the ET events in solution.^[21] To evaluate the changes in the binding interface with the conformational state of P450cam, the crystal structures of Pdx-P450cam complex (PDB entries, 3W9C, 4JX1 and 4JWS)^[7, 8] were superimposed with the closed state of free P450cam (PDB entry, 1DZ4),^[22] as shown in Figure 4.

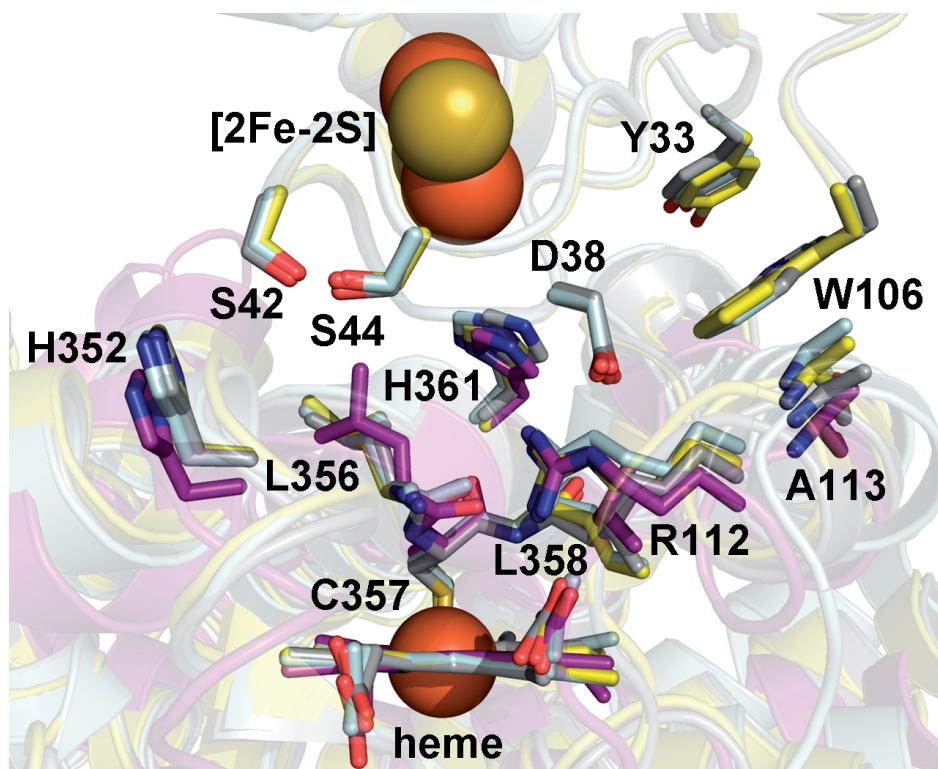


Figure 4. Superimposed structures of Pdx-P450cam complex. Gray, purple, yellow and cyan represent the oxidized complex (PDB entry, 3W9C), the closed conformation of P450cam (1DZ4), the reduced, cross-linked Pdx-P450cam complex with camphor bound (4JX1) and oxidized, cross-linked Pdx-P450cam complex (4JWS), respectively.

The crystal structures of both the oxidized (3W9C^[8] and 4JWS^[7]) and dithionite reduced, CO bound (4JX1^[7]) Pdx-P450cam complex have been reported. However, the actual redox state of the metals is difficult to establish in the crystal because the metals are probe to reduction by X-ray radiation.^[18]

The comparison reveals that majority of the prominent interactions in the binding interface changes only very subtly between the different P450cam conformations (open, semi-open and closed). The hydrogen bond between Asp38_(Pdx)-Arg112_{(P450cam)}}

important for ET, remains intact. The minimal distance between Pdx Trp106 and P450cam A113 is only slightly larger in the model of the complex of Pdx with the closed state of P450cam than in the ox-ox complex (4.4 Å vs. 3.8 Å in 3W9C). The H-bond between the Pdx Tyr33 and P450cam Asp125 is also present in both these complexes. Only the P450cam His352 is significantly further from Pdx Ser42 (5.5 Å vs. 4.2 Å). Given that the complex of the closed state with Pdx bound is not a crystal structure but a superposition, these differences can be considered small and it is reasonable to assume that Pdx is capable to bind both closed and open conformational states of P450cam. Thus, we believe it is plausible that the open/closed state of the complex is influenced by the crystal packing effects, as we suggested before (see chapter 3)^[8] and was also concluded by Myers *et al.*^[21] This implies that the question of what represents the effector activity remains open. Various suggestions have been made. The classic model of a “push” effect suggests that Pdx binding is physically transmitted to the heme-binding loop of P450cam and accelerates ET by influencing the axial thiolate ligand of heme iron.^[23] Another mechanism suggested by Ascitutto *et al.* involves *cis/trans* isomerization of the Ile88–Pro89 peptide bond of P450cam.^[24] Upon the complex formation, the structural perturbation in the Pdx binding site mechanically conveys to remote regions of P450cam, which leads to the closure of the substrate access channel. The substrate is thereby trapped in the active site of P450cam, which minimizes the solvation of the substrate and the diffusion of physiologically harmful peroxide intermediates.^[24] Structural studies of the complex in solution using NMR spectroscopy can complement the frozen solution (EPR) and crystal studies (X-ray diffraction) and may be able to shed more light on the issue.

In conclusion, mutagenesis studies presented in this report show the importance of the interactions of the polar residues in the Pdx-P450cam interface. These polar interactions were found to be important in the partner recognition, rather than in ET.

Experimental procedures

Cloning

The plasmid harboring the cDNA of PdR was purchased from GeneArt®, Life technologies (Invitrogen). The gene was designed to be subcloned into the pET28a expression vector by introducing NcoI and XhoI restriction sites. A His tag sequence was not included. The pET28a vectors containing cDNA of Pdx and P450cam were prepared as described in chapter 3.^[8] Pdx Y33A, Pdx S42A, Pdx S44A, P450cam D125A/C334A, P450cam H352A/C334A and P450cam H361A/C334A constructs were prepared by following the Quikchange® site-directed mutagenesis protocol (Stratagene, La Jolla, CA). The cysteine of P450cam at position 334 was substituted with alanine. The C334A mutation has been reported to prevent the dimerization of the protein and retain the catalytic turnover activity.^[17] P450cam C334A was treated as WT in this report.

Protein production

All Pdx and P450cam variants were produced as described in chapter 3.^[8] The gene expression and purification of PdR was performed by following the previous report with several modifications.^[25] Briefly, pET28a plasmid harboring PdR gene was transformed into the BL21 Star™ (DE3) chemically competent *E. coli* strain (Life technologies, Invitrogen). Single colonies were picked and inoculated into 5 mL LB medium with 50 µg/mL kanamycin at 37°C for 4 hours. Two mL of pre-culture was transferred into 500 mL LB medium with 50 µg/mL kanamycin and incubated at 37°C until $A_{600\text{nm}} = 0.6\text{--}0.7$. Gene expression was induced by adding 0.5 mM IPTG. The cultures were incubated at 22°C for 40–50 hours. Cells were resuspended in a KP_i buffer (20 mM KP_i , pH 8.0, 150 mM KCl, 1 mM DTT, 1 mM PMSF and 1 mM DNase). Samples were flash frozen in N_2 (l) and stored at -80°C .

The resuspended cells were defrosted rapidly at room temperature. A few mg of crystals of lysozyme were added and the sample was stirred for 30 minutes at 22 °C. The lysate was further disrupted by French-press and sonication and spun down by centrifugation at 35000 r.p.m. for 30 minutes at 4°C. The pH of supernatant was adjusted to ~7.5 by addition of a few drops of KOH. Ammonium sulfate powder was added slowly to the sample to 30% (w/v). The sample was then stirred in cold room for 30 minutes. Following centrifugation at 35000 r.p.m. for 30 minutes at 4°C, the supernatant was dialyzed overnight against 4 L of KP_i buffer A (20 mM KP_i , pH 7.5, 1 mM DTT). The dialysate was loaded on a HiTrap DEAE FF anion-exchange column (60 mL). The protein was eluted with a linear gradient of 0.1–0.3 M KCl in KP_i buffer A and the yellow fractions were collected. The fractions were pooled and concentrated by ultrafiltration using a Centricon 3K (Millipore) and injected into a Superose 12 size exclusion column pre-equilibrated with KP_i buffer B (20 mM KP_i , pH 7.4, 150 mM KCl, 1 mM DTT). Ammonium sulfate crystals were added (30% w/v) to the pooled fractions and the sample was stirred for 20 minutes at 4°C. Subsequently, the sample was centrifuged for 20 minutes to remove precipitation and the supernatant was applied to a HiTrap Phenyl FF hydrophobic column (10 mL). The yellow fractions containing PdR were collected after elution with a linear gradient 20–0% ammonium sulfate in KP_i buffer A. The fractions with the $A_{280\text{nm}}/A_{455\text{nm}}$ value below 7.0 were collected. Then the fractions were pooled and dialyzed overnight against 4 L of KP_i buffer B. The concentration of PdR was calculated using extinction coefficient of $11.0 \text{ mM}^{-1}\text{cm}^{-1}$ at 455 nm wavelength.^[26] Approximately 30 mg of PdR was obtained from 1 L of culture.

Stopped flow spectrophotometry assay

Stopped flow experiments were performed on SX-18MV Microvolume Stopped-Flow Spectrofluorometer (Applied Photophysics). D-glucose (1 mM) and 1 unit/mL (final concentration) of oxygen scrubbing proteins, glucose oxidase and catalase were added to Tris buffer C (50 mM Tris-HCl, pH 7.4, 100 mM KCl, 1 mM camphor, 1% MeOH) and made anaerobic by flushing argon and subsequently carbon monoxide (CO) gases for

20 minutes each. Immediately prior to experiment, NADH was added to Pdx reaction mixtures and incubated for a few minutes at room temperature. Final reaction mixtures contained 5–150 μM Pdx^{red}, 0.1 μM PdR^{red}, 400 μM NADH and saturated level of CO, whereas the P450cam reaction mixture contained 2 μM P450cam^{ox} and CO. The absorption at 447 nm wavelength was monitored for one second at 22°C.

DMC analysis

The dissociation constant (K_D) relates to the difference in free energy between bound and unbound states, equation (4)

$$\Delta G_B = RT \ln K_D \quad (4)$$

The difference in ΔG_B caused by a substitution of a residue by alanine ($\Delta\Delta G_B$) is calculated by equation (5)

$$\Delta\Delta G_B = RT \ln (K_D^{\text{mut}} / K_D^{\text{WT}}) \quad (5)$$

where K_D^{mut} and K_D^{WT} are the dissociation constants of the Pdx and/or P450cam mutants and WT complex, respectively. The free energy of interaction ($\Delta\Delta G_{\text{int}}$) between two residues equals to:

$$\Delta\Delta G_{\text{int}} = \Delta\Delta G_B^{\text{mut, mut}}_{(\text{Pdx, P450cam})} - \Delta\Delta G_B^{\text{mut}}_{(\text{Pdx})} - \Delta\Delta G_B^{\text{mut}}_{(\text{P450cam})} \quad (6)$$

where $\Delta\Delta G_B^{\text{mut, mut}}_{(\text{Pdx, P450cam})}$ represents $\Delta\Delta G_B$ of P450cam and Pdx variants derived from equation (5). A negative value of $\Delta\Delta G_{\text{int}}$ indicates that the interaction between the mutated residues is attractive whereas a positive value of $\Delta\Delta G_{\text{int}}$ suggests a repulsive interaction.^[16]

NADH consumption rates

All of the P450cam WT and variants were exchanged into Tris buffer C by Superprose 12 size exclusion column immediately before each experiment. The NADH consumption rates were measured on Perkin Elmer Lambda 25 spectrophotometer as described by Nickerson and Wong.^[17] Briefly, 400 μM of NADH (final concentration) was added to 0.2 mL reaction mixture containing 0.05 μM P450cam, 100 μM Pdx, 1.0 μM PdR to initiate the reaction. The absorption at 340 nm was monitored for 180 s at 22°C. The catalytic turnover of NADH oxidation was determined from the slope of a linear region in the plot of A_{340} vs. time. The concentration of NADH was estimated using extinction coefficient of 6.22 $\text{mM}^{-1}\text{cm}^{-1}$ at 340 nm.

NMR

Approximately 1 mM of ¹⁵N Pdx WT and variants were prepared in Tris buffer C with 6% D₂O for lock. All NMR samples were measured on a Bruker Avance III 600-MHz spectrometer equipped with a TCI-Z-GRAD cryoprobe at 298 K. ¹⁵N HSQC spectra were processed with NMRPipe^[27] and analyzed by CCPNMR.^[28] The NMR assignment

of Pdx amide resonances were based on previous work.^[29] Chemical shift perturbations (CSP average) were analyzed as previously described.^[30]

References

1. D. R. Nelson, *Hum Genomics* **2009**, *4*, 59-65.
2. T. Sakaki, *Biol Pharm Bull* **2012**, *35*, 844-849.
3. M. Katagiri, B. N. Ganguli, I. C. Gunsalus, *J Biol Chem* **1968**, *243*, 3543-3546.
4. C. A. Tyson, J. D. Lipscomb, I. C. Gunsalus, *J Biol Chem* **1972**, *247*, 5777-5784.
5. S. G. Sligar, P. G. Debrunner, J. D. Lipscomb, M. J. Namtvedt, I. C. Gunsalus, *Proc Natl Acad Sci U S A* **1974**, *71*, 3906-3910.
6. J. D. Lipscomb, S. G. Sligar, M. J. Namtvedt, I. C. Gunsalus, *J Biol Chem* **1976**, *251*, 1116-1124.
7. S. Tripathi, H. Li, T. L. Poulos, *Science* **2013**, *340*, 1227-1230.
8. Y. Hiruma, M. A. Hass, Y. Kikui, W. M. Liu, B. Olmez, S. P. Skinner, A. Blok, A. Kloosterman, H. Koteishi, F. Lohr, H. Schwalbe, M. Nojiri, M. Ubbink, *J Mol Biol* **2013**, *425*, 4353-4365.
9. W. Zhang, S. S. Pochapsky, T. C. Pochapsky, N. U. Jain, *J Mol Biol* **2008**, *384*, 349-363.
10. H. Koga, Y. Sagara, T. Yaoi, M. Tsujimura, K. Nakamura, K. Sekimizu, R. Makino, H. Shimada, Y. Ishimura, K. Yura, M. Go, M. Ikeguchi, T. Horiuchi, *Febs Lett* **1993**, *331*, 109-113.
11. V. Y. Kuznetsov, T. L. Poulos, I. F. Sevrioukova, *Biochemistry* **2006**, *45*, 11934-11944.
12. T. Toshi, S. Yoshioka, H. Hori, S. Takahashi, K. Ishimori, I. Morishima, *Biochemistry* **2002**, *41*, 13883-13893.
13. M. J. Hintz, J. A. Peterson, *J Biol Chem* **1981**, *256*, 6721-6728.
14. M. J. Hintz, D. M. Mock, L. L. Peterson, K. Tuttle, J. A. Peterson, *J Biol Chem* **1982**, *257*, 14324-14332.
15. R. A. Marcus, N. Sutin, *Biochim Biophys Acta* **1985**, *811*, 265-322.
16. M. Harel, M. Cohen, G. Schreiber, *J Mol Biol* **2007**, *371*, 180-196.
17. D. P. Nickerson, L. L. Wong, *Protein Eng* **1997**, *10*, 1357-1361.
18. I. F. Sevrioukova, *J Mol Biol* **2005**, *347*, 607-621.
19. N. Sari, M. J. Holden, M. P. Mayhew, V. L. Vilker, B. Coxon, *Biochemistry* **1999**, *38*, 9862-9871.
20. I. F. Sevrioukova, T. L. Poulos, I. Y. Churbanova, *J Biol Chem* **2010**, *285*, 13616-13620.
21. W. K. Myers, Y. T. Lee, R. D. Britt, D. B. Goodin, *J Am Chem Soc* **2013**, *135*, 11732-11735.
22. I. Schlichting, J. Berendzen, K. Chu, A. M. Stock, S. A. Maves, D. E. Benson, R. M. Sweet, D. Ringe, G. A. Petsko, S. G. Sligar, *Science* **2000**, *287*, 1615-1622.
23. S. Shaik, D. Kumar, S. P. de Visser, A. Altun, W. Thiel, *Chem Rev* **2005**, *105*, 2279-2328.
24. E. K. Asciotto, J. D. Madura, S. S. Pochapsky, B. OuYang, T. C. Pochapsky, *J Mol Biol* **2009**, *388*, 801-814.
25. I. F. Sevrioukova, J. T. Hazzard, G. Tollin, T. L. Poulos, *Biochemistry* **2001**, *40*, 10592-10600.
26. I. C. Gunsalus, G. C. Wagner, *Methods Enzymol* **1978**, *52*, 166-188.
27. F. Delaglio, S. Grzesiek, G. W. Vuister, G. Zhu, J. Pfeifer, A. Bax, *J Biomol NMR* **1995**, *6*, 277-293.
28. W. F. Vranken, W. Boucher, T. J. Stevens, R. H. Fogh, A. Pajon, M. Llinas, E. L. Ulrich, J. L. Markley, J. Ionides, E. D. Laue, *Proteins* **2005**, *59*, 687-696.
29. T. A. Lyons, G. Ratnaswamy, T. C. Pochapsky, *Protein Science* **1996**, *5*, 627-639.
30. S. Grzesiek, A. Bax, G. M. Clore, A. M. Gronenborn, J. S. Hu, J. Kaufman, I. Palmer, S. J. Stahl, P. T. Wingfield, *Nat Struct Biol* **1996**, *3*, 340-345.

CHAPTER 5

Paramagnetic NMR analysis
reveals the encounter state of the
Pdx-P450cam complex

Abstract

The physiological complex of putidaredoxin (Pdx) and cytochrome P450cam (P450cam) is a paradigm for the electron transfer process of the P450 superfamily. In this project, we have determined the major and minor states of Pdx-P450cam complex by using three different types of paramagnetic NMR techniques. The results of pseudocontact shifts and residual dipolar couplings support the previously determined structures of the complex. On the other hand, the distance restraints derived from paramagnetic relaxation enhancements (PREs) showed the significant deviations from the expected values. We performed PRE analysis at multiple positions of Pdx and P450cam and concluded that small fractions of the complex exhibit dynamic nature of the interactions. Our finding of the encounter complex provides the insight of the specificity of protein-protein interaction and the efficiency of electron transfer in Pdx-P450cam complex.

Introduction

Recently, the concept of encounter complex has gained attention to describe protein–protein complex formation. It is an intermediate stage in the binding process in which proteins adopt multiple orientations to search for the specific binding site on the protein partner. This transient state of the protein complex often exists only as a small fraction compared with the large population of free proteins and final complex.^[1] Therefore, it was technically challenging to study such a lowly populated state of the complex in a sample. However, recent development of paramagnetic NMR analysis,^[1] flash photolysis^[2] as well as double-mutant cycles in the combination of kinetics^[3] have opened up possibilities to study the nature of encounter complex. The biological function of encounter complex is thought to accelerate the formation of the final complex by reducing the dimensionality of the search of specific binding site.^[1] The encounter complex is particularly well-documented in the complex formation of electron carrier proteins where rapid ET and sufficient specificity of the protein–protein interaction are required to achieve high turnover rate of the complex.^[1]

In *Pseudomonas putida*, putidaredoxin (Pdx) and cytochrome P450cam (P450cam) form a redox complex in the camphor hydroxylation reaction. Pdx shuttles electrons from putidaredoxin reductase (Pdr) to P450cam, which in turn acts as a terminal oxygenase to catalyze regio- and stereo-specific hydroxylation of D-camphor.^[4] Recently, the atomic resolution structure of Pdx-P450cam complex has been solved by X-ray crystallography as well as paramagnetic NMR analysis (see Chapter 3).^[5–6] The binding interface of Pdx and P450cam is dominated by hydrophobic contacts and polar interactions, including the prominent hydrogen bond between Pdx Asp38 and P450cam Arg112.^[5–6] As suggested in previous studies, Pdx was found to interact with P450cam and Pdr with the same interface.^[5–8] A mutagenesis study showed that surface exposed Tyr33, Arg66 and Trp106 of Pdx are primarily involved in partner recognition.^[9] Interestingly, they exhibit large mobility on protein surface when Pdx is not bound to redox partners.^[10] As previously proposed for the Pdr-Pdx complex formation,^[8] the interaction between Pdx and P450cam is most likely facilitated by Pdx searching for the steric complementarity on the P450cam surface area. Upon reaching the optimal binding geometry, the mobility of the bulky side chains is reduced by specific interactions with P450cam or ordered water molecules in the interface.

The presence of an encounter complex of Pdx-P450cam has been implicated by paramagnetic NMR analysis in our previous study (Chapter 3).^[5] Three different paramagnetic NMR effects, namely, pseudocontact shifts (PCS), paramagnetic relaxation enhancements (PRE) and residual dipolar couplings (RDC) were generated by lanthanoid probes and 446 restraints were used for structural calculations. The distance restraints derived from PCS and PRE agree well with those calculated for the final solution structure and the crystal structure, except for one set of PRE data. Curiously, the results of this dataset indicated that a minor population of Pdx visits a remote

region on P450cam (Chapter 3).^[5] To further characterize the encounter complex of the Pdx-P450cam complex, a caged lanthanoid NMR probe (CLaNP) as well as a MTSL spin label were attached to P450cam and Pdx, respectively. In line with the previous study (Chapter 3),^[5] many of the obtained PRE data were not in agreement with a single binding orientation of Pdx. The present study indicates that Pdx explores the region nearby the J and K helices as well as $\beta 1$ sheet of P450cam in the encounter state.

Results

Protein tagging with paramagnetic probes

To study the interaction of Pdx-P450cam complex, a paramagnetic probe, CLaNP-7, was attached to P450cam. In our previous study, CLaNP-7 was demonstrated to be a useful tool for the structure determination of the Pdx-P450cam complex (see Chapter 3).^[5] The bidentate fashion of CLaNP attachment requires two surface-exposed Cys residues that are in close vicinity.^[11] In addition to the previously described P450cam mutants, K126C/R130C/C334A (mutant A) and A333C/C334A/H337C (mutant B), two other variants were prepared, namely, Q272C/E276C/C334A (mutant C) and E195C/A199C/C334A (mutant D). The probe attachment site of mutant C is relatively close to the mutation site B. The PRE data from this site provided the evidence for an encounter complex in the previous study.^[5] The position of mutant D is located at the G-helix of P450cam, which is in proximity to putative potassium binding site.

Intramolecular PCSs were measured for P450cam mutants C and D and the derived distance and orientation restraints were used to calculate the position of the lanthanoid ion (Ln^{3+}) and the orientation of the anisotropy of the magnetic susceptibility, the $\Delta\chi$ tensor. These are essential parameters to convert intermolecular paramagnetic NMR effects to accurate restraints, especially for the structure calculations on the encounter complex. To perform the intramolecular PCS experiments, P450cam mutant C and D were uniformly labeled with ^{15}N isotopes. Subsequently, the proteins were linked to Lu^{3+} or Tm^{3+} loaded CLaNP-7 ($\text{Lu}^{3+}/\text{Tm}^{3+}$ -CLaNP-7) and two-dimensional HSQC spectra were recorded in the absence of Pdx. The principle axial and rhombic components of $\Delta\chi$ tensors ($\Delta\chi_{ax}$, $\Delta\chi_{rh}$) were calculated to be $\Delta\chi_{ax} = 44.7 \pm 0.8$, $\Delta\chi_{rh} = 21.3 \pm 1.1$ and $\Delta\chi_{ax} = 44.7 \pm 2.0$, $\Delta\chi_{rh} = 8.0 \pm 2.0$ ($\ast 10^{-32} \text{ m}^3$) for Tm^{3+} -CLaNP-7 labeled P450cam mutant C and D, respectively. The variability of $\Delta\chi_{rh}$ values is attributed to the mobility of the tag on protein surfaces.^[12] The $\Delta\chi$ tensor values derived from intramolecular PCS analysis were summarized in Table 2 in Chapter 2.

Intermolecular paramagnetic NMR effects

Having established the attachment site of CLaNP-7, we next measured three types of paramagnetic NMR effects, PCS, RDC and PRE to determine the binding mode of Pdx-P450cam complex. Tm^{3+} -containing CLaNP-7 has been shown to induce both PCS and RDC, which were extensively used for the structural calculations of Pdx-P450cam complex in the previous study (see Chapter 3).^[5] PCSs provide long-range

distance information (up to 60 Å) as well as orientation restraints since it depends on the orientation of the $\Delta\chi$ tensor.^[13] In addition to PCS, orientation restraints can be independently determined by RDC analysis. The attachment of Tm³⁺-CLaNP-7 partially aligns the protein complex to the external magnetic field, which gives rise to amide proton residual dipolar couplings. Gd³⁺-containing CLaNP-7 (Gd³⁺-CLaNP-7) causes PREs, which provides distance restraints up to 45 Å. In contrast to PCS derived distances, which often agree well with those calculated from the crystal structure, the distance information obtained from PREs can reflect the lowly populated states of protein conformations. To obtain intermolecular paramagnetic NMR restraints, NMR spectra were acquired for isotopically enriched ²H, ¹⁵N Pdx in the presence of Lu³⁺/Tm³⁺/Gd³⁺-CLaNP-7 labeled P450cam. The PCS, RDC and PRE data for mutant C are shown in Figure 1. For the mutant D, only PREs were obtained, Figure 2. To illustrate the correlation with the previously determined structures of the final complex, a comparison was made between experimentally measured (red circles) and back-calculated restraints (blue lines) from the ensemble of ten solution structures (PDB entry 2M56^[5]).

Although small deviations were observed for Pdx residues 50-70 and 90-95, the intermolecular PCS of mutant C are in reasonable agreement with those predicted from the final complex. The predicted RDCs also correspond reasonably well with most of the experimental data. The Q factors (eq. 2 in the Materials and Methods) calculated from the experimental and back-predicted data are 0.07 and 0.34 for PCS and RDC, respectively. In contrast to the PCSs and RDCs, the PRE derived distances show poor correlations between experimentally determined and back-calculated distances. For almost all of the residues, experimental distances were shorter than predicted. To illustrate the extent of deviations, the additional PREs (Δ PRE) were calculated by subtracting the calculated PRE from the experimentally measured PRE and color coded on the Pdx surface as shown in Figure 1D. The Pdx residues with the largest Δ PRE (Figure 1D, red) were observed not only at the region closest to the probe attachment site but also on the other side of Pdx. The distribution of the Δ PREs on the protein surface cannot be explained by a single orientation of Pdx-P450cam complex since these residues are too far away from the paramagnetic center to be affected. The additional PRE effects are in line with those found for mutant B.^[5] Taken together, intermolecular PRE analysis of mutant C indicates that Pdx visits other orientations than the one observed in the final, well-defined complex. The agreement of RDC and PCS data with the predicted values suggests the population of the encounter complex to be small.

To investigate the extent of surface area being sampled by the encounter complex, paramagnetic tags were attached also Pdx. Pdx V6C/R12C/C73S/C85S (mutant I) was linked to Gd³⁺-CLaNP-7 to measure intermolecular PRE on P450cam. Moreover, Pdx wild type (WT) was produced for the attachment of an MTSL spin label. Zhang *et al.* demonstrated that the endogenous surface-exposed Cys73 can be labeled with MTSL

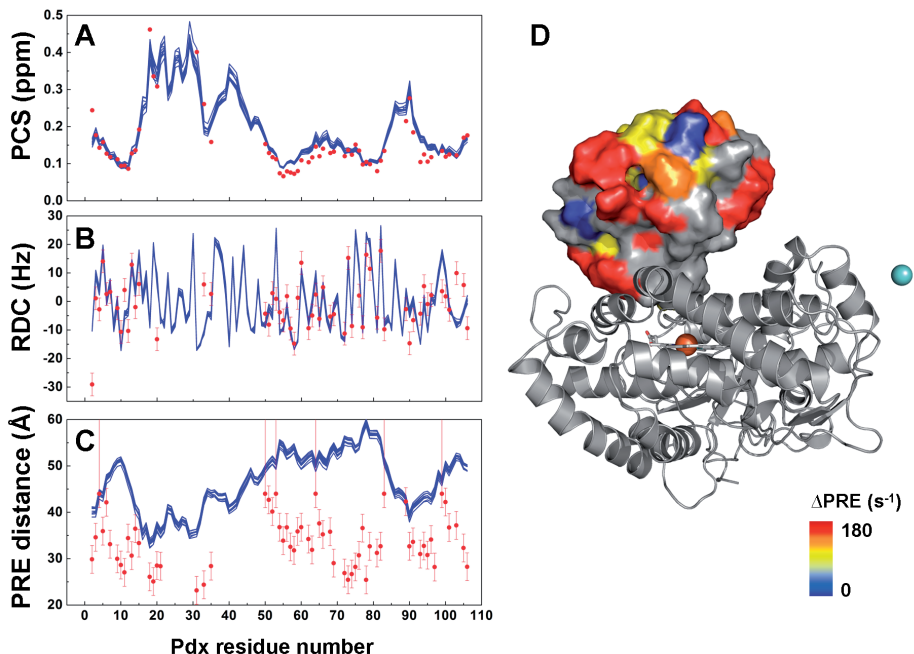


Figure 1. Intermolecular paramagnetic NMR effects on Pdx for P450cam mutant C tagged with CLaNP-7. The PCSs (A), RDCs (B) and PRE derived distances (C) were plotted against the Pdx residue number. Red circles and blue lines illustrate the experimentally measured restraints and back-calculated restraints from ten best solution structures of the complex (PDB entry 2M56), respectively. The experimental errors associated with PCS are within the circular symbols. (D) Surface representation of Pdx, showing the additional PREs (ΔPRE) caused by Gd³⁺-CLaNP-7 labeled P450cam mutant C. Pdx residues were color coded according to $\Delta\text{PRE} \geq 30$ s⁻¹, red; 20-30 s⁻¹, orange; 5-20 s⁻¹, yellow; < 5 s⁻¹, blue. Unassigned residues and P450cam are shown in gray. The blue sphere represents the position of the Gd³⁺. P450cam is shown in ribbon representation with the heme in sticks and the iron as a red sphere. Pdx is shown in the orientation found in the final complex.

without causing significant perturbations in the Pdx-P450cam complex.^[14] Figure 2 illustrates the PRE derived distances for the respective positions of paramagnetic probes on Pdx and P450cam.

The experimental PRE distances and those calculated from the final structure were found to be in good agreement for mutant A. For mutant D, with the exception of a few residues, significant PREs were not detected, which is represented by large lower limit of error bars in Figure 2. The absence of the additional PREs indicates that Pdx does not sample the region around position D of P450cam. However, several stretches of P450cam residues exhibit stronger PRE than those predicted for Pdx mutant I and MTSL at Cys73. In comparison to Gd³⁺-CLaNP-7, the distances that MTSL allows to measure are limited to the range of 14–22 Å.^[15] As illustrated in the Figure 3, additional PREs are observed at the remote regions from the predicted Gd³⁺/MTSL attachment

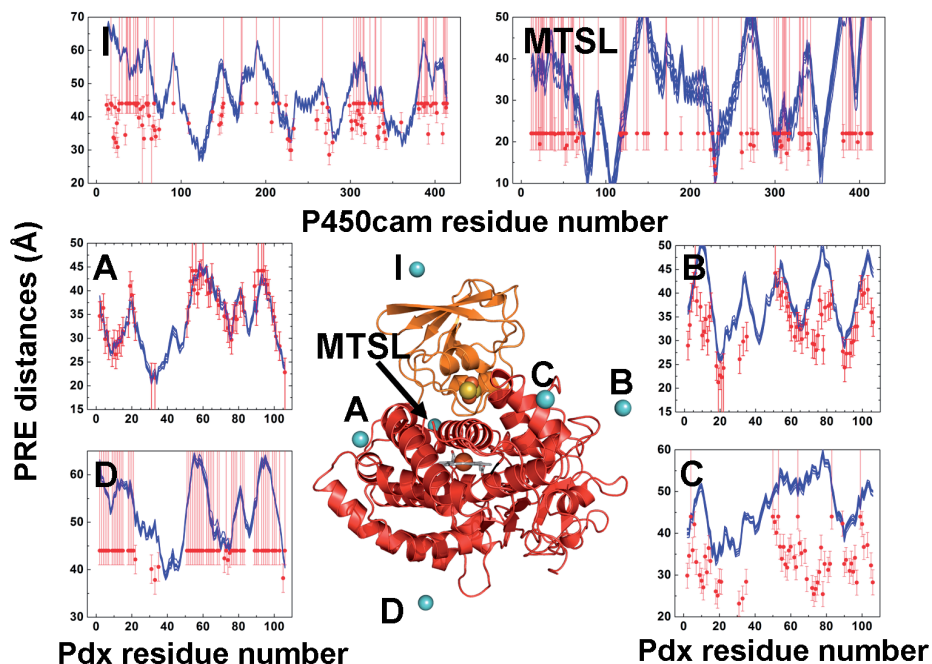


Figure 2. PRE analysis of Pdx-P450cam complex. In the central panel, the positions of Gd^{3+} and MTSL are represented by blue spheres on the Pdx-P450cam complex (PDB entry, 2M56). In the side panels, inter-protein PRE distances are plotted against the protein residue number for the respective positions.

sites. The regions with significant ΔPRE ($>5 \text{ s}^{-1}$) include 21–26 and 65–70 and 332–333, which are located in the proximity of the J, K helices as well as $\beta 1$ sheet of P450cam.

The largest deviations were observed for Pdx residues from the position B and C on P450cam. The Q factors calculated from the experimental and back-predicted PREs show 0.58 and 0.86 for mutant B and C, respectively (Table 1).

Table 1. Summary of Q factors for intermolecular paramagnetic NMR restraints.

Sample	Probes	Q (PRE)	Q (PCS)	Q (RDC)
P450cam mutant A	CLaNP-7	0.25 ^a	0.03 ^a	0.14 ^a
P450cam mutant B	CLaNP-7	0.58 ^a	0.07 ^a	0.34 ^a
P450cam mutant C	CLaNP-7	0.86	0.08	0.47
P450cam mutant D	CLaNP-7	0.42		
Pdx mutant I	CLaNP-7	0.59	0.08 ^a	0.28 ^a
Pdx WT	MTSL	0.76		

described in Chapter 3^[5]

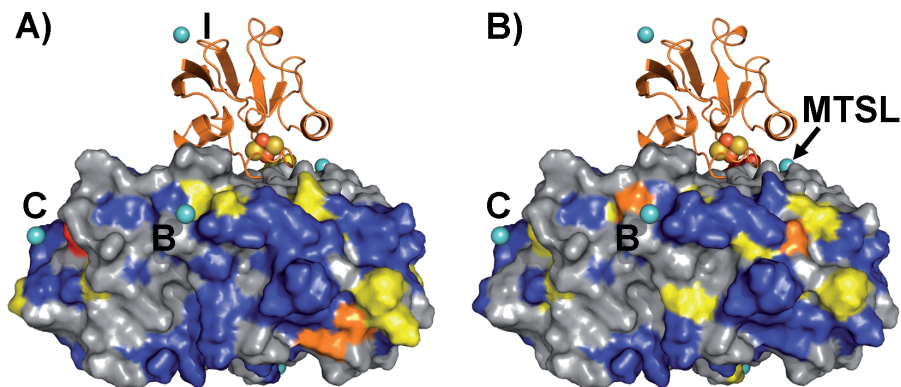


Figure 3. Surface representation of P450cam, showing the additional PREs. (A) Gd³⁺-CLaNP-7 labeled Pdx mutant I. The scheme of color code was the same as given in the caption of Figure 1D. (B) Pdx WT labeled with MTSL at Cys73. P450cam residues were color coded according to Δ PRE with ≥ 50 s⁻¹, red; 30-50 s⁻¹, orange; 7-30 s⁻¹, yellow; < 7 s⁻¹, blue. Unassigned residues and P450cam are shown in gray. The blue spheres represent the positions of the Gd³⁺ ions. Pdx is shown in ribbon representation with the [2Fe-2S] cluster as brown and yellow spheres.

It is worth mentioning that experimental PCSs correlate well with the predicted ones, with *Q* factors of 0.07–0.08. Therefore, the observed PRE deviations cannot be explained by significant perturbations in the complex caused by Ln³⁺-CLaNP-7 attachment. Taken together, the results indicate that the surface area of P450cam being sampled by Pdx in the encounter complex is localized nearby J, K helices as well as β 1 sheet. It should be noted that the conformational space being sampled by Pdx can be larger than the surface area covered in the current study. It can be further characterized by attaching paramagnetic probes at multiple locations of the protein surfaces.

To investigate the interactions that drive the encounter state of Pdx-P450cam complex, the regions nearby J, K helices as well as β 1 sheet were analyzed in the crystal structure (PDB entry 3W9C).^[5] It is worth mentioning that both of the proteins contain a large number of acidic residues, which results in isoelectric points (pI) of Pdx and P450cam of 4.5 and 5.2, respectively. As illustrated in Figure 4, the regions of P450cam affected by Δ PREs compose the clusters of basic and hydrophobic residues.

Previous mutagenesis studies as well as the structural analysis of the crystal structures revealed the importance of the hydrogen bond between Pdx Asp38 and P450cam Arg112 as well as the hydrophobic contact between Pdx Trp106 and P450cam Ala113 for the formation of Pdx-P450cam complex.^[5-6, 9, 16] Moreover, the mutagenesis and kinetics data presented in the Chapter 4 highlighted interactions of several polar residues in the Pdx-P450cam interface. These polar interactions were found to be important in partner recognition, rather than in ET. Taken together, we propose that the encounter state of Pdx-P450cam complex is driven by polar interactions as well as short-range interactions, including hydrogen bonding and hydrophobic contacts.

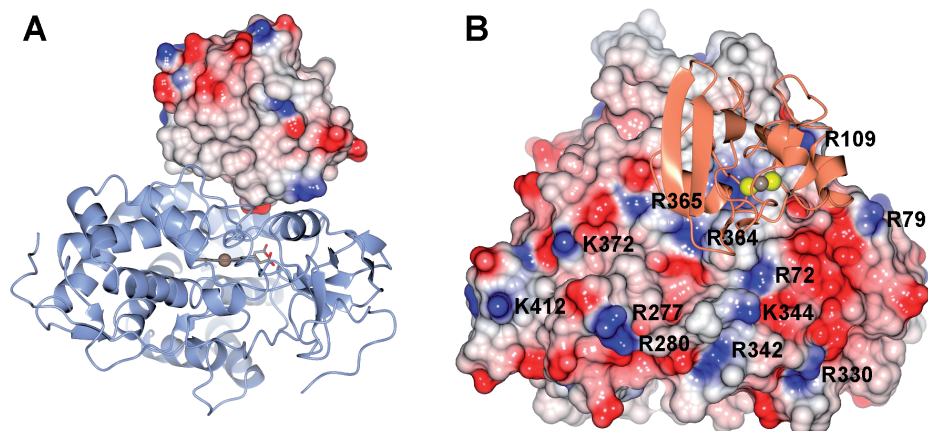


Figure 4. Electrostatic surface of Pdx-P450cam complex (PDB entry 3W9C). Blue and red represent basic and acidic, respectively. (A) Electrostatic surface representation of Pdx. Blue ribbon represents P450cam. (B) Electrostatic surface representation of P450cam. Orange ribbon represents Pdx. Basic patches of P450cam were annotated.

5

Discussion

The paramagnetic NMR analysis with lanthanoid probes provides information about both the structural and dynamic nature of the protein-protein interaction in the solution state. PCSs and RDCs caused by Tm^{3+} -containing CLaNP-7 generate distance and orientation restraints that help to determine the major conformational state, which often agrees well with those of crystal structures.^[5, 17-18] On the other hand, due to the strong distance dependency, PRE is known to be extremely sensitive to detect lowly populated conformational states of proteins.^[11] We compared the results of the PCS, RDC and PRE analyses of Ln^{3+} -CLaNP-7 labeled mutants (A, B, C and I) and showed that Pdx visits minor orientation(s) in the Pdx-P450cam complex. The Q factors were found to be as small as 0.03–0.07 for PCS, which reflects the good correlations between experimentally measured and predicted PCS. Reasonably small Q factors were also found in RDC datasets. In contrast, poor correlations were observed for PRE derived distances. All of the residues with significant deviations showed stronger PREs than expected and also the distributions of the PREs on the Pdx surface are not consistent with the stereospecific complex and this effect was observed for probes at multiple positions on P450cam. Clearly, a single Pdx-P450cam complex cannot account for the observed PREs. In line with the suggestions to the previous study,^[5] we concluded that additional PREs can be attributed to a lowly populated encounter state of the Pdx-P450cam complex.

To compare the results of the PREs obtained by Zhang *et al.* and those in the current study with Gd^{3+} -CLaNP-7, a nitroxide spin label was attached to Pdx WT, using the endogenous surface exposed Cys73. Significant PREs were observed for

nuclei in several stretches across P450cam in addition to the previously described residues.^[14] Some of these affected residues were located at more than 22 Å away from the predicted MTSL attachment site. Moreover, the regions with ΔPRE caused by MTSL correspond to those induced by Gd³⁺-CLaNP-7 from mutant I. The results of PRE analysis with nitroxide spin label indicate that the encounter complex of Pdx-P450cam is not an artifact of the attachment of Gd³⁺-CLaNP-7, but rather represents true dynamics in the Pdx-P450cam interaction.

The fraction of encounter complex, relative to the fraction of the stereospecific structure, varies among protein complexes. For the interaction of yeast cytochrome c and cytochrome c peroxidase it has been shown that the fraction of its encounter state is 30%.^[19] Other complexes have been described to exist only as encounter complexes.^[20-21] In our current study, the fraction of encounter state of Pdx-P450cam complex was not quantified. However, the good agreement of PCS and RDC data with the predicted values suggests the population of the encounter complex to be relatively small (less than 10%).

The PRE analysis for multiple positions of Pdx and P450cam indicates that in the encounter state Pdx is localized close to the J and K helices as well as the β1 sheet. These regions all have basic and hydrophobic residues clustered together. Previous mutagenesis studies as well as X-ray crystallography demonstrated that the interactions of Pdx and P450cam are dominated by polar interactions, hydrogen bonding and hydrophobic contacts.^[5-6, 9, 22] Given the overall negative charge of both proteins, it is reasonable to assume that Pdx visits mostly basic/hydrophobic patches of the P450cam surface. Based on isothermal titration calorimetric results, Aoki *et al.* compare the association of Pdx with P450cam to antigen-antibody binding.^[23] The specificity of an antigen-antibody interaction is established by van der Waals interactions, hydrogen bonding and loss of the mobility upon the complex formation. The C-terminal Pdx Trp106 plays an essential role in the partner recognition in complex formation.^[5-6, 9, 22] Moreover, it exhibits significant flexibility on protein surface.^[10] The dynamics of the bulky hydrophobic residue could be a key determinant in the search for optimal binding geometry.

In general, the encounter state facilitates the formation of final well-defined complex. However, recent experimental evidences demonstrated that not all encounter state of protein complexes proceed to final productive complexes such complexes are called futile encounters.^[1, 24-25] In general, the further away the partner binds in the encounter complex, the higher the chances that it dissociates without forming the productive complex. The surface of P450cam sampled by Pdx extends from the proximal side to the regions nearby J and K helices as well as β1 sheet. Some of these sites are rather far away from the putative binding site. Therefore, it is reasonable to conclude that not every Pdx binding leads to the formation of the ET complex. Nonetheless, the localized areas of P450cam being visited by Pdx suggest that the lowly populated encounter complex is relevant to the formation of the final

Pdx-P450cam complex. As illustrated in the electrostatic surface of P450cam (Figure 4), the prominent basic patches of R342, K344, R72 and R364 compose a path to guide the Pdx to the putative binding site. Thereby, it reduces the three dimensional search via collisions to a two dimensional search on the P450cam surface. Moreover, the charge interaction prolongs the lifetime of the encounter facilitating the formation of the ET active complex. It has been shown that Pdx shuttles electrons between PdR and P450cam through the same interface.^[8]

In conclusion, we investigated the dynamics of the Pdx^{ox}-P450cam^{ox} interaction by PRE analysis. A small population of the complex is found to exist as an encounter state. Further biochemical and structural studies are required to elucidate the biological function of the encounter complex.

Material and Methods

Chemicals

CLaNP-7^[13] was kindly provided by Wei-Min Liu (Leiden University) and chelated to Lu³⁺, Gd³⁺ and Tm³⁺ ions. MTSL ((1-oxyl-2,2,5,5-tetramethyl-3-pyrroline-3-methyl)-methanesulfonothioate) and MTS ((1-acetyl-2,2,5,5-tetramethyl-3-pyrroline-3-methyl)-methanesulfonothioate) were purchased from Toronto Research Chemicals, North York, Ontario, Canada.

Mutagenesis

To prepare double cysteine mutants of Pdx and P450cam, site-directed mutagenesis was carried out using QuikChange protocol (Stratagene, La Jolla, CA).

Protein production

Pdx and P450cam variants were produced as described in Chapter 3.

Paramagnetic probe attachments

Pdx and P450cam variants were labeled with Ln³⁺-CLaNP-7 as previously described.^[5] For MTS(L) tagging, Pdx WT was incubated with 5 mM DTT in 20 mM KP_i, pH 7.0, 50 mM KCl for 30 minutes on ice. DTT was removed by using a PD-10 column. The protein solution was mixed with five molar equivalents of MTS(L) and incubated for one hour at 4°C. Oligomers and surplus of spin labels were removed by two steps of chromatography, on a HiTrap Q HP anion-exchange column and a Superose 12 size exclusion column, respectively. The MTS(L) incubated sample was filtered and loaded on a HiTrap Q HP anion-exchange column (2 mL). The protein was eluted with a linear gradient of 0.1–0.4 M KCl in 20 mM KP_i, pH 7.4 and the first peak fractions were collected and subsequently loaded on a Superose 12 size exclusion column pre-equilibrated with 50 mM Tris-HCl, pH 7.4, 100 mM KCl and 1 mM camphor, 1% MeOH, 6% D₂O. The eluted brown fractions were pooled and concentrated. Approximately, 80–90% of proteins were lost during the labeling procedure presumably because

MTSL labeling hampers the stability of the iron sulfur cluster. The loss of [2Fe-2S] cluster results in unfolding and oligomerization of the protein.

NMR samples and experiments

NMR samples contained 100–200 μM [^2H , ^{15}N] Pdx (WT) or [^2H , ^{15}N] P450cam (C334A) with two molar equivalents of Ln^{3+} -CLaNP-7 labeled P450cam or Ln^{3+} -CLaNP-7/MTS(L) tagged Pdx mutants, respectively, in 50 mM Tris-HCl, pH 7.4, 100 mM KCl, 1 mM camphor and 7% D_2O . 2D ^{15}N - ^1H HSQC and ^{15}N - ^1H TROSY spectra^[22] were recorded at 290 K on a Bruker Avance III 600 MHz spectrometer equipped with a TCI-Z-GRAD cryoprobe.

NMR assignment

All NMR data were processed in NmrPipe^[26] and analyzed in CCPNMR^[27]. The amide resonances of oxidized Pdx and P450cam were assigned based on previous work and Chapter 3.^[5, 28]

PCS and RDC analysis

PCS and RDC measurements were performed as reported in Chapter 3.^[5]

PRE analysis

PRE datasets of Gd^{3+} -CLaNP-7 and MTSL were analyzed as described in Chapter 3.^[5, 15] The peak height of the amide resonances of the proteins were compared in the presence of partner protein with diamagnetic probe (Lu^{3+} -CLaNP-7 or MTS) and with paramagnetic probe (Gd^{3+} -CLaNP-7 or MTSL) and they were represented as I_{dia} and I_{para} , respectively. The $I_{\text{para}}/I_{\text{dia}}$ ratios were normalized by dividing them by the averaged values of the 10 largest $I_{\text{para}}/I_{\text{dia}}$ values (0.96, 1.09, 1.15, 0.95, 1.0 and 0.97 for P450cam mutant A, B, C, D, Pdx mutant I and MTSL samples, respectively). Intermolecular distance restraints were calculated using the equation 1.

$$r = \sqrt[6]{\frac{f_{\text{bound}} \cdot f_{\text{labeled}}}{R_{2,\text{para}}} \frac{\gamma^2 g^2 \beta^2 \mu_0^2 (S+1) S}{240\pi^2} \left(4\tau_c + \frac{3\tau_c}{1 + \omega_h^2 \tau_c^2} \right)} \quad [1]$$

where r is the distance between an unpaired electron (Gd ion or nitroxide) and a given amide proton; f_{bound} is the fraction of the bound ^{15}N protein. Given a dissociation constant of Pdx-P450cam as 5–10 μM , f_{bound} was set to 0.9; f_{labeled} is the fraction of the paramagnetic probe attached protein. f_{labeled} were estimated to be 0.8-0.9 as described in Chapter 2 and 1.0 for Gd^{3+} -CLaNP-7 and MTSL, respectively; γ is the proton gyromagnetic ratio; g is the electronic g-factor; β is the Bohr magneton; ω_h is the Larmor frequency of protons; μ_0 is vacuum permeability; S is spin quantum number of nitroxide and Gd^{3+} ; τ_c is the rotational correlational time of nitroxide/ Gd^{3+} -proton vector. τ_c was estimated to be 30 ns on the basis of HYDRONMR^[29] for the Pdx-P450cam complex. The intermolecular distances were divided in three classes

of restraints: i) residues with resonance peaks that broaden out beyond detection in the paramagnetic spectrum. For these residues, only an upper limit of the distance was calculated and found to be 14 and 20 Å for MTSL and Gd³⁺ samples, respectively. ii) residues with $R_{2,\text{para}} \geq 7.0 \text{ s}^{-1}$ (MTSL) and $R_{2,\text{para}} \geq 3.0 \text{ s}^{-1}$ (Gd³⁺). Error margins were set to $\pm 4 \text{ Å}$ and $\pm 3 \text{ Å}$ for MTSL and Gd³⁺ samples, respectively. iii) residues with $R_{2,\text{para}} < 7.0 \text{ s}^{-1}$ (MTSL) and $R_{2,\text{para}} < 3.0 \text{ s}^{-1}$ (Gd³⁺). These residues were considered to be too remote from the paramagnetic center to induce a significant PRE and therefore only the lower limit was calculated and found to be 22 Å and 44 Å for MTSL and Gd³⁺ samples, respectively.

The correlations between observed (O^{obs}) and back-predicted (O^{sim}) observables (PRE, PCS and RDC) were assessed with Q values using equation 2.^[19]

$$Q = \sqrt{\frac{\sum_i \{O^{\text{obs}}(i) - O^{\text{sim}}(i)\}^2}{\sum_i \{|O^{\text{obs}}(i)| + |O^{\text{sim}}(i)|\}^2}} \quad [2]$$

For Q (PRE), the residues with observed PRE of $R_{2,\text{para}} < 7.0 \text{ s}^{-1}$ (MTSL) and $R_{2,\text{para}} < 3.0 \text{ s}^{-1}$ (Gd³⁺) were excluded from the calculation. These residues were considered to be too remote from the paramagnetic center to induce a significant PRE.

References

1. J. Schilder, M. Ubbink, *Curr Opin Struct Biol*, **2013**, *23*, 911-918.
2. J. M. Nocek, A. K. Knutson, P. Xiong, N. P. Co, B. M. Hoffman, *J Am Chem Soc*, **2010**, *132*, 6165-6175.
3. G. Schreiber, G. Haran, H. X. Zhou, *Chem Rev*, **2009**, *109*, 839-860.
4. M. Katagiri, B. Ganguli, I. C. Gunsalus, *Fed Proc*, **1968**, *27*, 525-&.
5. Y. Hiruma, M. A. Hass, Y. Kikui, W. M. Liu, B. Olmez, S. P. Skinner, A. Blok, A. Kloosterman, H. Koteishi, F. Lohr, H. Schwalbe, M. Nojiri, M. Ubbink, *J Mol Biol*, **2013**, *425*, 4353-4365.
6. S. Tripathi, H. Li, T. L. Poulos, *Science*, **2013**, *340*, 1227-1230.
7. I. F. Sevrioukova, T. L. Poulos, I. Y. Churbanova, *The Journal of biological chemistry*, **2010**, *285*, 13616-13620.
8. I. F. Sevrioukova, T. L. Poulos, *Arch Biochem Biophys*, **2011**, *507*, 66-74.
9. V. Y. Kuznetsov, T. L. Poulos, I. F. Sevrioukova, *Biochemistry*, **2006**, *45*, 11934-11944.
10. N. Sari, M. J. Holden, M. P. Mayhew, V. L. Vilker, B. Coxon, *Biochemistry*, **1999**, *38*, 9862-9871.
11. P. H. Keizers, A. Saragliadis, Y. Hiruma, M. Overhand, M. Ubbink, *J Am Chem Soc*, **2008**, *130*, 14802-14812.
12. D. Shishmarev, G. Otting, *J Biomol NMR*, **2013**, *56*, 203-216.
13. W. M. Liu, P. H. Keizers, M. A. Hass, A. Blok, M. Timmer, A. J. Sarris, M. Overhand, M. Ubbink, *J Am Chem Soc*, **2012**, *134*, 17306-17313.
14. W. Zhang, S. S. Pochapsky, T. C. Pochapsky, N. U. Jain, *J Mol Biol*, **2008**, *384*, 349-363.
15. S. Scanu, J. Forster, M. G. Finiguerra, M. H. Shabestari, M. Huber, M. Ubbink, *Chembiochem*, **2012**, *13*, 1312-1318.
16. S. G. Sligar, P. G. Debrunner, J. D. Lipscomb, M. J. Namtvedt, I. C. Gunsalus, *Proc Natl Acad Sci U S A*, **1974**, *71*, 3906-3910.
17. P. H. Keizers, B. Mersinli, W. Reinle, J. Donauer, Y. Hiruma, F. Hannemann, M. Overhand, R. Bernhardt, M. Ubbink, *Biochemistry*, **2010**, *49*, 6846-6855.

18. J. Evenas, V. Tugarinov, N. R. Skrynnikov, N. K. Goto, R. Muhandiram, L. E. Kay, *J Mol Biol*, **2001**, *309*, 961-974.
19. Q. Bashir, A. N. Volkov, G. M. Ullmann, M. Ubbink, *J Am Chem Soc*, **2010**, *132*, 241-247.
20. J. A. Worrall, Y. Liu, P. B. Crowley, J. M. Nocek, B. M. Hoffman, M. Ubbink, *Biochemistry*, **2002**, *41*, 11721-11730.
21. X. Xu, W. Reinle, F. Hannemann, P. V. Konarev, D. I. Svergun, R. Bernhardt, M. Ubbink, *J Am Chem Soc*, **2008**, *130*, 6395-6403.
22. K. Pervushin, R. Riek, G. Wider, K. Wuthrich, *Proc Natl Acad Sci U S A*, **1997**, *94*, 12366-12371.
23. M. Aoki, K. Ishimori, H. Fukada, K. Takahashi, I. Morishima, *Biochim Biophys Acta*, **1998**, *1384*, 180-188.
24. S. Scanu, J. M. Foerster, G. M. Ullmann, M. Ubbink, *J Am Chem Soc*, **2013**, *135*, 7681-7692.
25. A. Spaar, C. Dammer, R. R. Gabdouliline, R. C. Wade, V. Helms, *Biophys J*, **2006**, *90*, 1913-1924.
26. F. Delaglio, S. Grzesiek, G. W. Vuister, G. Zhu, J. Pfeifer, A. Bax, *J Biomol NMR*, **1995**, *6*, 277-293.
27. W. F. Vranken, W. Boucher, T. J. Stevens, R. H. Fogh, A. Pajon, M. Llinas, E. L. Ulrich, J. L. Markley, J. Ionides, E. D. Laue, *Proteins*, **2005**, *59*, 687-696.
28. T. A. Lyons, G. Ratnaswamy, T. C. Pochapsky, *Protein Sci*, **1996**, *5*, 627-639.
29. J. Garcia de la Torre, M. L. Huertas, B. Carrasco, *J Magn Reson*, **2000**, *147*, 138-146.

CHAPTER 6

Structural characterization
of the substrate access
channel of P450cam with
a paramagnetic inhibitor

Abstract

P450 enzymes bind to a variety of different compounds to catalyze monooxygenation reactions. However, the mechanisms of substrate recognition and product release of P450 enzymes are poorly understood. In the presence of substrates, the crystal structures of P450cam have been shown to adapt the closed conformation. In this state, there is no channel through which substrates can access the active site of P450cam. In this project, utilizing the paramagnetic inhibitor, N-(3-(1H-imidazole-1-yl)phenyl)-1-oxylradical-2,2,5,5-tetramethyl- δ -3-pyrroline-3-carboxamide (1-PIM-3), the nature of the substrate access channel was investigated by X-ray crystallography as well as paramagnetic NMR techniques. X-ray crystallography revealed that P450cam exhibits the open conformation in the complex with 1-PIM-3. The substrate access channel was traced by paramagnetic relaxation enhancements, indicating that the A helix and the region nearby β 1 sheet are part of the substrate access channel.

Introduction

Cytochrome P450cam (CYP101A1) is an archetypical bacterial P450 for which more than a hundred structures have deposited in the protein data bank. Recently, crystal structures of artificially cross-linked Pdx and P450cam were solved,^[1] which raised questions about the conformational states of P450cam. In the presence of the substrate almost all of the P450cam structures show the “closed” conformation, in which there is no channel present large enough to allow substrate access to the active site. Substrate entry into P450cam had puzzled researchers for decades until Dunn *et al.* co-crystallized the protein with elongated substrate analogues.^[2] These analogues protruded from the active site to the protein surface, forcing the substrate access channel to be opened. In 2010, Goodin and co-workers solved the crystal structure of P450cam in the absence of substrates, revealing that the opening of the substrate access channel primarily involves the movement of the F and G helices.^[3] While the structure of the “open” conformation provides valuable information for understanding P450cam catalysis, it also leaves many questions to be unresolved: how fast is the exchange between the open and closed conformations? Which factors trigger the equilibrium shift? Is there a secondary substrate binding site inside the channel as suggested by a recent study?^[4] Paramagnetic NMR techniques can be used to examine the substrate access channel in solution. When a substrate or inhibitor analogue with a paramagnetic center binds to the active site of P450cam, it should cause PREs mark on the residues comprising the substrate access channel. The PRE is dependent on distance between a paramagnetic center and observed residue and the sensitivity of the PRE allows the detection of minor conformational states of proteins.^[4] Tracking the PRE effect on P450cam residues, the structure and dynamics of substrate access channel can be analyzed (Figure 1). In this chapter, the paramagnetic substrate analogue, 1-PIM-3-para, was used to characterize the substrate access channel of P450cam. The work demonstrates the proof-of-principle that small paramagnetic centers attached to ligands rather than protein can be helpful to characterize a complex.

Results & Discussion

1-PIM-3 binding to P450cam

The paramagnetic substrate analogue, 1-PIM-3-para, was designed on the basis of the known type I inhibitor of P450cam, 1-phenylimidazole, and a commonly used paramagnetic spin label, 1-oxyl-2,2,5,5-tetramethyl- δ -3-pyrroline-3-methyl (OTPM). The crystal structure of 1-phenylimidazole bound P450cam indicates that the closed conformation of P450cam remains intact while one nitrogen atom of the imidazole group binds the heme iron.^[5] The coordination of the sixth ligand to the iron provides an important advantage to the NMR analysis since it suppresses the endogenous PRE effect caused by the high spin state of the heme iron. The diamagnetic inhibitor analogue, 1-PIM-3-dia was prepared by replacing OTPM with 1-methoxy-2,2,5,5-tetramethyl- δ -3-pyrroline-3-methyl (MTPM) group of 1-PIM-3-para.

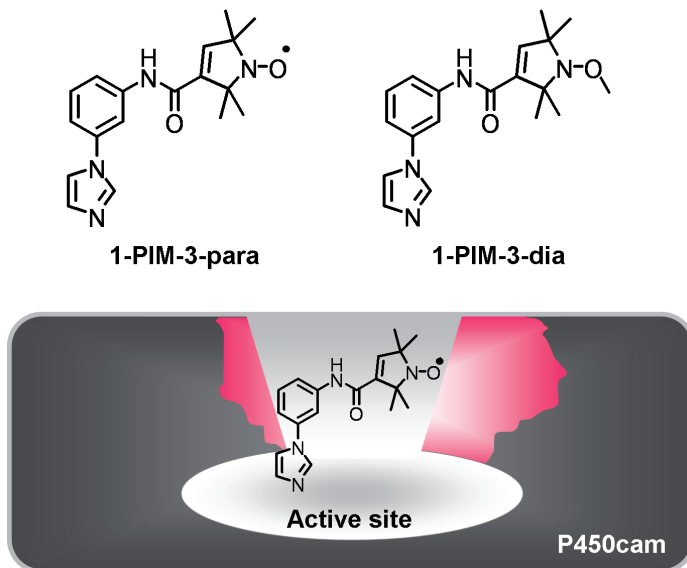


Figure 1. Schematic representation of mapping the channel with PREs. The paramagnetic inhibitor analogue, 1-PIM-3-para reaches the active site of P450cam through the substrate access channel. The red colored regions of P450cam represent the residues that exhibit PRE.

To determine the affinity of 1-PIM-3 to P450cam, a competitive binding assay was carried out with UV/VIS spectrophotometry (Figure 2).

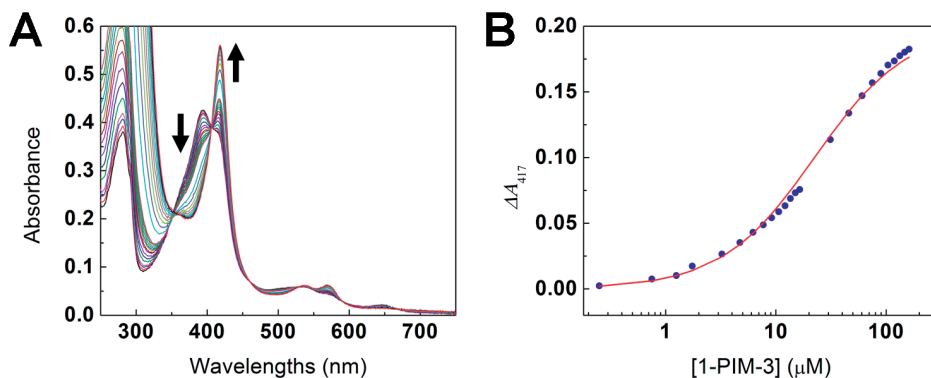


Figure 2. Competitive binding assay of 1-PIM-3 and camphor to P450cam. (A) Overlaid traces of absorption spectra of P450cam. Upon the titration of 1-PIM-3, the maximum absorption peak at 391 nm shifts to the 417 nm. (B) The plot of ΔA_{417} against the concentration of 1-PIM-3. The blue points and red line represent the experimentally derived ΔA_{417} values and the simulated curve, respectively.

In the presence of the physiological substrate, camphor, the changes of the Soret maximum peak at 417 nm wavelength of P450cam were monitored with increasing concentration of 1-PIM-3. The dissociation constant (K_D) of 1-PIM-3 was estimated to be $7.5 \pm 0.5 \mu\text{M}$ by simulating the curve with the binding affinity for 1-PIM-3 as well as camphor and the maximal change of the absorbance at 417 nm (ΔA_{417}) as variable (Figure 2B). The K_D of camphor was found to be $7 \pm 1 \mu\text{M}$, which is in line to the previous study of $K_D = 10.2 \pm 0.6 \mu\text{M}$.^[6] The details of the simulation are described in the Materials and Methods. The obtained K_D value of 1-PIM-3 is compared with those of camphor and 1-phenylimidazole in Table 1. The binding affinity of 1-PIM-3 is comparable to that of camphor. The difference of K_D by 70–80 folds with 1-phenylimidazole is attributed to the presence of OTPM function group.

Table 1. Dissociation constant (K_D) of P450cam substrate and inhibitors.

Compounds	K_D (μM)
Camphor	7 ± 1
1-phenylimidazole	0.1 ^a
1-PIM-3	7.5 ± 0.5

(a) previously determined by Poulos, T.L. and Howard, A.J.^[5]

Crystal structure of P450cam bound to 1-PIM-3

Having established the affinity of 1-PIM-3 for P450cam, we obtained the structural information of P450cam bound to 1-PIM-3 by X-ray crystallography. The formation of crystal was observed under the same conditions as described by Lee, Y.T. *et al.*^[7] The crystal structures of both 1-PIM-3-para and -dia bound P450cam were solved with maximum resolution of 2.2 Å and 2.0 Å, respectively. Data processing and refinement were carried out by Dr. Igor Nederlof (Biophysical Structural Chemistry group at Leiden University).

In line with the findings for 1-phenylimidazole,^[5] the crystal structure of 1-PIM-3 shows that the nitrogen atom of imidazole group coordinates the heme iron (Figure 3A). While the electron density of the 1-phenylimidazole group as well as the amide linker is well-defined, that of the OTPM functional group was less clear. This observation points toward mobility of the OTPM group, which has also been reported for MTSL labeled samples in NMR studies.^[8-9]

To further characterize the 1-PIM-3 binding, a comparison was made with the crystal structure of P450cam bound to 1-phenylimidazole.^[5] The position of the axial nitrogen atom of imidazole group is very similar (Figure 3B), indicating that the nature of type I inhibition of 1-phenylimidazole is conserved in 1-PIM-3. However, the orientation of the 1-PIM-3 imidazole ring was found to be rotated by 55 degrees relative to that

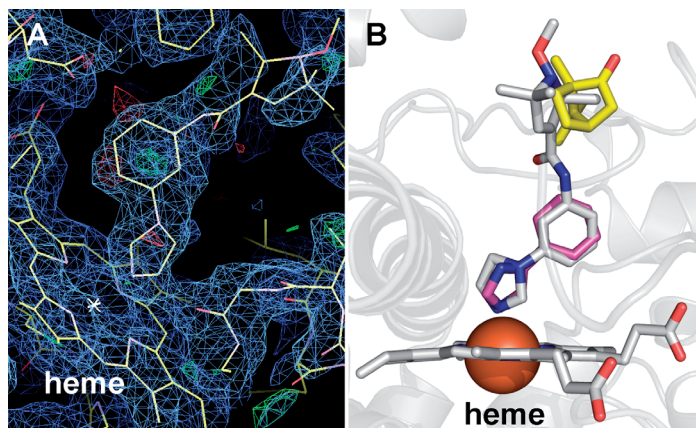


Figure 3. Crystal structure of P450cam bound to 1-PIM-3-dia. (A) Details of the electron density map with a maximum resolution of 2.0 Å. The structure was solved by molecular replacement using P450cam in the open conformation (PDB entry 3L61^[10]). (B) Positions and orientations of ligands are superimposed. Gray, pink and yellow sticks represent 1-PIM-3-dia, 1-phenylimidazole and camphor, respectively.

of 1-phenylimidazole. It is also worth mentioning that the position of OTPM group coincides to the previously observed second substrate binding site.^[1] The potential link between the occupancy of the second binding site and conformation state of P450cam will be studied in future.

Interestingly, 1-PIM-3 bound P450cam is present with substrate access channel in the open conformation, which distinctively differs from the closed conformation of P450cam bound to 1-phenylimidazole (Figure 4). The conformations of substrate access channel can be classified by the structural features of antiparallel F and G helices and intervening F–G loop.^[7] The F–G loop region exhibits the largest movement upon the conformational change in P450cam.

The superimposed structures of the F–G loop illustrate that 1-PIM-3 bound P450cam adopts the structural features of the open conformation (Figure 4). In fact, the degree opening appears to be even slightly larger than in the substrate-free structure. It is plausible that the presence of bulky OTPM functional group forces the protein into this conformation. Other residues that are known to correlate with the conformation change are shown in Figure 4B and C. The formation of the unusual hydrogen bond between hydroxyl group of Thr252 and carboxyl backbone of Gly248 is a unique feature of the closed conformation. It has been reported to regulate the position of catalytic water in the active site.^[10] Another characteristic aspect of P450cam conformational states is the arrangement of the B' helix. In the intermediate and open states, the B' region exhibit large mobility and does not form the defined secondary structure. However, the binding of a potassium ion enhances the stability

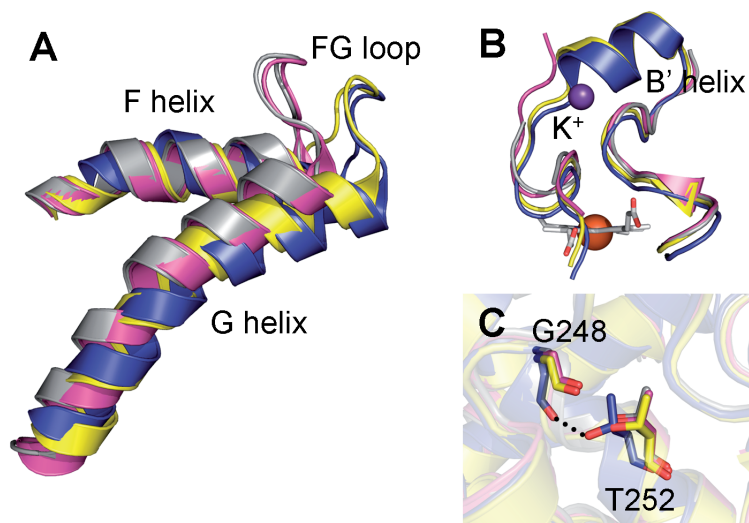


Figure 4. Superimposed structures of P450cam in different conformations. Blue, yellow, purple and gray structures represent closed (PDB entry, 1DZ4),^[11] intermediate (1K2O),^[2] open (3L61)^[10] and 1-PIM-3, respectively. (A) Ribbon representation of the F and G helices and the F–G loop. (B) Cartoon representation of the B' helix. The purple sphere represents a potassium ion. (C) Sticks depict the conformations for the indicated residues. Black dots represent a hydrogen bond.

of B' helix. It increases the binding affinity of camphor by ten-folds, which leads to the closed conformation.^[10] Taken together, we concluded that 1-PIM-3 binding forces the substrate access channel of P450cam into the open state.

PRE analysis of P450cam bound to 1-PIM-3

To investigate the dynamics and structural components involved in the substrate access channel, a paramagnetic NMR experiment was carried out. In the current study, due to the limited availability of [²H, ¹⁵N] labeled proteins, [¹⁵N] isotopically enriched P450cam C334A/H352A mutant was used to optimize the experimental conditions. The catalytic activity of this mutant was shown to be intact in a previous study (Chapter 4). The two dimensional ¹⁵N–¹H HSQC spectra were acquired for the P450cam samples in the presence of 1-PIM-3-para/-dia. In addition to the amide-proton resonances of P450cam, large peaks caused by dimethylformamide (DMF) were observed across the indirect dimension at 7.8 ppm of the ¹H chemical shift (Figure 5A). The 3% of DMF used to solubilize 1-PIM-3 in the sample is the cause of this signal. The contribution of DMF peaks can be minimized by utilizing deuterated DMF in the future. The NMR spectra were overlaid with the closed conformation of P450cam in high spin and low spin states (kindly provided by Simon Skinner at Leiden University). Most of the assigned peaks in closed state were either shifted or disappeared, presumably due

to the P450cam being in the open conformation and the chemical shift perturbations caused by 1-PIM-3 binding. Out of 414 residues, 116 residues were assigned on the basis of the assignments of closed conformation. As a future perspective, the number of unambiguous assignments can be increased by acquiring NMR spectra in a titration of camphor. In addition, the exchange regime (on the NMR time-scale) of the association and dissociation of 1-PIM-3-dia binding needs to be established. From the ratios of the peak intensities of 1-PIM-3-para/-dia (I_{para}/I_{dia}), the PREs were calculated. The observed PREs are a weighted average of 1-PIM-3 bound form and substrate-free P450cam. Given the $K_D = 7.5 \mu\text{M}$, ca. 90% of P450cam was bound to 1-PIM-3 in this experiment. Therefore, the observed PREs were extrapolated to the 100% bound

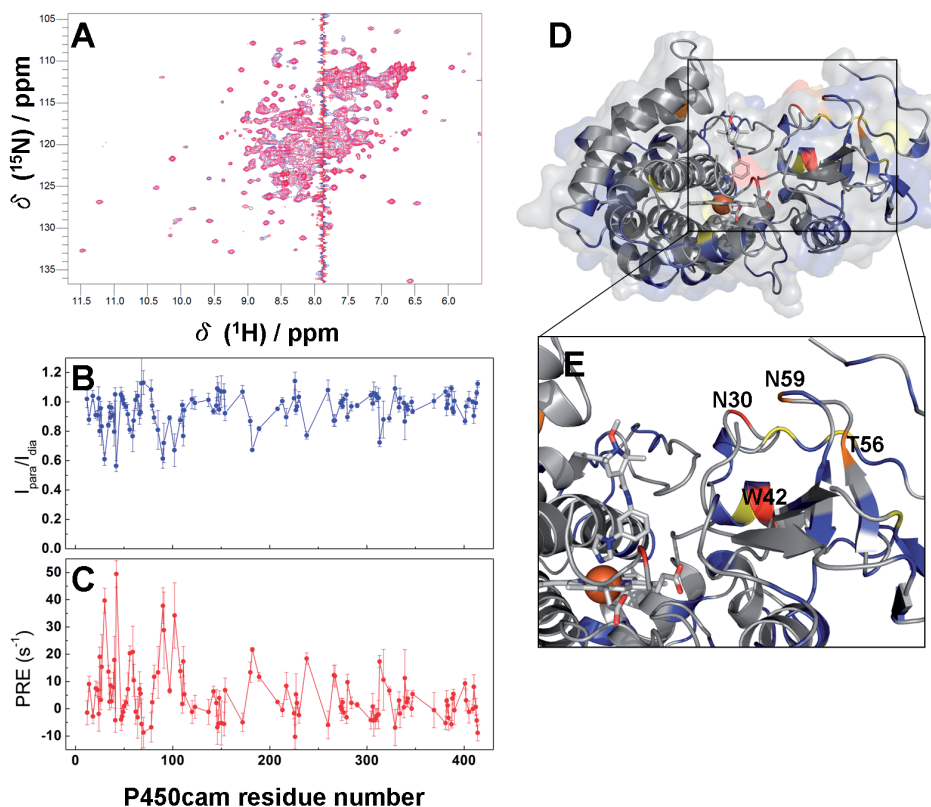


Figure 5. PRE analysis of P450cam bound to 1-PIM-3. (A) Overlaid HSQC spectra of P450cam. Blue and red peaks represent 1-PIM-3-dia and -para samples, respectively. (B) I_{para}/I_{dia} ratios (B) and PREs (C) are plotted against P450cam residue number. (D) Ribbon representation of the crystal structure of P450cam bound to 1-PIM-3. P450cam residues were color coded according to PRE with $\geq 30 \text{ s}^{-1}$, red; 20–30 s^{-1} , orange; 15–20 s^{-1} , yellow; $< 15 \text{ s}^{-1}$, blue. Unassigned residues are shown in gray. (E) Zoom-in of the region affected by PRE. Sticks and sphere represent 1-PIM-3-dia and heme.

state by dividing the PREs by 0.9. The calculated PREs were color coded on P450cam as shown in Figure 5.

It has been reported that the secondary structural elements helices, F, G and I as well as the F–G loop exhibit distinct movements in the transition between the conformational states.^[7] Due to the significant chemical shift changes, it was impossible to assign the resonances of residues in those elements. The B' helix, comprising residues 90–95, is also known to be important for the conformation shift of P450cam. Significant PREs ($>25 \text{ s}^{-1}$) indicate that those residues are in close proximity of the paramagnetic center of 1-PIM-3. In addition to the previously described structural motifs, other regions, such as the A helix and the nearby $\beta 1$ sheet also display strong PREs (Figure 5E). Most of these residues are located within 22 Å from the paramagnetic center, which agrees well with the distance range in which a nitoxide spin label is expected to cause PREs (14–22 Å). Further NMR experiments are required to characterize the dynamics and nature of the substrate access channel in the solution state.

Conclusions

The current study demonstrated binding of a paramagnetic inhibitor analogs to P450cam. The binding affinity of 1-PIM-3 was found to be $K_D = 7.5 \text{ }\mu\text{M}$, which is comparable to the physiological substrate, camphor. The crystal structure of P450cam bound to 1-PIM-3 exhibits a more open conformation than that of substrate-free form. The preliminary results of the PRE analysis indicate that paramagnetic ligand analogues can be used to characterize protein-ligand complexes.

Materials and Methods

Chemicals

1-PIM-3-para/-dia were kindly provided by Wei-Min Liu (Leiden University).

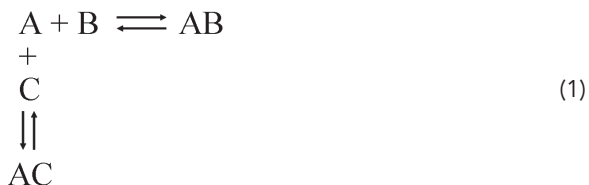
Protein production

P450cam C334A as well as [¹⁵N] isotopically enriched P450cam C334A/H352A were produced and purified as described in Chapters 3 and 4. Camphor was removed by Superose 12 gel filtration column (120 mL) pre-equilibrated with 20 mM Hepes, pH 7.4. The fractions containing P450cam with absorbance ratio of $A_{417}/A_{280} > 1.55$ were pooled.

Competitive binding assay

The reaction mixtures (2 mL) contained 5 μM P450cam C334A in 20 mM Hepes, pH 7.4 and 100 mM KCl. First, P450cam was saturated with three molar equivalents of camphor. 1-PIM-3 was titrated into camphor bound P450cam and the change of the Soret maximum peak at 417 nm (ΔA_{417}) was monitored at 293K.

The following model was used to describe the binding of camphor and 1-PIM-3.



where A, B, C, AB and AC represent P450cam, camphor, 1-PIM-3, camphor bound P450cam and 1-PIM-3 bound P450cam, respectively. The system is described by two K_D values and the mass laws (eq. 2-7)

$$K_D^{AB} = \frac{A \cdot B}{AB} \tag{2}$$

$$K_D^{AC} = \frac{A \cdot C}{AC} \tag{3}$$

$$B = \frac{B_t \cdot K_D^{AB}}{K_D^{AB} + A} \tag{4}$$

$$B_t = B + AB \tag{5}$$

$$C = \frac{C_t \cdot K_D^{AC}}{K_D^{AC} + A} \tag{6}$$

$$C_t = C + AC \tag{7}$$

The experimental absorbance change at 417 nm was simulated with eq. 8 for each point (*i*) in the titration, by varying K_D^{AB} , K_D^{AC} and ΔA_{417}^{\max} , the maximal change in absorbance (for 100% P450cam-1-PIM-3 complex).

$$\Delta A_{417}(i) = \frac{AC_i}{A_t} \cdot \Delta A_{417}^{\max} \tag{8}$$

The error associated with the dissociation constant was estimated by measuring the agreement between experimental and simulated data.

Crystallization

The stock solution contained 200 μ M P450cam C334A in 20 mM Hepes, pH 7.4 and 2 mM 1-PIM-3-para/-dia (10% DMF). Crystals of P450cam bound to 1-PIM-3 were grown by the sitting-drop vapor diffusion method at room temperature from 12–22% PEG 8000, 100 mM sodium cacodylate, pH 5.5–7.0 and 100–200 mM KCl. The crystals were mounted on nylon loops containing glycerol as a cryoprotectant and flash-frozen in liquid nitrogen.

X-ray diffraction data were collected at European synchrotron radiation facility in Grenoble. Data collection and crystal structure determination were performed by Dr. Igor Nederlof (Biophysical Structural Chemistry group at Leiden University).

NMR samples and experiments

The fractions from Superose 12 column were pooled and buffer exchanged to 100 mM cacodylic acid, pH 6.5, 200 mM KCl, 12.5% D₂O by ultrafiltration using a centricon (5K). The NMR samples contained 250 μM [¹⁵N] P450cam C334A/H352A and 300 μM 1-PIM-3-para/-dia in 80 mM cacodylic acid, 160 mM KCl, pH 6.5, 5 mM HEPES, 10% D₂O and 3% DMF. Two-dimensional ¹⁵N–¹H HSQC spectra were recorded at 298 K on a Bruker Avance III HD 850-MHz spectrometer equipped with a TCI-Z-GRAD cryoprobe. NMR data were processed in NMRPipe^[13] and analyzed in CCPNMR.^[14]

NMR assignment

The amide resonances of P450cam C334A/H352A bound to 1-PIM-3-dia/-para were assigned on the basis of cyanide and camphor-bound oxidized P450cam C334A (provided by Simon Skinner, Leiden University).

Restraint analysis

The ratios of $I_{\text{para}}/I_{\text{dia}}$ were normalized by dividing them by the averaged values of the 85 largest $I_{\text{para}}/I_{\text{dia}}$ ratios (0.96). PREs were determined as described in the Chapter 3 and 5.

References

1. S. Tripathi, H. Li, T. L. Poulos, *Science*, **2013**, *340*, 1227-1230.
2. A. R. Dunn, I. J. Dmochowski, A. M. Bilwes, H. B. Gray, B. R. Crane, *Proc Natl Acad Sci U S A*, **2001**, *98*, 12420-12425.
3. Y. T. Lee, R. F. Wilson, I. Rupniewski, D. B. Goodin, *Biochemistry*, **2013**, *49*, 3412-3419.
4. M. Ubbink, *Biochem Soc Trans*, **2012**, *40*, 415-418.
5. T. L. Poulos, A. J. Howard, *Biochemistry*, **1987**, *26*, 8165-8174.
6. D. P. Nickerson, L. L. Wong, *Protein Eng*, **1997**, *10*, 1357-1361.
7. Y. T. Lee, E. C. Glazer, R. F. Wilson, C. D. Stout, D. B. Goodin, *Biochemistry*, **2011**, *50*, 693-703.
8. N. L. Fawzi, M. R. Fleissner, N. J. Anthis, T. Kalai, K. Hideg, W. L. Hubbell, G. M. Clore, *J Biomol NMR*, **2011**, *51*, 105-114.
9. J. Iwahara, C. D. Schwieters, G. M. Clore, *J Am Chem Soc*, **2004**, *126*, 5879-5896.
10. Y. T. Lee, R. F. Wilson, I. Rupniewski, D. B. Goodin, *Biochemistry*, **2010**, *49*, 3412-3419.
11. I. Schlichting, J. Berendzen, K. Chu, A. M. Stock, S. A. Maves, D. E. Benson, R. M. Sweet, D. Ringe, G. A. Petsko, S. G. Sligar, *Science*, **2000**, *287*, 1615-1622.
12. E. K. Ascutto, J. D. Madura, S. S. Pochapsky, B. OuYang, T. C. Pochapsky, *J Mol Biol*, **2009**, *388*, 801-814.
13. F. Delaglio, S. Grzesiek, G. W. Vuister, G. Zhu, J. Pfeifer, A. Bax, *J Biomol NMR*, **1995**, *6*, 277-293.
14. W. F. Vranken, W. Boucher, T. J. Stevens, R. H. Fogh, A. Pajon, M. Llinas, E. L. Ulrich, J. L. Markley, J. Ionides, E. D. Laue, *Proteins*, **2005**, *59*, 687-696.

CHAPTER 7

General discussion

Pdx-P450cam complex

At the start of this research in 2009, the molecular details of interaction and ET in the Pdx-P450cam complex had yet to be elucidated due to the lack of atomic resolution structures. Zhang *et al.* had generated a model of the Pdx-P450cam complex by NMR experiments,^[1] in which the interactions in the interface agreed well with mutagenesis studies.^[2-3] The initial aim of the project was to validate their model by paramagnetic NMR techniques. By attaching Ln^{3+} -CLaNP-7 at multiple locations on Pdx and P450cam surfaces, 446 distance and orientation restraints were obtained (Chapter 3). An ensemble of solution structures with average RMSD from the mean of 1.3 Å for the position of Pdx has obtained. Similar approach has been demonstrated by Keizers *et al.*^[4] The structure complex of adrenodoxin (Adx) and adrenodoxin reductase (AdR) was determined by the combination of chemical shift perturbation, pseudocontact shift and paramagnetic relaxation enhancement. Adx is also [2Fe-2S] cluster containing ferredoxin, which hampers NMR studies by broadening the residual peaks around [2Fe-2S] cluster. However, using long-range restraints obtained from two Ln^{3+} attachment sites, they showed that the mean of ensemble solution structures is close to the crystal structure of the complex with an RMSD of 4.0 Å.^[4] Strikingly, our structure generated by paramagnetic NMR restraints differs from the previously proposed model. Our collaborators, Dr. Nojiri and co-workers at Osaka University in Japan, crystallized the Pdx-P450cam complex. Their crystal structure closely resembles the solution structure. Structural analysis of the interface shows two potential ET pathways as well as several interaction networks. In addition to a putative hydrogen bond between Pdx Asp38 and P450cam Arg112 as well as hydrophobic contacts between Pdx Trp106 and P450cam Ala113, several polar residues are found in the interface. Site-directed mutagenesis and kinetics analysis revealed that these residues, which had not been recognized to be relevant for the binding before, play an important role in the binding affinity of Pdx-P450cam (Chapter 4). While our manuscript was under review, Tripathi *et al.* published the crystal structure of the Pdx-P450cam complex that was obtained via cross linking of the two proteins.^[5] Tripathi *et al.* found that P450cam is present in a state that resembles the open state of P450cam. On the basis of this observation, they concluded that the nature of effector role of Pdx (see Chapter 1) is to cause a conformation change in P450cam from the closed to open state.^[5] The crystal structure of the complex solved by Dr. Nojiri and co-workers showed that the conformation of P450cam is in an intermediate state between open and closed.^[6] It is not clear whether the open state found in the crystal structures is a consequence of crystal packing. In both cases, contacts of the F or G helices with neighboring molecules in the crystal are observed, which could imply that only the open state of P450cam in complex with Pdx is able to crystallize. To investigate whether Pdx binding indeed causes the opening of P450cam, Myers *et al.* used double electron-electron resonance (DEER) spectroscopy.^[7] The results of DEER indicated that the conformation change of P450cam is dependent

on the redox state of Pdx. Reduced Pdx binding to reduced P450cam-CO does not induce the transition of the P450cam conformation. However, the binding of oxidized Pdx shifts the equilibrium to the open state.^[7] Further NMR experiments that are able to distinguish between the open and closed states of P450cam in the complex in solution are required. In Chapter 2, intramolecular PCS experiments are described, that were aimed at observing the dynamics of P450cam upon binding of oxidized Pdx. In contrast to the previous findings, our results indicated that a major conformational change of P450cam was not observed between presence and absence of Pdx. The discrepancy between the results of X-ray crystallography, DEER and paramagnetic NMR experiments can most likely be attributed to the experimental conditions. Crystal formation was only observed at low concentrations of potassium,^[5-6] which favors the shift to the open state.^[8] The DEER experiments were carried out in frozen solutions at 30/50K.^[7] Paramagnetic NMR experiments allow the investigation of the sample in the solution state under a variety of the conditions at ambient temperature. Previously, Pochapsky and co-workers proposed the alternative roles of Pdx effector activity.^[9] On the basis of the NMR data and structure calculations, they found that Pdx binding induces the *trans*-to-*cis* isomerization of Ile88-Pro89 amide bond.^[10] The change to the *cis* conformer facilitates the rearrangement of the substrate to the orientation appropriate for hydroxylation reaction.^[9] Furthermore, they reported that the effect of Pdx binding transmits to the distal side of P450cam, which leads to the complete closure of the substrate access channel. This mechanism potentially prevents the dissociation of the substrate and minimizes the formation of the unwanted peroxide intermediate.^[9] Currently, further intramolecular PCS experiments are undertaken to elucidate the dynamics of P450cam upon Pdx binding.

Encounter complex

The results in Chapter 3 demonstrated the accuracy of the paramagnetic NMR approach for structure determination. The long-range distance and orientation restraints provided by PCS, RDC and PRE analysis allowed the characterization of the 58 kDa redox complex, which could not easily have been achieved by conventional NMR methods. Moreover, PRE analysis provided information about a lowly populated encounter state of Pdx-P450cam interaction (Chapter 5). The encounter complex is the intermediate state of protein-protein interaction, in which one protein samples the partner surface to find the binding site. This transient state accelerates the formation of the final, stereo-specific complex.^[11] In the encounter state, Pdx visits the regions nearby the J and K helices as well as the β 1 sheet of P450cam. Structural analysis revealed that almost entire surfaces of both Pdx and P450cam are covered by acidic residues. The local electrostatic interaction alone is insufficient to describe the driving force of Pdx-P450cam encounter complex. Mutagenesis and kinetics described in Chapter 4 demonstrated that the polar residues in the interface contribute to the binding affinity

of Pdx-P450cam interaction. Given that the formation of stereo-specific complex is stabilized by the hydrogen bonds between Pdx Asp38 and P450cam Arg112 as well as hydrophobic contacts between Pdx Trp106 and P450cam Ala113,^[6] we postulated that encounter state of Pdx-P450cam complex is driven by local electrostatic interactions as well as short-range interactions. The significance of hydrophobic interactions in the encounter complex has been also described in the ET complex of cytochrome *f* (cyt *f*) and plastocyanin (Pc) in cyanobacterium *Nostoc* sp PCC 7119.^[12] The hydrophobic patch of cyt *f* guides Pc to the specific binding site. Further structure calculation of Pdx-P450cam encounter complex are currently undertaken to illustrate the functional significance of the encounter state.

P450cam substrate channel

The mechanism of the substrate entry and product release of P450cam has been illuminated by solving the crystal structure of P450cam bound to the ruthenium-linker substrate analogue.^[13] It traps the structure of P450cam to be in open state and allows to visualize the substrate access channel. In Chapter 6, a paramagnetic inhibitor molecule, 1-PIM3-para, was used to characterize the substrate binding channel by X-ray crystallography as well as paramagnetic NMR spectroscopy. In the biophysical structural chemistry group at Leiden University, Dr. Nederlof solved the crystal structure of P450cam bound to 1-PIM-3 with a maximum resolution of 2.0 Å. In contrast to other substrate analogues, P450cam was shown to adapt an open conformation when it is bound to 1-PIM-3. Preliminary results of PRE experiments indicated that the dynamics of substrate access channel extends over a wide range of P450cam structural component. Further NMR studies are required to elucidate the nature of substrate binding of P450cam.

In conclusion, the structure and dynamics of P450cam system were analyzed by paramagnetic NMR techniques. The stereo-specific final complex and transient encounter complex of Pdx and P450cam have been uncovered by pseudocontact shift, residual dipolar coupling and paramagnetic relaxation enhancement. Moreover, the result of X-ray crystallography has provided the significant insights of the interaction and raised the questions of the Pdx effector activity. Since paramagnetic NMR experiments detect the complex in solution under ambient temperature, paramagnetic NMR will further illuminate the molecular mechanism of P450cam system in future.

References

1. W. Zhang, S. S. Pochapsky, T. C. Pochapsky, N. U. Jain *J Mol Biol.* **2008**, *384*, 349-363.
2. V. Y. Kuznetsov, T. L. Poulos, I. F. Sevrioukova *Biochemistry.* **2006**, *45*, 11934-11944.
3. I. F. Sevrioukova, T. L. Poulos *Arch Biochem Biophys.* **2011**, *507*, 66-74.
4. P. H. Keizers, B. Mersinli, W. Reinle, J. Donauer, Y. Hiruma, F. Hannemann, M. Overhand, R. Bernhardt, M. Ubbink *Biochemistry.* **2010**, *49*, 6846-6855.
5. S. Tripathi, H. Li, T. L. Poulos *Science.* **2013**, *340*, 1227-1230.

General discussion

6. Y. Hiruma, M. A. Hass, Y. Kikui, W. M. Liu, B. Olmez, S. P. Skinner, A. Blok, A. Kloosterman, H. Koteishi, F. Lohr, H. Schwalbe, M. Nojiri, M. Ubbink *J Mol Biol.* **2013**, *425*, 4353-4365.
7. W. K. Myers, Y. T. Lee, R. D. Britt, D. B. Goodin *J Am Chem Soc.* **2013**, *135*, 11732-11735.
8. B. OuYang, S. S. Pochapsky, G. M. Pagani, T. C. Pochapsky *Biochemistry.* **2006**, *45*, 14379-14388.
9. E. K. Ascitutto, J. D. Madura, S. S. Pochapsky, B. OuYang, T. C. Pochapsky *J Mol Biol.* **2009**, *388*, 801-814.
10. B. OuYang, S. S. Pochapsky, M. Dang, T. C. Pochapsky *Structure.* **2008**, *16*, 916-923.
11. J. Schilder, M. Ubbink *Curr Opin Struct Biol.* **2013**, *23*, 911-918.
12. S. Scanu, J. M. Foerster, G. M. Ullmann, M. Ubbink *J Am Chem Soc.* **2013**, *135*, 7681-7692.
13. A. R. Dunn, I. J. Dmochowski, A. M. Bilwes, H. B. Gray, B. R. Crane *Proc Natl Acad Sci U S A.* **2001**, *98*, 12420-12425.

ADDENDUM

Summary

Samenvatting

Publication list

Curriculum Vitae

Acknowledgements

Summary

Among the 15,000 reported cytochrome P450s, the best characterized P450 family member is P450cam (CYP101A1). The aim of the research described in this thesis is to advance our understanding of the mechanisms of P450cam-ligand interactions. The results of the studies provide general insights into P450 systems, since their catalytic mechanisms are closely related to that of P450cam. Chapter 1 provides a general introduction about the P450 superfamily, the catalytic cycle and electron transfer partners of P450cam as well as paramagnetic NMR methods.

In chapter 2, a study is described in which a paramagnetic NMR probe, CLaNP-7, was attached at multiple sites of P450cam and Pdx to determine the structure of their complex in solution. The size and orientation of $\Delta\chi$ tensors of Ln^{3+} -CLaNP-7 and the metal positions were experimentally determined by pseudocontact shift (PCS) analysis. Out of twelve P450cam constructs, six P450cam mutants were produced. The other six constructs yielded very little protein and therefore, it was decided not to use them for CLaNP-7 labeling. The low yield of P450cam constructs was attributed to the substitution of double Cys mutations, which apparently leads to instable or incorrectly folded protein in some cases. The $\Delta\chi$ tensors derived from the experimentally obtained PCS suggested that all of the mutants were labeled with CLaNP-7 via two arms, except for P450cam mutant F (A113C/N116C). Fitting of the Ln^{3+} position based on the PCS showed that CLaNP-7 was anchored at P450cam mutant F via a single disulfide bond. Two of the mutants were found either too close or far away from the Pdx binding site. In total, four out of twelve mutants were used for the calculations, which indicates that designing probe positions on protein contains the elements of trial and error. These results form the prelude for the intermolecular paramagnetic NMR experiments to study Pdx-P450cam complex, which are discussed in chapter 3.

In this chapter the structure of the oxidized Pdx-P450cam complex in solution is reported, based on a set of 446 restraints for structure calculation obtained by PCS, PRE and RDC analysis. After the structure had been determined, our collaborators also solved the crystal structure of the complex. The solution structure based on paramagnetic restraints is represented by an ensemble of ten structures with an average RMSD from the mean of 1.3 Å for the position of Pdx. The position for Pdx relative to P450cam observed in the crystal structure is identical to the one in the solution structure within the experimental precision of the ensemble. These results demonstrate the accuracy of the paramagnetic approach for structure determination. The structure demonstrated that the metal centers are 16Å away, allowing for a sufficiently fast ET. Two coupling pathways could be distinguished, connecting the FeS cluster to the conjugated heme ring system and iron, respectively. Strikingly, our structure of the Pdx-P450cam complex differs from the previously proposed model by Zhang *et al.* While our manuscript was under review, Tripathi *et al.* published the crystal structure of the Pdx-P450cam complex that was obtained via cross linking of the two proteins. Tripathi *et al.* found that P450cam is present in a state that resembles



the open state of P450cam. On the basis of this observation, they concluded that the nature of effector role of Pdx is to cause a conformation change in P450cam from the closed to open state. Further NMR experiments that are able to distinguish between the open and closed states of P450cam in the complex are required to establish whether Pdx binding causes the opening of P450cam also in solution.

The importance of the interactions of polar residues that were newly identified to be part of the interface of the Pdx-P450cam complex, is demonstrated by mutagenesis and kinetic experiments (Chapter 4). These polar interactions contribute to partner recognition but do not influence the electron transfer rates.

In the Chapter 5, we have characterized the encounter state of the Pdx-P450cam complex using paramagnetic data from additional probes. The results of PCS and RDC analysis support the previously determined structures of the complex. At the same time the distance restraints derived from PRE showed significant deviations from the expected values for some probes. It is concluded that a small fraction of the complex exhibits a dynamic nature. In the encounter state Pdx is localized close to the J and K helices as well as the β 1 sheet. These regions all have basic and hydrophobic residues clustered together. Previous mutagenesis studies as well as X-ray crystallography demonstrated that the interactions of Pdx and P450cam are dominated by polar interactions, hydrogen bonding and hydrophobic contacts. Given the overall negative charge of both proteins, it is reasonable to assume that Pdx visits mostly basic/hydrophobic patches of the P450cam surface. The lowly populated encounter complex could be relevant to the formation of the final Pdx-P450cam complex. The prominent basic patches compose a path to guide the Pdx to the putative binding site. Thereby, it reduces the three-dimensional search via collisions to a two-dimensional search on the P450cam surface. Moreover, the charge interaction prolongs the lifetime of the encounter facilitating the formation of the ET active complex.

The paramagnetic substrate analogue, 1-PIM-3-para, was used to characterize the substrate access channel of P450cam (Chapter 6). The crystal structure of P450cam bound to 1-PIM-3 exhibits a more open conformation than that of substrate-free form. The preliminary results of the PRE analysis indicate that paramagnetic ligand analogues can be used to characterize protein-ligand complexes. This work demonstrates the proof-of-principle that small paramagnetic centers attached to ligands rather than protein can be helpful to characterize a complex.

In conclusion, by utilizing paramagnetic NMR techniques, the structure and dynamics of the P450cam system were investigated. The analysis of PCS and RDC illuminated the stereo-specific final complex of Pdx and P450cam, while the results of PRE demonstrated the presence of a transient encounter complex. Furthermore, the significant insights of the interaction in the interface were uncovered by X-ray crystallography. Currently, the nature of Pdx effector activity is under debate. Since paramagnetic NMR experiments are applicable to solution studies at ambient temperature, PCS, RDC and PRE methods can further resolve the molecular mechanism of P450cam in the future.

Samenvatting

Van de 15.000 in de literatuur vermeldde cytochromen P450, is P450cam (CYP101A1) het best gekarakteriseerd. Het doel van het onderzoek dat wordt beschreven in dit proefschrift is het vergroten van onze kennis van het mechanisme van interacties tussen P450cam en liganden. De resultaten van de studies geven een algemeen inzicht in P450 systemen, aangezien hun katalytische mechanismen nauw verwant zijn aan dat van P450cam. Hoofdstuk 1 geeft een algemene inleiding over de P450 superfamilie, de katalytische cyclus en elektronenoverdrachtpartners van P450cam alsmede over paramagnetische kernspinresonantie (*Nuclear Magnetic Resonance, NMR*) technieken.

In Hoofdstuk 2 wordt een studie beschreven waarin een paramagnetische NMR sonde, CLaNP-7, is aangebracht op verschillende plaatsen op P450cam en Pdx om de structuur te bepalen van hun complex in oplossing. De grootte en oriëntatie van de $\Delta\chi$ -tensors van Ln^{3+} -CLaNP-7 en de positie van het metaal zijn experimenteel bepaald door analyse van pseudocontact verschuivingen (*pseudocontact shift, PCS*). Van twaalf P450cam constructen zijn zes mutanten geproduceerd. De resterende constructen gaven een te lage eiwitopbrengst en zijn daarom niet gebruikt voor *Caged Lanthanide NMR Probe (CLaNP)* aanhechting. De lage eiwitopbrengst van de P450cam-constructen is te wijten aan het aanbrengen van dubbele cysteïne mutaties, die in sommige gevallen kunnen leiden tot instabiele of incorrecte vouwing van het eiwit. De $\Delta\chi$ -tensoren afgeleid uit de analyse van experimenteel verkregen PCS suggereren dat alle varianten CLaNP-7 binden via twee armen, met uitzondering van mutant F (A113C/N116C). Bij het bepalen van de Ln^{3+} -positie gebaseerd op PCS, is aangetoond dat CLaNP-7 met een enkele zwavelbrug is gebonden aan deze P450cam variant. Twee van de mutanten bleken een CLaNP-aanhechtingsplaats te hebben die zich te ver weg of juist te dicht bij de Pdx bindingsplaats bevond. In totaal zijn 4 van de 12 mutanten gebruikt in de berekeningen, wat aantoont dat het ontwerpen van de posities van de sonde een kwestie is van uitproberen. Deze resultaten vormen de inleiding tot de paramagnetische NMR-experimenten gebruikt om het P450cam-Pdx complex te bestuderen zoals beschreven in hoofdstuk 3. In dit hoofdstuk wordt de structuur van het geoxideerde Pdx-P450cam complex in oplossing beschreven, gebaseerd op een set van 446 *restraints* voor structuurberekeningen, verkregen uit PCS, paramagnetische relaxatieversterking (*Paramagnetic Relaxation Enhancement, PRE*) en residuële dipolaire koppeling (*Residual Dipolar Coupling, RDC*) analyse. Nadat de structuur in oplossing was bepaald, hebben onze collega's tevens de kristalstructuur van dit complex bepaald. De structuur in oplossing gebaseerd op paramagnetische NMR-gegevens wordt weergegeven door een ensemble van tien structuren met een gemiddelde *RMSD* van 1.3 Å voor de positie van Pdx. De positie van Pdx ten opzichte van P450cam zoals gezien in de kristalstructuur is identiek aan die in oplossing, gegeven de experimentele precisie van het ensemble. Deze resultaten tonen de nauwkeurigheid aan van een paramagnetische methode voor



structuurbepaling. De structuur laat zien dat de metaalcentra zich 16 Å van elkaar bevinden, waardoor elektronenoverdracht met voldoende snelheid mogelijk is. Twee trajecten van elektronische koppeling konden worden bepaald, door de FeS cluster te koppelen aan respectievelijk de geconjugeerde heemring en de heemijzer. Onze structuur van het Pdx-P450cam complex wijkt af van de eerder voorgestelde structuur van Zhang *et al.* Terwijl ons manuscript werd beoordeeld voor publicatie, publiceerde Tripathi *et al.* de kristalstructuur van het Pdx-P450cam complex verkregen door de twee eiwitten te verbinden via een flexibel molecule. Tripathi *et al.* zagen dat P450cam in een toestand is die lijkt op de open vorm van P450cam. Gebaseerd op deze observatie concluderen zij dat het de functie is van Pdx om een conformationele verandering van de gesloten naar de open vorm bij P450cam te bewerkstelligen. Verdere NMR experimenten die onderscheid kunnen maken tussen de open en gesloten vorm van P450cam zijn nodig om te bepalen of binding van Pdx ook in oplossing het openen van P450cam veroorzaakt.

Het belang van polaire residuen die zijn geïdentificeerd als onderdeel van het bindingsoppervlak van het Pdx-P450cam complex is aangetoond met behulp van mutagenese en kinetische experimenten (Hoofdstuk 4). Deze polaire interacties dragen bij aan partnerherkenning, maar hebben geen invloed op de snelheid van elektronenoverdracht.

In hoofdstuk 5 wordt beschreven hoe wij de ontmoetingsstaat (*encounter state*) van het Pdx-P450cam complex hebben gekarakteriseerd door gebruik te maken van paramagnetische gegevens van aanvullende sondes. De resultaten van PCS- en RDC-analyse onderschrijven de eerder bepaalde structuren van het complex. Tegelijkertijd laten de experimentele afstanden verkregen met PRE significante afwijkingen van de verwachte waardes zien voor sommige sondes. Hieruit wordt geconcludeerd dat een klein deel van het complex dynamisch van aard is. In de ontmoetingsstaat bevindt Pdx zich dicht bij de J en K helices en de $\beta 1$ sheet. Deze gebieden bezitten geclusterde basische en hydrofobe residuen. Eerdere mutagenesestudies evenals Röntgen kristallografie tonen aan dat de interacties tussen Pdx en P450cam worden gedomineerd door polaire interacties, waterstofbruggen en hydrofobe contacten. Gezien de algehele negatieve lading van beide eiwitten, lijkt het redelijk om aan te nemen dat Pdx voornamelijk de basische/hydrofobe delen van het oppervlak van P450cam bezoekt. Het ontmoetingscomplex kan relevant zijn bij het vormen van het uiteindelijke Pdx-P450cam complex. De prominent aanwezige basische delen aan het oppervlak vormen een pad die Pdx naar de vermeende bindingsplaats kan leiden. Hierdoor wordt een drie-dimensionale zoektocht door botsingen beperkt tot een tweedimensionale over het oppervlak van P450cam. Bovendien verlengt de ladingsinteractie de levensduur van de ontmoeting, wat de vorming van een elektronenoverdracht-actief complex vergemakkelijkt.

1-PIM-3-para is een paramagnetisch substraatanalogon en is gebruikt om het substraat-toegangskanaal van P450cam te karakteriseren (Hoofdstuk 6). De

kristalstructuur van P450cam gebonden aan 1-PIM-3 vertoont een opener configuratie dan de substraatvrije vorm. De eerste resultaten van PRE-analyse geven aan dat paramagnetisch ligand-analogen gebruikt kunnen worden om eiwit-ligand complexen te karakteriseren. Dit werk levert het *proof-of-principle* dat kleine paramagnetische centra, gebonden aan liganden in plaats van aan eiwitten, zeer behulpzaam kunnen zijn bij het karakteriseren van een complex.

Concluderend, door gebruik te maken van paramagnetische NMR technieken is de structuur en dynamiek van het P450cam-systeem onderzocht. De analyse van PCS en RDC heeft een stereospecifiek eindcomplex van Pdx en P450cam aan het licht gebracht, terwijl de resultaten van PRE de aanwezigheid van een kortlevend ontmoetingscomplex hebben aangetoond. Daarnaast is door gebruik te maken van Röntgen kristallografie significant inzicht verkregen in de interacties in het bindingsoppervlak van dit complex. Op dit moment staat de aard van de functie van Pdx ter discussie. Omdat paramagnetische technieken toepasbaar zijn op studies in oplossing bij kamertemperatuur, zijn PCS-, RDC- en PRE-methoden in staat in de toekomst het moleculaire mechanisme van P450cam verder op te lossen.



Publication list

Keizers, P.H.J.; Saragliadis, A.; Hiruma, Y.; Overhand, M.; Ubbink, M. (2008) Design, Synthesis, and Evaluation of a Lanthanide Chelating Protein Probe: CLaNP-5 Yields Predictable Paramagnetic Effects Independent of Environment. *J Am Chem Soc* **130**, 14802–14812.

Takahashi, I.; Kuroiwa, S.; Lindfors, H.E.; Ndamba, L.A.; Hiruma, Y.; Yajima, T.; Okishio, N.; Ubbink, M.; Hirota, S. (2009) Modulation of protein-ligand interactions by photocleavage of a cyclic peptide using phosphatidylinositol 3-kinase SH3 domain as model system, *J Pept Sci* **15**, 411–416.

Hass, M.A.S.; Keizers, P.H.J.; Blok, A.; Hiruma, Y.; Ubbink, M. (2010) Validation of a Lanthanide Tag for the Analysis of Protein Dynamics by Paramagnetic NMR Spectroscopy, *J Am Chem Soc* **132**, 9952–9953.

Keizers, P.H.J.; Mersinli, B.; Reinle, W.; Donauer, J.; Hiruma, Y.; Hannemann, F.; Overhand, M.; Bernhardt, R.; Ubbink, M. (2010) A Solution Model of the Complex Formed by Adrenodoxin and Adrenodoxin Reductase Determined by Paramagnetic NMR Spectroscopy, *Biochemistry* **49**, 6846–6855.

Keizers, P.H.J.; Hiruma, Y.; Ubbink, M. (2012) Protein-Paramagnetic Protein Interactions. In: *NMR of Biomolecules Towards Mechanistic Systems Biology*: (Bertini, I., McGreevy, K.S. and Parigi, G., eds.) Wiley-Blackwell, pp. 204–217.

Hiruma, Y.; Hass, M.A.; Kikui, Y.; Liu, W.M.; Olmez, B.; Skinner, S.P.; Blok, A.; Kloosterman, A.; Koteishi, H.; Löhr, F.; Schwalbe, H.; Nojiri, M.; Ubbink, M. (2013) The Structure of the Cytochrome P450cam-Putidaredoxin Complex Determined by Paramagnetic NMR Spectroscopy and Crystallography, *J Mol Biol* **425**, 4353–4365.

Hiruma, Y.; Gupta, A.; Kloosterman, A.; Olijve, C.; Olmez, B.; Hass, M.A.; Ubbink, M. (2014) Hot Spot Residues in the Cytochrome P450cam-Putidaredoxin Binding Interface, *ChemBioChem* **15**, 80-86



Curriculum Vitae

Yoshitaka Hiruma was born on the 15th of December 1983 in Tokyo, Japan. After obtaining his diploma in Soka high school in Tokyo, he decided to move to the U.K. to continue his education. He spent one year at University College London to pursue a British university entrance exam and enrolled in the University of Edinburgh in Scotland. In 2007, he obtained his BSc with honors in Biological sciences. He then moved to the Netherlands to pursue his MSc degree in Leiden University. Here, he joined the group of Prof. Dr. Marcellus Ubbink. Under the supervision of Dr. Peter Keizers and Hanna Lindfors, he completed his MSc thesis entitled "The characterization of protein interactions by NMR spectroscopy". During the MSc study, he joined in the Erasmus exchange program and performed his second internship in Ludwig Maximilians University Munich, Germany. In 2009, he obtained his MSc degree in the department of Chemistry in Leiden University. He then joined in the Protein Chemistry group headed by Prof. Dr. Marcellus Ubbink as a PhD student. His research was focused on the characterization of the Pdx-P450cam complex formation by paramagnetic NMR spectroscopy. During his PhD degree, he collaborated with Dr. Masaki Nojiri in Osaka University, Japan. This led to the determination of the atomic resolution structure of the Pdx-P450cam complex by both paramagnetic NMR spectroscopy and X-ray crystallography, which is presented in this thesis.

He joined the research groups of Prof. Dr. Geert Kops in the University Medical Center in Utrecht and Dr. Anastassis Perrakis in Netherlands Cancer Institute as a post-doctoral researcher in November 2013. In this collaborative project between both groups, he will perform his research concerning the biochemical characterization of the mitotic checkpoint machinery.



Acknowledgements

I would like to express my deepest gratitude to Prof. Dr. Marcellus Ubbink for providing me the opportunity to study for PhD as well as MSc degrees in his group. Over six years, I truly enjoyed being a member of his group and I was always very proud to present paramagnetic NMR techniques in a science conference. I am also deeply indebted to Dr. Peter Keizers who supervised me during my MSc project and introduced me to cytochromes P450. I have learned so many things from Peter and I would like to present this thesis to him with a sincere gratitude as one of his students. I also greatly appreciate the huge help provided by Dr. Mathias A.S. Hass, who shared his expertise throughout my PhD degree.

I owe a big thanks to all members in Protein Chemistry group. Especially, I would like to acknowledge Anneloes Blok, who makes a wonderful research environment as well as plays a role as a sister/mother in the lab. Also I would like to thank Lionel Ndamba, who not only gave me technical support but also helped me to move my house. Whenever Lionel was around, I shared the progress of my experiments and my personal life without any hesitations. I am very grateful to Dr. Wei-Min Liu for synthesizing and providing me his paramagnetic NMR probes. Without his wonderful compound, CLaNP-7, my PhD project would never be fruitful. I would like to acknowledge BSc and MSc project students, Alexander Kloosterman, Caroline Olijve and Betül Ömez. While working together, I realized the solutions of many problems. Thanks also to Dr. Monika Timmer and Ingrid Bekooy, whose help was fundamental in and out of the laboratory.

I am very fortunate to have had an outstanding collaboration with Osaka University in Japan during my PhD project. Dr. Masaki Nojiri, who shared his expertise of X-ray crystallography, solved the crystal structure of Pdx-P450cam complex. Masaki visited Leiden in 2011 and I was grateful to be able to introduce him and his family to the beauty of the historical Leiden city center. I would like to thank Ankur Gupta in Leiden Institute of Physics for technical support for stopped-flow experiments. I was shocked to see the computer operating the stopped-flow equipment, which dated back to 1990's. I would also like to acknowledge Dr. Navraj Pannu and Dr. Igor Nederlof in Biophysical Structure Chemistry in Leiden Institute of Chemistry. Without their support, I would have never managed to perform X-ray crystallography.

I am very thankful to the SGI Buddhist members in the Netherlands, who continuously encouraged me to go through my PhD degree. A particular thank goes to Olivier Hijmans, Ann Ferrara and Lianna Hartanto. At the final year of my PhD, my mother had a breast cancer. They provided me with a lot of support during that difficult time.

I would like to mention my brother, mother and father, who brought me up no matter how difficult my childhood was. When I was in primary school, I never liked studying and my grades were horrifying. Today, I am going to present this thesis to



my family for paying a debt of gratitude. And great thank goes to my wife, Mika Hiruma. Whenever I was disappointed at my experiments and my manuscript being rejected so many times from journals, Mika supported me without any doubts. She also introduced me to the top dermatologist in Japan. I was suffering so much from unknown allergic reactions in the Netherlands and I was used to wear white gloves on my bleeding hands. My allergic condition has dramatically improved since Mika came to my life.

Last but not least, I am very thankful to my mentor, Dr. Daisaku Ikeda, who believes in my potential and gave me a dream to become a great scientist.